Title
Synthesis and Modification of Carbon Nanomaterials for Potential Device Applications

Author
Cha, Kitty

Publication Date
2012

Peer reviewed|Thesis/dissertation

UNIVERSITY OF CALIFORNIA

Los Angeles

Synthesis and Modification of Carbon Nanomaterials for Potential Device Applications

A dissertation submitted in partial satisfaction of the

requirements for the degree Doctor of Philosophy

in Materials Science and Engineering

by

Kitty Chih-Pei Cha

2012

ABSTRACT OF THE DISSERTATION

Synthesis and Modification of Carbon Nanomaterials for Potential Device Applications

by

Kitty Chih-Pei Cha

Doctor of Philosophy in Materials Science and Engineering

University of California, Los Angeles, 2012

Professor Yang Yang, Chair

Graphene and its derivatives have shown potential to replace indium tin oxide in electronic applications because of their high theoretical conductivity and high optical transmittance. While certain factors prevent the immediate incorporation of graphene as a general transparent electrode material, particularly in solution-processible organic electronics, advances have been made in bringing this material closer to commercial applications. This work explores graphene derived from two popular synthesis methods as an electrode material in organic electronic devices, namely solution processible reduced graphene oxide and chemical vapor deposition (CVD) on copper. Chemical modification with thionyl chloride greatly enhanced the conductivity of chemically reduced graphene. When examined in detail, it was found that thionyl chloride adsorbed on the surface induces charge transfer from the graphitic base to the adsorbed molecule. Although the conductivity of this material is now almost comparable with

conventional transparent electrode materials, the process requires blending with carbon nanotubes to achieve consistency in production of continuous large area films.

Chemical vapor deposition is an effective method to deposit large areas of graphene, and after optimization of the growth and transfer conditions, continuous single layer graphene with minimal defects was synthesized on copper foils. When used as a transparent anode at the bottom of an organic bulk heterojunction device, the surface roughness and hydrophobicity hinder its performance. To improve adhesion and conductivity of the electrode, a layer of the conducting polymer poly(3,4-ethylenedioxythiophene) was electropolymerized directly and conformally on the graphene surface. The surface morphology and thickness of the polymer material was tracked with the growth time, and was also found to be heavily dependent on the quality of the graphene and contact with the potentiostat. With further optimization, this process could be an important advance toward creating multilayer polymer devices on graphene electrodes.

The dissertation of Kitty Chih-Pei Cha is approved.

Xiangfeng Duan

Yu Huang

Richard B. Kaner

Yang Yang, Committee Chair

University of California, Los Angeles

2012

In memory of Chia Ah-Pu and Joseph Henry

Table of Contents

List of Figures

Acknowledgments

It is with the support and guidance of many over the last several years that this dissertation and the work behind it are possible.

I thank Professor Yang Yang, my research supervisor, for the honor of being a member of his group. His advising has been instrumental in shaping my research and career goals. I am also grateful for the mentorship of Professor Richard Kaner, my co-advisor, and for the assistance of my committee members Professors Yu Huang and Xiangfeng Duan.

I owe sincere thanks to my mentors at the Claremont Colleges and Los Alamos National Laboratory, whose distinguished careers served as inspiration for my own ambitions. The guidance and encouragement of Dr. Elshan Akhadov, Dr. Gabriel Montaño and Dr. Rico Del Sesto enabled me to discover the thrill and joy of scientific research. I also thank my collaborators at the Center for Integrated Nanotechnologies at Los Alamos National Laboratory, Dr. Andrew Dattelbaum, Dr. Aditya Mohite, and Dr. Gautam Gupta, for the use of their facilities and providing their generous technical assistance and insight.

I also appreciate the help of all my colleagues in the Yang lab. Dr. Wei Lek Kwan, Dr. William Hou, Dr. Srinivas Sista, Dr. Li-Min Chen, and Ms. Reneé Green provided me with peer mentorship and technical input. Mr. Wenbing Yang spent many evenings acquiring X-ray photoelectron spectra. Mr. Steven Hawks assisted with the finer points of organic electronic devices. Mr. Eric Richard provided valuable insight and suggestions on a number of topics, particularly in electrochemistry. Mr. Brion Bob contributed his energy and enthusiasm as a sounding board during data analysis and in proofreading a number of drafts, including this dissertation. I thank Dr. Vincent Tung and Dr. Matthew Allen for laying the groundwork on this research project, Mr. Sergey Dubin for providing graphite oxide, and Dr. Jonathan Wassei for our lengthy discussions and fruitful collaboration.

I am especially grateful to all my friends, without whom this experience would not be complete. Dr. Paul Brochu, Dr. James Dorman, Mr. James Ma and Ms. Stephanie Reed sustained me through the trials of graduate school with their wit, kindness and friendship.

And finally, I thank my family for their unwavering support of my goals and appreciate the sacrifices they have made to enable them.

Chapter Two is adapted from “Wassei, J. K.; Cha, K. C.; Tung, V. C.; Yang, Y.; Kaner, R. B. “The effects of thionyl chloride on the properties of graphene and graphene-carbon nanotube composites.” *Journal of Materials Chemistry* **2011**, 21, 3391.”

VITA

2006	B.A., Chemistry, Scripps College, Claremont, California
2006-2007	Post-baccalaureate, Los Alamos National Laboratory, Los Alamos, New Mexico
2008	National Science Foundation IGERT Fellowship
2010	M.S., Materials Science and Engineering, University of California, Los Angeles, California
2010	Editorial Intern, Wiley-VCH Verlag GmbH, Weinheim, Germany
2011-2012	Teaching Associate, Department of Materials Science and Engineering, University of California, Los Angeles, California

PUBLICATIONS

Y. He, J. You, L. Dou, C.-C. Chen, E. Richard, K. C. Cha, Y. Wu, G. Li, Y. Yang. High performance low band gap polymer solar cells with a non-conventional acceptor. *Chem. Commun.* **48**, 7616 (2012).

R. Zhu, C.-H. Chung, K. C. Cha, W. Yang, Y. B. Zheng, H. Zhou, T.-B. Song, C.-C. Chen, P. S. Weiss, G. Li, Y. Yang. Fused Silver Nanowires with Metal Oxide Nanoparticles and Organic Polymers for Highly Transparent Conductors. *ACS Nano* **5**, 9877 (2011).

J. K. Wassei*, K. C. Cha*, V. C. Tung, Y. Yang and R. B. Kaner. The effects of thionyl chloride on the properties of graphene and graphene-carbon nanotube composites. *J. Mater. Chem.* **21**, 3391 (2011).

S. Dubin, S. Gilje, K. Wang, V. C. Tung, K. Cha, A. S. Hall, J. Farrar, R. Varshneya, Y. Yang and R. B. Kaner. A One-Step, Solvothermal Reduction Method for Producing Reduced Graphene Oxide Dispersions in Organic Solvents. *ACS Nano* **4**, 3845 (2010).

J. K. Wassei, V. C. Tung, S. J. Jonas, K. Cha, B. S. Dunn, Y. Yang, and R. B. Kaner. Stenciling Graphene, Carbon Nanotubes, and Fullerenes Using Elastomeric Lift-Off Membranes. *Adv. Mater.* **22**, 897 (2010).

E. Nazaretski, Y. Obukhov, I. Martin, D. V. Pelekhov, K. C. Cha, E. A. Akhadov, P. C. Hammel, and R. Movshovich. Localized ferromagnetic resonance force microscopy in Permalloy-cobalt films. *J. Appl. Phys*. **106**, 046103 (2009).

D. M. Tournear, M. A. Hoffbauer, E. A. Akhadov, A. T. Chen, S. J. Pendleton, T. L. Williamson, K. C. Cha, and R. I. Epstein. Gamma-ray waveguides. *Appl. Phys. Lett*. **92**, 153502 (2008).

E. Nazaretski, D. V. Pelekhov, I. Martin, K. C. Cha, E. A. Akhadov, P. C. Hammel, and R. Movshovich. Localized Ferromagnetic Resonance Force Microscopy of a Continuous Permalloy-Cobalt Film. *Mater. Res. Soc. Symp. Proc*. **1025** (2008).

E. Nazaretski, E. A. Akhadov, K. C. Cha, D. V. Pelekhov, I. Martin, K. S. Graham, P. C. Hammel, and R. Movshovich. Ferromagnetic resonance force microscopy studies of a continuous permalloy–cobalt film. *phys. stat. sol. (a)* **205**, 1758 (2008).

A. F. Fucaloro, Y. Pu, K. Cha, A. Williams, and K. Conrad. Partial Molar Volumes and Refractions of Aqueous Solutions of Fructose, Glucose, Mannose, and Sucrose at 288.15, 293.15, and 298.15K. *J. Solution Chem* **36**, 61 (2007).

A. Niemz, K. Bandyopadhyay, E. Tan, K. Cha, and S. M. Baker. Fabrication of Nanoporous Templates from Diblock Copolymer Thin Films on Alkylchlorosilane-Neutralized Surfaces. *Langmuir* **22**, 11092 (2006).

Chapter 1: Introduction to Graphene and Recent Developments

1.1 Introduction to Graphene Research

In recent years, concern about the future of energy supplies worldwide has caused increasing demand for innovation in the fields of energy, electronics, and biology. In turn, this has accelerated research interest into alternative and functional materials. Traditionally, many devices built for electronics, biomedical applications, and energy generation and storage have been made from metals or inorganic semiconductors. However, the evolution of these technologies has seen the scaling down of these devices and the discovery of new materials which offer either advantages of cost, performance, or both. From an economic standpoint, materials made from carbon are more earth abundant, and therefore lower cost. Nanoscale forms of carbon, namely fullerene, carbon nanotubes, and graphene have shown to exhibit some very interesting properties that allow them the potential of replacing traditional materials in a wide swath of applications. This introduction will describe how nanostructured carbon, particularly graphene, is a versatile material with great potential for a wide range of high performance applications.

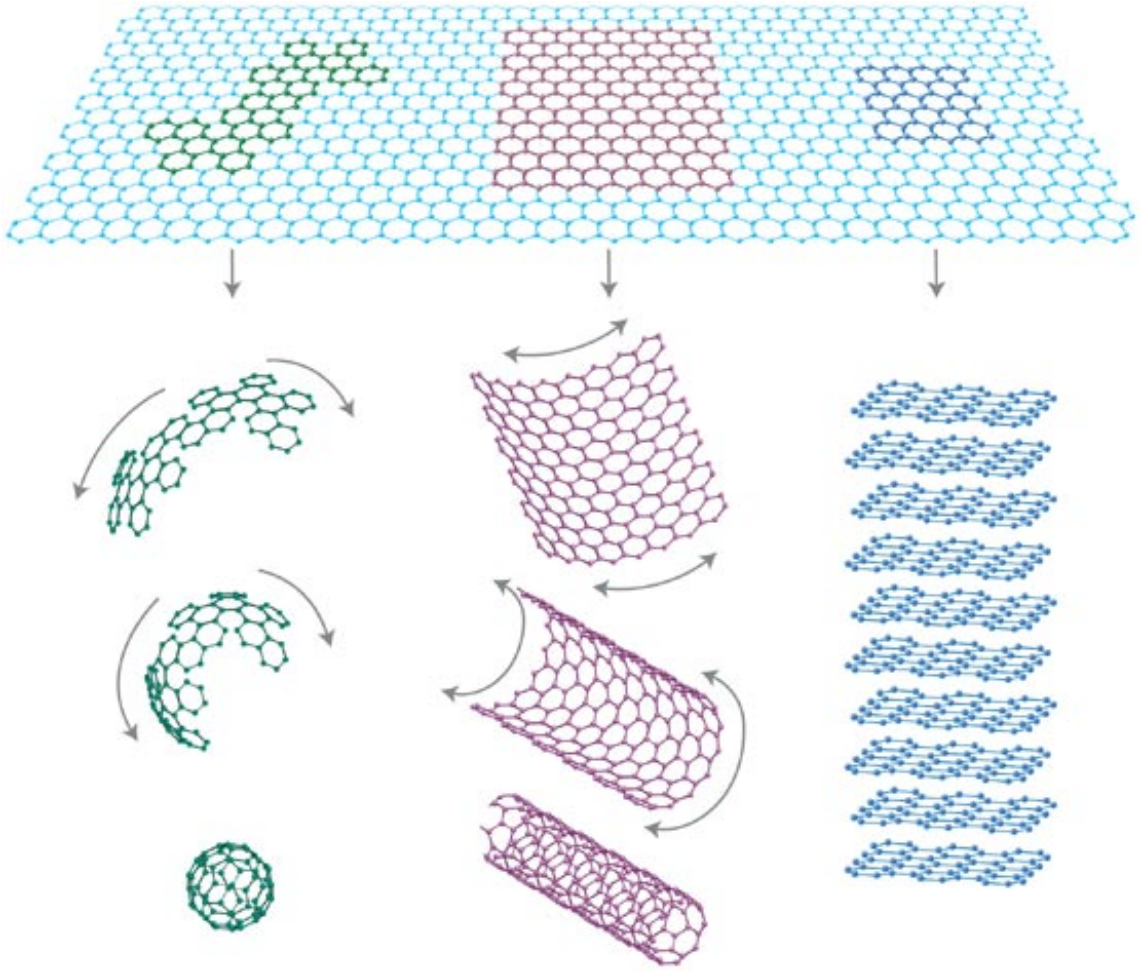

Figure 1.1 Graphene (top) as the structural basis for crystalline forms of carbon: (left) 0-dimensional fullerene; (middle) 1-dimensional carbon nanotube; (right) 3-dimensional graphite. From Reference 1. Reprinted by permission from Macmillan Publishers.

Graphene, a single, two-dimensional layer of sp^2-networked carbon, can be thought of as the mother of all different graphitic forms. Graphene is the basic structure for various carbon allotropes, including graphite, which consist of stacks of individual graphene layers bonded via van der Waals forces. The high strength of the covalent bonding within the layers and weak

interlayer bonding allows them to slide quite easily. This has led to use of graphite in pencils: exfoliating layers with every stroke occasionally down to single monolayers. Single layer graphene was thought to be thermodynamically unstable in its free state until 2004 when it was isolated by a group of scientists led by Andre Geim.[2] Although no experimental tools existed to search for one-atom-thick flakes among the pencil debris covering macroscopic areas, graphene was eventually spotted due to the subtle optical effect it creates on top of a substrate of silicon dioxide (SiO_2) of a certain thickness, which allows its observation with an optical microscope.[3,4]

Because of these extraordinary properties and range of potential applications, naturally there is a natural impetus to produce large quantities. Unfortunately the original methods of synthesizing graphene were not scalable, and restricted to characterization studies or novel proof-of-concept devices. Methods for the large scale synthesis of graphene have so far been unable to exactly replicate the properties observed in pristine graphene, but these synthetic materials themselves have had their own fascinating properties which allow them to be topics of research.

1.2 Physical and Chemical Properties of Graphene

1.2.1 Physical Characteristics

The extraordinary electronic properties of single and few-layer graphene have been discussed in great depth in the literature, and these phenomena were confirmed in the pioneering study of experimentally isolated graphene.[2] First, its charge carriers behave as massless relativistic particles, or Dirac fermions, and under ambient conditions they move with little scattering. The symmetry of its unit cell results in its unique band structure: a zero-bandgap 2D semiconductor with a tiny overlap between valence and conduction bands. This in turn causes it

to exhibit a strong ambipolar electric field effect so that the charge carrier concentrations of up to 10^{13} cm^{-2} and room-temperature mobilities of ~10 000 $cm^{-2}s^{-1}$ are measured, paving the way for unique field effect transistors. The two-dimensional structure of graphene confines electron transport within the plane, giving it a half-integer quantum Hall effect (QHE) for both electron and hole carriers in graphene has been observed by adjusting the chemical potential using the electric field effect.[5,6] In addition, graphene is highly transparent, with an absorption of ~2.3% towards visible light.[7] Although this number is significant when thought of in the context of the atomically thin layer, the electrical characteristics imparted only by a single layer of material makes it suitable for transparent conductive applications.

Graphene, like other graphitic forms, is thermally stable.[8,9] For instance, graphene nanosheets can withstand temperatures up to 700°C before decomposing,[10] and annealing temperatures higher than 250°C have been incorporated in some processes. Vapor-based synthetic methods occur around 1000 °C. As yet, a clear melting temperature is unknown. As it has a negative thermal expansion coefficient due to its two-dimensionality and out of plane phonons,[11] Graphene exhibits an exceptionally high in-plane thermal conductivity up to 5300 W/mK.[8] These outstanding thermal properties of graphene make it an attractive material for heat dissipation in a wide range of devices from nanometer-scale silicon complementary metal-oxide-semiconductor (CMOS) technology, to photonics, and bioengineering.

The strength of the carbon-carbon double bond causes graphene to be mechanically very strong while remaining flexible. Indentation experiments conducted on pristine graphene have yielded an intrinsic strength of about 130 GPa, a Young's modulus of 1 TPa, and a third order elastic stiffness of about 2 TPa with a strength of 42 N/m, which is the strongest ever

measured.[12] Measurements conducted with single layer graphene deposited by CVD, which contains some defects, had an average shear modulus of 280 GPa, which is five times as large as that of multilayer graphene at 53 GPa, which is also five times that of graphite (10 GPa).[13] While these measurements were made from small samples and are not necessarily directly scalable to a macroscopic sample, these benchmarks have led to the use of graphene in composites to supplement the mechanical strength and flexibility of ceramics, metals and polymers.[14,15]

Although graphene is hydrophobic,[16,17] a single layer has wetting transparency when laid on certain substrates, so the surface energy of the underlying substrate is generally unchanged.[18] Additionally, graphene can inhibit oxidation on certain metals, making it a potential corrosion resistant coating.[19,20]

1.2.2 Chemical Properties

Because graphene is a chemically inert material and stable in air up to 200°C,[19] it needs relatively high energetic species to break its sp^2 bonds and initiate functionalization reactions. Atomic H generated with a hot tungsten filament has enough reactivity to reduce the graphene to graphane.[21] The first successful hydrogenation was performed on mechanically exfoliated graphene.[22] Oxidation of graphene is also possible through oxygen plasma. The ease at which the graphitic base is functionalized enables graphene to be a versatile backbone for chemical reactions. Most of the time, graphite oxide is used as a starting material, which will be explained in more detail later in this chapter.

Molecular sensors based on chemically derived graphene have been reported, which utilize the principle of increasing or decreasing the electrical conductivity of a graphene sheet in response to electron donating or withdrawing groups. Recent reports have shed some light on

covalent functionalization of graphene through aryl diazonium salts.[23] Graphene substrates originating from different chemical processes have varied reactivity toward aryl diazonium salts, from a high reactivity of chemically converted graphene, which is derived from the reduction of graphene oxide, , while epitaxial graphene grown from SiC is surface grafted using diazonium salts.[24] The diazonium reaction with graphite or mechanically exfoliated graphene shows preferential edge reactivity. As diazonium salts are moderately reactive, they can be used as a path for further graphene chemical reactions.

1.3 Structure and Characterization of Graphene

1.3.1 Raman Spectroscopy

Raman spectroscopy is an effective, convenient and nondestructive way to determine the structure, thickness and quality of graphene-based materials. Specifically, the in-plane optical vibrations of sp^2-bonded carbon atoms give rise to the G peak, occurring at a Raman shift of ~1580 cm^{-1}, while the 2D peak, located at about 2700 cm^{-1}, arises from second-order boundary phonons. The D peak, also known as the “defect” peak, is absent in defect-free graphene such as peeled graphene, is attributed to first order zone boundary phonons. A small D’ peak is also sometimes visible around 1620 cm^{-1}. Therefore, the presence of the D peak is indicative of bonds other than sp^2-carbon.[25] The D peak is attributed to first-order zone boundary phonons, which is absent from defect-free graphene, and is therefore a useful measure of quality. The quality and number of layers in a peeled graphene sample can be determined by the shape, width, and position of the 2D peak. Figure 1.2 shows how the number of graphene layers changes the number of subpeaks present, increasing the full-width at half maximum (FWHM) of the 2D peak and upshifting in wavenumber, while the peak height is roughly unchanged. In a single layer, the

D+ and D− subpeaks degenerate into a single 2D peak, while in a bilayer it splits into 4 subpeaks. The G peak of single layer graphene is found upshifted by 3 to 5 cm^{-1} from bulk graphite and is much less intense. The position and the height ratio of peaks between G and 2D bands vary with the number of layers: the relative G peak intensity is about 10% to 50% of the 2D height for monolayers, roughly equivalent in bilayers, and higher than the 2D peak in few-layer (>2) graphenes and bulk graphite.

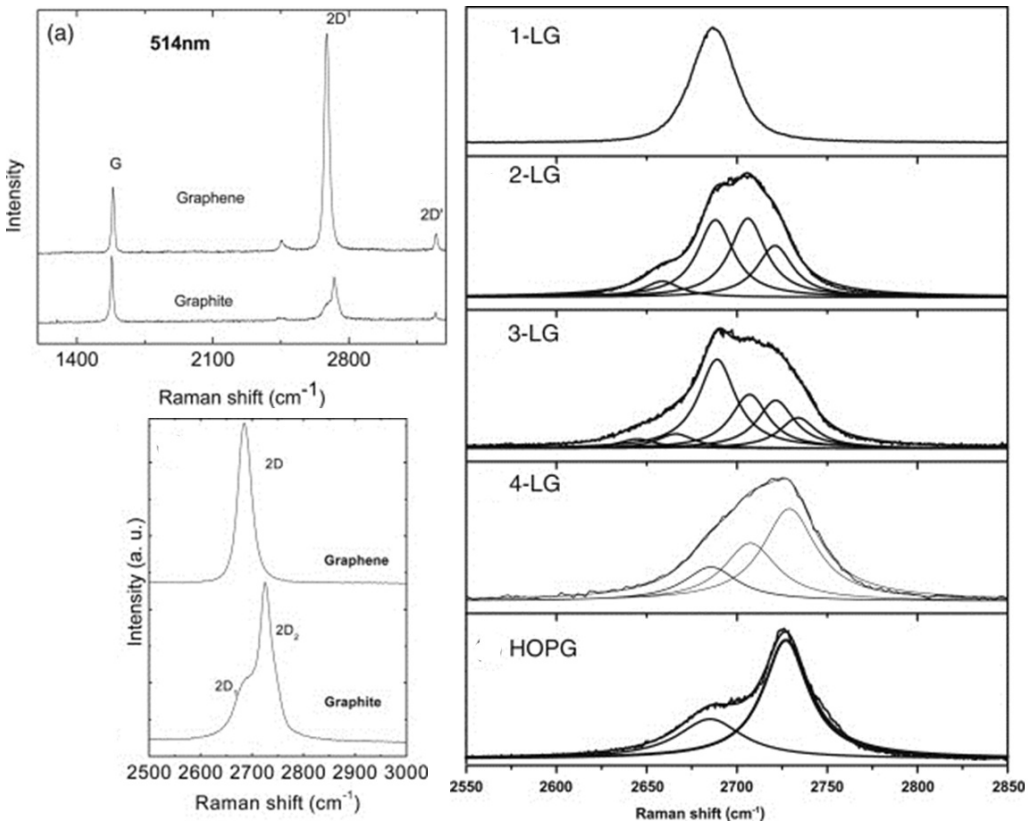

Figure 1.2 A comparison of the Raman spectra of graphene and graphite with increasing number of layers, in particular the 2D peak. Reproduced with permission from References 25 and 26 from Elsevier.

The frequency and intensity ratio of the G and 2D peaks is also found to be modulated by charge carriers: the G peak stiffens and sharpens for both n- and p-type samples, and the ratio of the intensities between the G and 2D peaks shows a strong dependence on doping.[26] Therefore, Raman peaks are commonly used to deduce the character of a graphene sample and reported in the literature.

1.3.2 Microscopic Characterization

For a trained eye, a quick observation under optical microscopy can identify graphene. It was found that graphene affects the interference in silicon oxide, allowing it to be observed on a SiO_2 substrate. The change in the contrast is thickness-dependent, so subtle differences in the color of the film on the substrate can be indicative of the relative thickness of the sample.[3]

Scanning electron microscopy (SEM) provides a higher resolution observation of graphene grown on both metals and dielectrics. The contrast of SEM images is mainly induced by the different conductivity between the graphene and the underlying surface. Dark areas indicate the boundaries of the graphene film while light areas are the exposed metal oxide surface. While it does not provide specific quantitative information on the graphene structure and characteristics, it is valuable for locating graphene devices or determining the approximate dimensions of a graphene sheet up to several tens of microns. Transmission electron microscopy (TEM) is a powerful tool that can show the atomic features of single layered graphene down to the arrangement of individual carbon atoms.[27] This makes it valuable for mapping features such as atomic defects,[28] or in the case of large area CVD graphene, grain boundaries.

Scanning probe microscopy, including AFM and scanning tunneling microscopy (STM) are the most powerful tools for determining layer thickness, structure and quality.[29,30] Scanning

tunneling spectroscopy can also provide information on electronic properties.[31] The thickness of a single graphene sheet should be 0.34 nm, or the equivalent of the diameter of a carbon atom, which is larger than the 0.1 nm detection limit in AFM. Often, in a topographic scan, oxides or other functionalities on the graphene sheet cause step heights of more than 0.34 nm. These are taken into consideration during data analysis, and usually, especially in the case of functionalized graphene, a step height between 0.34 nm and 1.0 nm indicates a single layer graphene sample.[32,33] The STM technique has become especially valuable to image graphene grown by epitaxial growth to reveal domains and grain boundaries.[34-36] In all, the microscopic techniques highlighted are valuable tools in analyzing the quality of the graphene material, and by extension, shed light on the success of a particular synthetic or modification method.

1.4 Synthetic Methods of Graphene and its Derivatives

1.4.1 Mechanical Exfoliation

The exfoliation of graphite is a process in which bulk graphite can be separated into single atomic planes. On a small scale, this is achieved using the simple method of peeling away layers of highly oriented pyrolytic graphite (HOPG) using Scotch™ tape. The simplicity of this method, formally known as micromechanical cleavage of bulk graphite, has caused it to be widely used to prepare graphene samples. Because of the high quality of the starting graphite material and subsequently of the peeled graphene samples, it is also known as pristine graphene. After being peeled away from each other, the layers are then transferred directly to the desired substrate, typically silicon oxide for identification and electrical measurements. An initial wet transfer technique was supplanted by a simpler dry transfer from the tape directly onto the oxide. Sizes of individual crystals can reach millimeter range, but is it still a low throughput method.

The pristine quality of these samples still makes them attractive for studying fundamental properties but they are not used in any practical applications.

1.4.2 Epitaxial Growth

Wafer-scale growth of graphene has been demonstrated through epitaxial graphene (EG) growth on a silicon carbide (SiC) surface.[37,38] The work in this bottom-up approach was conducted by heating 6H- or 4H-SiC in ultrahigh vacuum (UHV) in the temperature range of 1200 to 1600°C.[37] The process involves the sublimation of silicon atoms on the surface, after which the exposed carbons reconstruct to a layers. This method can be implemented on a large scale, and enables growth directly on an insulating surface which is suitable for electronics. However, the high cost of single crystal SiC wafers and the ultrahigh vacuum requirement are barriers to industrial scale growth.

1.4.3 Chemical Methods

Chemical routes to graphene were explored in response to the demand for large quantities of graphene for experimental purposes and practical implementation. Intercalation and exfoliation of bulk graphite is a successful method for producing high volumes of graphene. Another distinct advantage is that these sheets, through their covalent functionalities, remain stable in organic solvents.[39] Several liquid-phase exfoliation approaches have been reported,[40-42] but most of these have given way to oxidation of bulk graphite and its subsequent reduction.

Bulk graphite is most commonly oxidized through Hummers method, which is the most effective in overcoming the van der Waals forces that hold the graphite layers together.[43] The oxidized flakes contain negative charges that are stabilized in solution by electrostatic repulsion.[44] The oxidation disrupts the sp^2-hybridization of the basal plane carbon atoms,

converting them to sp^3 carbons with oxygen functionalities such as hydroxides, carboxylic acids and epoxides. Graphene oxide is soluble in water and other polar solvents without the assistance of surfactants. Ultrasonication is typically used to increase the concentration of graphite oxide sheets in dispersion, although at high power, the ultrasonic forces can break up the sheets into smaller dimensions.

As graphite oxide is electrically insulating, the complete reduction of graphite oxide to restore the conductivity is desired. Methods of reduction range from chemical,[32,45] thermal,[46] microwave,[47] electrochemical,[48] and optical (through a camera flash or laser beam).[49-51] Some of these techniques, such as chemical reduction via hydrazine, are able to preserve the single flake exfoliated structure, while others form more aggregated structures. It has been found that graphite oxide reduced by laser scribing is extremely advantageous for supercapacitor applications.[50] Hydrazine is the most effective chemical reducing agent for graphite oxide, and it offers the added advantage of enabling stable surfactant-free dispersions[32,52] but its toxicity is a concern. Other chemical reducing agents such as $NaBH_4$[53] and ascorbic acid[54] have been effectively used. Nevertheless, chemical reduction does not restore the planar sp^2 network that is found in pristine graphene, but does decrease its electrical resistance through lowering the defect concentration and dramatically reducing the density of oxygen groups.

1.4.4 Chemical Vapor Deposition

The preparation of graphene by chemical vapor deposition on transition metal surfaces is an effective way to obtain single or few layer graphene on a large scale. Given the right growth conditions, the continuous area of the graphene is limited only by the dimensions of the metal on which it is grown. Currently this is the most promising, inexpensive and readily accessible

approach for deposition of reasonably high quality graphene, and prototypes using CVD graphene as a transparent electrode in an electronic device have been fabricated in industry. Field effect mobilities of up to 7350 $cm^2V^{-1}s^{-1}$ have been measured.[55] As will be elaborated in Chapter 3, in CVD, the growth of graphene layers occurs through the segregation of bulk-dissolved carbon to the surface of the metal during the annealing and cooling stages, and by the surface decomposition of carbon-containing molecules. Because of the high quality of the grown graphene and rapid progress in understanding the growth process, at present CVD is the most commonly adopted growth technique for producing graphene films for electronics research.

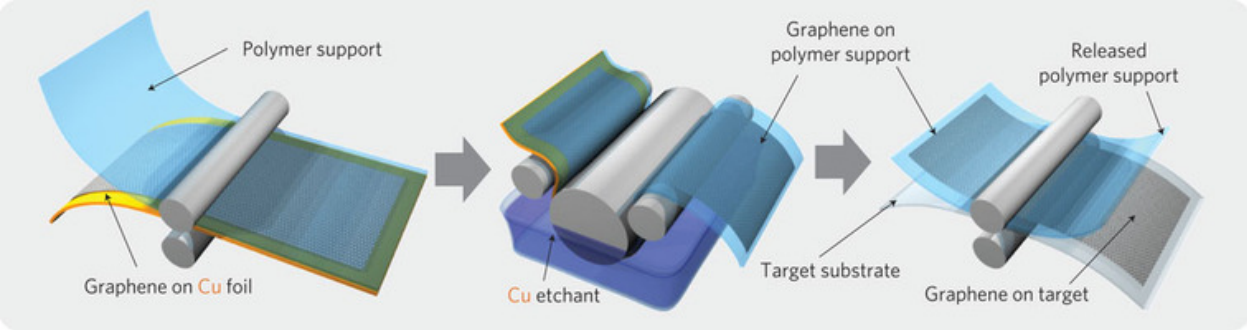

Figure 1.3 A schematic of the roll-to-roll CVD graphene growth and transfer process. The process includes adhesion of a thermal release polymer support, copper etching and dry transfer-printing on a target substrate. Reproduced from Reference 55 with permission from Macmillan Publishers Ltd.

1.5 Applications of Graphene

1.5.1 Electronics and Transparent Conductors

The unique electronic properties of graphene have led to furious exploration into using it in novel electronic devices such as high-frequency electronics and spintronics.[56,57] Its high conductivity at high optical transmittance can pave the way in making flexible, rollable, or stretchable electronics at the large scale. Graphene can also be applied in flexible and transparent integrated circuits, as shown by a recent report on a solution-processed graphene device operating in the gigahertz.[58] Although the conductivities of chemically derived graphene are usually lower than that produced by CVD or epitaxial growth, it offers the advantage of solution casting. Hybrids of graphene and other conductive materials such as polymers or carbon nanotubes can boost its conductivity while maintaining its solution processibility.[59] Using graphene to replace current transparent conductor technology, either from large area CVD growth or solution-processible graphene inks, would enable many types of electronics, such as sensors, memory devices, solar cells, touch screens, lighting, and displays,[60] to adopt bendable and rollable configurations.

1.5.2 Graphene in Devices for Energy Harvesting

Graphene is a promising material for a number of energy related applications, namely for photovoltaics and storage. With a theoretical specific surface area of 2630 m^2/g, and experimental values of up to 3100 m^2/g measured for a supercapacitor anode material created from graphite oxide, graphene has outperformed conventional activated carbon materials by two to three times.[61,62] Photovoltaic cells require a transparent conductive layer to allow complete

light absorption by the active layers in the device, and graphene has immense potential for this application.[60,63] Graphene produced both from chemical reduction and CVD methods has been used as the anode in organic,[64] dye-sensitized (DSSC)[65] and hybrid solar cells.[66] Solution-processed graphene has been used as a hole transport material in organic[67,68] cells. In DSSCs, a graphene-based material that was incorporated into the TiO_2 electron transport material and electrode reduced the recombination rate and increased the dye adsorption for higher efficiency.[69] The flexible nature of graphene was also utilized in ZnO nanowire piezeoelectric generators.[70,71]

Beyond transparent conductor and charge transport functions, graphene also exhibits a photothermoelectric effect, where a photocurrent was produced across a graphene junction upon illumination,[72] along with a large voltage difference. Therefore, along with high electrical conductivity, the tunability of the electrical properties in the presence of light or an electric field showcases its versatility for power generation.

1.6 Organization of the Dissertation

With the ultimate goal of improving the application of graphene in organic devices, this dissertation details work on the synthesis and manipulation of graphene material synthesized via two methods: chemical reduction of graphite oxide and chemical vapor deposition. Rather than improve upon already published figures of merit from other optimized systems, the focus of the work is to describe methods of manipulating graphene to make it a versatile, feasible electrode material for organic electronic devices. This is established through improvement of its electrical conductivity and its surface compatibility with conducting polymers.

References

(1) Geim, A. K.; Novoselov, K. S. *Nat Mater* **2007**, *6*, 183.

(2) Novoselov, K. S.; Geim, A. K.; Morozov, S. V.; Jiang, D.; Zhang, Y.; Dubonos, S. V.; Grigorieva, I. V.; Firsov, A. A. *Science* **2004**, *306*, 666.

(3) Roddaro, S.; Pingue, P.; Piazza, V.; Pellegrini, V.; Beltram, F. *Nano Letters* **2007**, *7*, 2707.

(4) Ni, Z. H.; Wang, H. M.; Kasim, J.; Fan, H. M.; Yu, T.; Wu, Y. H.; Feng, Y. P.; Shen, Z. X. *Nano Letters* **2007**, *7*, 2758.

(5) Novoselov, K. S.; Geim, A. K.; Morozov, S. V.; Jiang, D.; Katsnelson, M. I.; Grigorieva, I. V.; Dubonos, S. V.; Firsov, A. A. *Nature* **2005**, *438*, 197.

(6) Zhang, Y.; Tan, Y.-W.; Stormer, H. L.; Kim, P. *Nature* **2005**, *438*, 201.

(7) Nair, R. R.; Blake, P.; Grigorenko, A. N.; Novoselov, K. S.; Booth, T. J.; Stauber, T.; Peres, N. M. R.; Geim, A. K. *Science* **2008**, *320*, 1308.

(8) Balandin, A. A.; Ghosh, S.; Bao, W.; Calizo, I.; Teweldebrhan, D.; Miao, F.; Lau, C. N. *Nano Letters* **2008**, *8*, 902.

(9) Balandin, A. A. *Nat Mater* **2011**, *10*, 569.

(10) Campos-Delgado, J.; Kim, Y. A.; Hayashi, T.; Morelos-Gómez, A.; Hofmann, M.; Muramatsu, H.; Endo, M.; Terrones, H.; Shull, R. D.; Dresselhaus, M. S.; Terrones, M. *Chemical Physics Letters* **2009**, *469*, 177.

(11) Yoon, D.; Son, Y.-W.; Cheong, H. *Nano Letters* **2011**, *11*, 3227.

(12) Lee, C.; Wei, X.; Kysar, J. W.; Hone, J. *Science* **2008**, *321*, 385.

(13) Liu, X.; Metcalf, T. H.; Robinson, J. T.; Houston, B. H.; Scarpa, F. *Nano Letters* **2012**, *12*, 1013.

(14) Stankovich, S.; Dikin, D. A.; Dommett, G. H. B.; Kohlhaas, K. M.; Zimney, E. J.; Stach, E. A.; Piner, R. D.; Nguyen, S. T.; Ruoff, R. S. *Nature* **2006**, *442*, 282.

(15) Huang, X.; Qi, X.; Boey, F.; Zhang, H. *Chemical Society Reviews* **2012**, *41*, 666.

(16) Wang, S.; Zhang, Y.; Abidi, N.; Cabrales, L. *Langmuir* **2009**, *25*, 11078.

(17) Wang, G.; Yang, J.; Park, J.; Gou, X.; Wang, B.; Liu, H.; Yao, J. *The Journal of Physical Chemistry C* **2008**, *112*, 8192.

(18) Rafiee, J.; Mi, X.; Gullapalli, H.; Thomas, A. V.; Yavari, F.; Shi, Y.; Ajayan, P. M.; Koratkar, N. A. *Nat Mater* **2012**, *11*, 217.

(19) Chen, S.; Brown, L.; Levendorf, M.; Cai, W.; Ju, S.-Y.; Edgeworth, J.; Li, X.; Magnuson, C. W.; Velamakanni, A.; Piner, R. D.; Kang, J.; Park, J.; Ruoff, R. S. *ACS Nano* **2011**, *5*, 1321.

(20) Prasai, D.; Tuberquia, J. C.; Harl, R. R.; Jennings, G. K.; Bolotin, K. I. *ACS Nano* **2012**, *6*, 1102.

(21) Sun, Z.; Pint, C. L.; Marcano, D. C.; Zhang, C.; Yao, J.; Ruan, G.; Yan, Z.; Zhu, Y.; Hauge, R. H.; Tour, J. M. *Nat Commun* **2011**, *2*, 559.

(22) Elias, D. C.; Nair, R. R.; Mohiuddin, T. M. G.; Morozov, S. V.; Blake, P.; Halsall, M. P.; Ferrari, A. C.; Boukhvalov, D. W.; Katsnelson, M. I.; Geim, A. K.; Novoselov, K. S. *Science* **2009**, *323*, 610.

(23) Lomeda, J. R.; Doyle, C. D.; Kosynkin, D. V.; Hwang, W.-F.; Tour, J. M. *Journal of the American Chemical Society* **2008**, *130*, 16201.

(24) Bekyarova, E.; Itkis, M. E.; Ramesh, P.; Berger, C.; Sprinkle, M.; de Heer, W. A.; Haddon, R. C. *Journal of the American Chemical Society* **2009**, *131*, 1336.

(25) Malard, L. M.; Pimenta, M. A.; Dresselhaus, G.; Dresselhaus, M. S. *Physics Reports* **2009**, *473*, 51.

(26) Ferrari, A. C.; Meyer, J. C.; Scardaci, V.; Casiraghi, C.; Lazzeri, M.; Mauri, F.; Piscanec, S.; Jiang, D.; Novoselov, K. S.; Roth, S.; Geim, A. K. *Physical Review Letters* **2006**, *97*, 187401.

(27) Meyer, J. C.; Kisielowski, C.; Erni, R.; Rossell, M. D.; Crommie, M. F.; Zettl, A. *Nano Letters* **2008**, *8*, 3582.

(28) Hashimoto, A.; Suenaga, K.; Gloter, A.; Urita, K.; Iijima, S. *Nature* **2004**, *430*, 870.

(29) Lauffer, P.; Emtsev, K. V.; Graupner, R.; Seyller, T.; Ley, L.; Reshanov, S. A.; Weber, H. B. *Physical Review B* **2008**, *77*, 155426.

(30) Stolyarova, E.; Rim, K. T.; Ryu, S.; Maultzsch, J.; Kim, P.; Brus, L. E.; Heinz, T. F.; Hybertsen, M. S.; Flynn, G. W. *Proceedings of the National Academy of Sciences of the United States of America* **2007**, *104*, 9209.

(31) Li, G.; Luican, A.; Andrei, E. Y. *Physical Review Letters* **2009**, *102*, 176804.

(32) Tung, V. C.; Allen, M. J.; Yang, Y.; Kaner, R. B. *Nat Nano* **2009**, *4*, 25.

(33) Dubin, S.; Gilje, S.; Wang, K.; Tung, V. C.; Cha, K.; Hall, A. S.; Farrar, J.; Varshneya, R.; Yang, Y.; Kaner, R. B. *ACS Nano* **2010**, *4*, 3845.

(34) Zan, R.; Muryn, C.; Bangert, U.; Mattocks, P.; Wincott, P.; Vaughan, D.; Li, X.; Colombo, L.; Ruoff, R. S.; Hamilton, B.; Novoselov, K. S. *Nanoscale* **2012**, *4*, 3065.

(35) Yu, Q.; Jauregui, L. A.; Wu, W.; Colby, R.; Tian, J.; Su, Z.; Cao, H.; Liu, Z.; Pandey, D.; Wei, D.; Chung, T. F.; Peng, P.; Guisinger, N. P.; Stach, E. A.; Bao, J.; Pei, S.-S.; Chen, Y. P. *Nature Materials* **2011**, *10*, 443.

(36) Rasool, H. I.; Song, E. B.; Allen, M. J.; Wassei, J. K.; Kaner, R. B.; Wang, K. L.; Weiller, B. H.; Gimzewski, J. K. *Nano Letters* **2010**, *11*, 251.

(37) Berger, C.; Song, Z.; Li, X.; Wu, X.; Brown, N.; Naud, C.; Mayou, D.; Li, T.; Hass, J.; Marchenkov, A. N.; Conrad, E. H.; First, P. N.; de Heer, W. A. *Science* **2006**, *312*, 1191.

(38) Emtsev, K. V.; Bostwick, A.; Horn, K.; Jobst, J.; Kellogg, G. L.; Ley, L.; McChesney, J. L.; Ohta, T.; Reshanov, S. A.; Rohrl, J.; Rotenberg, E.; Schmid, A. K.; Waldmann, D.; Weber, H. B.; Seyller, T. *Nat Mater* **2009**, *8*, 203.

(39) Li, X.; Zhang, G.; Bai, X.; Sun, X.; Wang, X.; Wang, E.; Dai, H. *Nat Nano* **2008**, *3*, 538.

(40) Hernandez, Y.; Nicolosi, V.; Lotya, M.; Blighe, F. M.; Sun, Z.; De, S.; McGovern, I.; Holland, B.; Byrne, M.; Gun'Ko, Y. K. *Nature Nanotechnology* **2008**, *3*, 563.

(41) Lotya, M.; Hernandez, Y.; King, P. J.; Smith, R. J.; Nicolosi, V.; Karlsson, L. S.; Blighe, F. M.; De, S.; Wang, Z.; McGovern, I. T.; Duesberg, G. S.; Coleman, J. N. *Journal of the American Chemical Society* **2009**, *131*, 3611.

(42) Nuvoli, D.; Valentini, L.; Alzari, V.; Scognamillo, S.; Bon, S. B.; Piccinini, M.; Illescas, J.; Mariani, A. *Journal of Materials Chemistry* **2011**, *21*, 3428.

(43) Hummers, W. S.; Offeman, R. E. *Journal of the American Chemical Society* **1958**, *80*, 1339.

(44) Park, S.; Ruoff, R. S. *Nat Nano* **2009**, *4*, 217.

(45) Stankovich, S.; Dikin, D. A.; Piner, R. D.; Kohlhaas, K. A.; Kleinhammes, A.; Jia, Y.; Wu, Y.; Nguyen, S. T.; Ruoff, R. S. *Carbon* **2007**, *45*, 1558.

(46) Zhu, Y.; Stoller, M. D.; Cai, W.; Velamakanni, A.; Piner, R. D.; Chen, D.; Ruoff, R. S. *ACS Nano* **2010**, *4*, 1227.

(47) Chen, W.; Yan, L.; Bangal, P. R. *Carbon* **2010**, *48*, 1146.

(48) Guo, H.-L.; Wang, X.-F.; Qian, Q.-Y.; Wang, F.-B.; Xia, X.-H. *ACS Nano* **2009**, *3*, 2653.

(49) Gao, W.; Singh, N.; Song, L.; Liu, Z.; Reddy, A. L. M.; Ci, L.; Vajtai, R.; Zhang, Q.; Wei, B.; Ajayan, P. M. *Nat Nano* **2011**, *6*, 496.

(50) El-Kady, M. F.; Strong, V.; Dubin, S.; Kaner, R. B. *Science* **2012**, *335*, 1326.

(51) Kim, F.; Luo, J.; Cruz-Silva, R.; Cote, L. J.; Sohn, K.; Huang, J. *Advanced Functional Materials* **2010**, *20*, 2867.

(52) Li, D.; Müller, M. B.; Gilje, S.; Kaner, R. B.; Wallace, G. G. *Nature Nanotechnology* **2008**, *3*, 101.

(53) Shin, H.-J.; Kim, K. K.; Benayad, A.; Yoon, S.-M.; Park, H. K.; Jung, I.-S.; Jin, M. H.; Jeong, H.-K.; Kim, J. M.; Choi, J.-Y.; Lee, Y. H. *Advanced Functional Materials* **2009**, *19*, 1987.

(54) Zhang, J.; Yang, H.; Shen, G.; Cheng, P.; Guo, S. *Chemical Communications* **2010**, *46*, 1112.

(55) Bae, S.; Kim, H.; Lee, Y.; Xu, X.; Park, J.-S.; Zheng, Y.; Balakrishnan, J.; Lei, T.; Ri Kim, H.; Song, Y. I.; Kim, Y.-J.; Kim, K. S.; Ozyilmaz, B.; Ahn, J.-H.; Hong, B. H.; Iijima, S. *Nature Nanotechnology* **2010**, *5*, 574.

(56) Wu, Y.; Jenkins, K. A.; Valdes-Garcia, A.; Farmer, D. B.; Zhu, Y.; Bol, A. A.; Dimitrakopoulos, C.; Zhu, W.; Xia, F.; Avouris, P.; Lin, Y.-M. *Nano Letters* **2012**, *12*, 3062.

(57) Zhang, Q.; Chan, K. S.; Lin, Z. *Applied Physics Letters* **2011**, *98*, 032106.

(58) Sire, C.; Ardiaca, F.; Lepilliet, S.; Seo, J.-W. T.; Hersam, M. C.; Dambrine, G.; Happy, H.; Derycke, V. *Nano Letters* **2012**, *12*, 1184.

(59) Peng, L.; Feng, Y.; Lv, P.; Lei, D.; Shen, Y.; Li, Y.; Feng, W. *The Journal of Physical Chemistry C* **2012**, *116*, 4970.

(60) Bonaccorso, F.; Sun, Z.; Hasan, T.; Ferrari, A. *Nature Photonics* **2010**, *4*, 611.

(61) Zhu, Y.; Murali, S.; Stoller, M. D.; Ganesh, K. J.; Cai, W.; Ferreira, P. J.; Pirkle, A.; Wallace, R. M.; Cychosz, K. A.; Thommes, M.; Su, D.; Stach, E. A.; Ruoff, R. S. *Science* **2011**, *332*, 1537.

(62) Stoller, M. D.; Park, S.; Zhu, Y.; An, J.; Ruoff, R. S. *Nano Letters* **2008**, *8*, 3498.

(63) Luo, B.; Liu, S.; Zhi, L. *Small* **2012**, *8*, 630.

(64) Park, H.; Brown, P. R.; Bulović, V.; Kong, J. *Nano Letters* **2011**, *12*, 133.

(65) Wang, X.; Zhi, L.; Mullen, K. *Nano Letters* **2007**, *8*, 323.

(66) Yin, Z.; Wu, S.; Zhou, X.; Huang, X.; Zhang, Q.; Boey, F.; Zhang, H. *Small* **2010**, *6*, 307.

(67) Li, S. S.; Tu, K. H.; Lin, C. C.; Chen, C. W.; Chhowalla, M. *ACS Nano* **2010**, *4*, 3169.

(68) Murray, I. P.; Lou, S. J.; Cote, L. J.; Loser, S.; Kadleck, C. J.; Xu, T.; Szarko, J. M.; Rolczynski, B. S.; Johns, J. E.; Huang, J.; Yu, L.; Chen, L. X.; Marks, T. J.; Hersam, M. C. *The Journal of Physical Chemistry Letters* **2011**, *2*, 3006.

(69) Yen, M.-Y.; Hsiao, M.-C.; Liao, S.-H.; Liu, P.-I.; Tsai, H.-M.; Ma, C.-C. M.; Pu, N.-W.; Ger, M.-D. *Carbon* **2011**, *49*, 3597

(70) Choi, D.; Choi, M.-Y.; Choi, W. M.; Shin, H.-J.; Park, H.-K.; Seo, J.-S.; Park, J.; Yoon, S.-M.; Chae, S. J.; Lee, Y. H.; Kim, S.-W.; Choi, J.-Y.; Lee, S. Y.; Kim, J. M. *Advanced Materials* **2010**, *22*, 2187.

(71) Kumar, B.; Lee, K. Y.; Park, H.-K.; Chae, S. J.; Lee, Y. H.; Kim, S.-W. *ACS Nano* **2011**, *5*, 4197.

(72) Gabor, N. M.; Song, J. C. W.; Ma, Q.; Nair, N. L.; Taychatanapat, T.; Watanabe, K.; Taniguchi, T.; Levitov, L. S.; Jarillo-Herrero, P. *Science* **2011**, *334*, 648.

Chapter 2: Synthesis and Chemical Modification of Graphitic Materials

2.1 Introduction to Chemically Reduced Graphite Oxide

2.1.1 Synthesis and Processing Methods

The graphite oxide (GO) starting material used in this chapter was synthesized via a modified Hummers method that is commonplace in the research community.[1,2] The graphite oxide obtained was then stored in an aqueous suspension until it was processed for film deposition. The film deposition process is as follows: first, the aqueous suspension of GO is vacuum filtered through a Nucleopore™ track-etched polycarbonate membrane and allowed to dry for 24 hours. For reduction, the hydrated GO 'paper' was then dispersed and reduced in anhydrous hydrazine at a concentration of 1 mg/mL. The hydrazine was added to the GO directly in a glass vial. This reaction was performed in an inert atmosphere, and the dark brown GO turns black as it is reduced in an exothermic reaction.[3] The GO-hydrazine dispersion is given a few days to completely react. To isolate the single-layer and few-layer sheets of chemically converted graphene (CCG), the dispersion is centrifuged between 1200 rpm and 1500 pm for 45 to 60 minutes. For a 1 mL centrifuge vial, the top 100 μL is collected and redispersed in 900 μL fresh hydrazine.

The graphene layers were deposited on a substrate via spin-coating. As hydrazine is hydrophilic, the SiO_2 or glass substrates must first be activated by ozonation for about 15 minutes or by oxygen plasma for 3 to 5 minutes at 30 W power. A film is cast from the hydrazine dispersion within 5 minutes by static spin-coating or dip-coating. In spin-coating, the surface coverage is controlled via the spin speed, or by adding more coats of the dispersion. The sample is then baked on a hotplate at 150°C for 30 minutes to remove all traces of hydrazine.

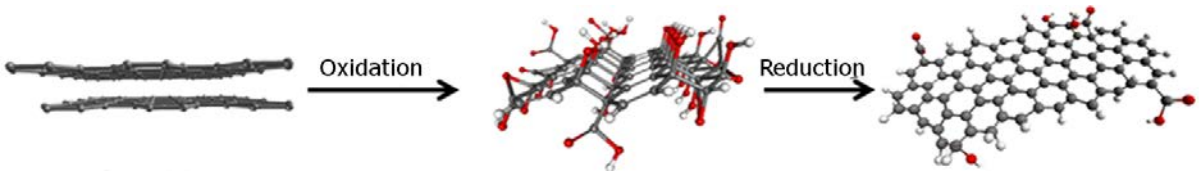

bulk graphite graphite oxide chemically reduced

Figure 2.1 Schematic of the reduction and dispersion of graphite oxide by hydrazine. Oxidation overcomes the van der Waals forces binding the sheets in bulk graphite, converting the sp^2 network in the graphene sheets to sp3 hybridized carbons with oxygen functionalities.

2.1.2 Hybrids of Graphene and Single-Walled Carbon Nanotubes

Synthetic constraints and the insolubility of CNTs and graphene in most common organic solvents have prevented their use in practical applications at manufacturing scales. Several approaches have been developed for the synthesis of these nanoscale carbon materials. The poor solubility characteristics of both graphene and CNTs has hindered their wide spread inclusion in practical commercial devices. Rigorous effort has been placed into improving the solubility of these graphitic materials. Many of the published strategies rely on the covalent addition of functional groups or self-assembled monolayers that are compatible with the desired solvent to the open ends or side walls of the nanostructures.[4] Unfortunately, these modifications often lead to the formation of local defects that disrupt the conjugated sp^2 carbon network that elicits the characteristic electronic behavior of these nanoscale graphitic materials. Other groups have utilized surfactants to enhance the solubility of CNTs and graphene. In these methods, the physical bonding between these materials and surfactant molecules tends to inhibit the formation

of extended π-π networks between the graphitic nanostructures, resulting in reduced carrier mobility and overall device performance.

The single-walled carbon nanotubes (CNTs) used in this chapter have been acid-treated as a purification step; therefore, they also have oxygen functionalities on the graphitic backbone.[5] Therefore, reduction via direct, surfactant-free dispersion in hydrazine is also effective for these species.[6] It has been found that carbon nanotubes that have not undergone the oxidation and purification steps do not form homogeneous dispersions in hydrazine. The CNTs, used as received, are dispersed in anhydrous hydrazine in an initial concentration of 10 mg/mL and allowed to reduce over several days. CNTs are known to form bundles, which have to be disintegrated by ultrasonication for an hour. The dispersion is then centrifuged at 11000 rpm and the top 100 μL of the supernatant is collected and diluted with 900 μL fresh anhydrous hydrazine.

The graphene and CNT dispersions in hydrazine were then mixed in a ratio of 1:1 (note that the initial concentrations of these materials are different, so the final ratio of CCG to CNTs is closer to 1:5 to 1:10). Films were then deposited from surfactant-free dispersions in hydrazine on to a variety of substrates by spin-coating. A mild annealing process, at 110°C, was applied to ensure adequate removal of the solvent. Additional studies on graphene were performed on sheets of mechanically exfoliated graphene, or pristine graphene, which were transferred onto silicon substrates with a thermally grown 300 nm silicon oxide.

2.1.3 Hydrazine as a Common Solvent for All Nanoscale Graphitic Materials

The use of hydrazine as a solvent and reducing agent was extended to the other nanoscale graphitic materials, namely carbon nanotubes and fullerenes. We have found that chemically

functionalized carbon nanotubes and the fullerene derivative [6,6]-phenyl-C_{61}-butyric acid methyl ester (PCBM) are soluble in hydrazine at high concentrations because of the oxygen functionalities that are present on the surface of these materials. Processing from hydrazine dispersions allows for a simple, scalable approach to disperse and controllably deposit CNTs, graphene, and PCBM via solution processing. By controlling the solution processing and spin coating conditions we are able to obtain various degrees of surface coverage and morphologies. Although PCBM is already soluble in common organic solvents that may be safer than hydrazine,[7] the universality of hydrazine as a solvent for all the graphitic forms eliminates the need for solvent mixtures which may form aggregations, permitting the formation of uniform mixtures where it is possible to homogeneously combine each of the three materials without the addition of surfactants that may hinder their electronic performance.

It is suspected that the underlying mechanism responsible for the stable dispersions relies on the formation of counter ion complexes between negatively charged graphitic materials and positively charged hydrazine. Upon dissolution in anhydrous hydrazine, the local polarity of these oxygen moieties facilitates redistribution of local dipoles. Electrons residing on carbon atoms will be pulled toward oxygen atoms, leading to negative charges at the material interface that ultimately form counterion complexes with positively charged hydrazine ions as illustrated in Scheme 2.1. The dispersions in hydrazine utilized in this work do not involve surfactants and are stable for months with no evidence of aggregation.

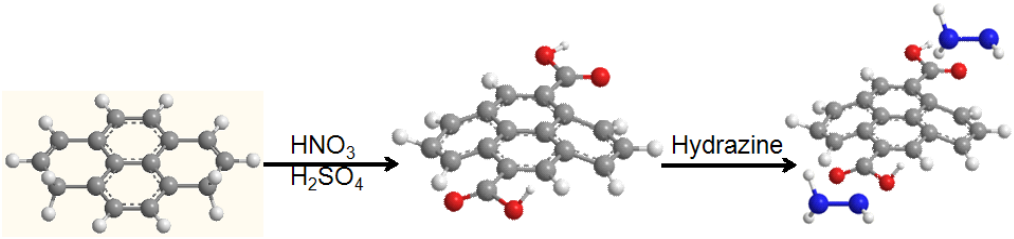

Scheme 2.1 Illustration of the interaction of hydrazine on oxidized graphene.

2.2 Conductivity Enhancement of Reduced Graphene Oxide by Chemical Doping

2.2.1 Adsorption of chemical p-dopants

Although the conductivity upon reduction of graphite oxide is dramatically increased, it does not meet the value required to compete with metals or ITO. Scientists and engineers have turned to doping to increase the conductivity of inorganic seminconductor materials and conducting polymers. The same concept has also been applied to carbon nanotubes and graphene in recently published work, with success. Doping of graphene and carbon nanotubes can be done by substitutional dopant atoms such as B and N.[8,9] In this area, the simplest, most effective processes for doping are still being explored. Doping processes of CVD graphene with nitric acid, nitromethane and $AuCl_3$ show characteristics of p-doping,[10-12] while polyvinyl alcohol has been reported to n-dope mechanically exfoliated graphene.[13] Doping can reduce the resistance of graphene films to a few hundreds of Ω, bringing it within a reasonable range of ITO. Modification of graphene and carbon nanotubes has been carried out using a number of species in the vapor and liquid phases.

A simpler way of noncovalently doping the graphitic network is through charge transfer of adsorbed chemical species. It has been found that charge transfer to and from adsorbed species

can shift the graphene Fermi level by a large fraction of an electron volt.[14] The main effect of charge transfer adsorbed species is a change in the Fermi level and the conductivity. The primary advantage to this method is the lack of any substitutional impurities which would disrupt the conjugated network. As such, adsorption-induced chemical doping may well become an important aspect of future graphene technologies. In graphenes consisting of only a few layers, chemical doping can result from both surface adsorption and intercalation between layers. Previous studies have employed halogens as dopants, specifically Br_2 and I_2. Metallic nanoparticles can also be incorporated as dopants, introduced to the surface in solution. Specifically, $AuCl_3$ solution which was introduced to the surface of graphene, left gold nanoparticles after heating.[12] The use of NO_2 as a charge transfer dopant for graphene, which can controllably shift its Fermi level,[15] has been shown to change the electrical response enough for it to be used as a chemical sensor.[16,17] The literature on doping with NO_2, Br_2 and I_2 has shown that, as these materials are more electronegative than graphite, they should dope graphene and carbon nanotubes positively when adsorbed. In the vapor phase, I_2 adsorbs on and dopes carbon nanotubes,[18-20] along with other conjugated carbon materials such as fullerenes,[21] pentacene,[22,23] and polyacetylene.[24,25] Charge transfer via doping by Br_2 and I_2 on the carbon network is typically characterized by Raman spectroscopy. The G peak appears upshifted by hole doping. An intercalated structure is created by Br, as is evident from an intercalated Br- band appearing near 240 cm^{-1}. However, it is thought that the longer I_2 bond length does not allow an intercalation structure, though the presence of anionic I_3^- and I_5^- is seen in the Raman spectra.[11]

2.2.2 Chemical doping with thionyl chloride

Thionyl chloride ($SOCl_2$) is a commonly used solvent and inorganic acid known for dehydrating and chlorinating oxygen containing hydrocarbons. Similar effects have been observed in nanotubes exposed to strong inorganic acids such as nitric and sulfuric acids, but these effects are believed to be due to oxidation and removal of surfactant groups.[26] Thionyl chloride is capable of comprehensively modifying the basal planes and open ends of graphitic materials, creating platforms for attachment of a variety of functionalities.[27,28] Previous work showed that the conductivity of single-walled carbon nanotubes increases upon treatment with $SOCl_2$.[28] The modification process involves simple immersion either in liquid or vapor phase $SOCl_2$, so the mechanism behind their increased conductivity warrants further analysis. The structural similarity of the graphitic backbone shared by carbon nanotubes and graphene makes it logical that graphene and composites comprised of these two (G-CNT) would be affected by this chemical treatment in an analogous manner. While there have been reports on dopant- or solvent-induced changes in the electronic properties of graphitic materials, there has been a lack of conclusive evidence to explain the improvement in conductivity in chemically converted graphene and graphene-CNT nanocomposites treated with $SOCl_2$. In this study, the effects of thionyl chloride on the physical and chemical properties of pristine graphene are explored, as well as the changes in the structure and morphology of G-CNT nanocomposites that lead to improvements in their transparent conducting properties.

Substrates with dried CCG, G-CNT composites and pristine graphene were placed into glass petri dishes and ~1 mL of liquid $SOCl_2$ was dispensed into the dishes and around the samples, with care taken to avoid direct contact. It was found that extended immersion in thionyl

chloride results in complete delamination of the carbon from the substrate. The dishes were covered and allowed to saturate with vapor at 135°C for at least 15 minutes, or until the vapor had dissipated.

2.2.3 Characterization of the doping mechanism of thionyl chloride

Raman spectra were obtained using a Renishaw 1000, with a 50x objective lens at an excitation wavelength of 514 nm. The peaks were fitted using the Renishaw software to confirm the location of the Raman peaks. X-ray photoemission spectroscopy (XPS) was carried out in an Omicron Nanotechnology system with a base pressure of 2×10^{-10} torr with Al Kα radiation (1486.6 eV) as the excitation source. The sheets of chemically converted graphene were scanned with a Veeco Dimension 5000 atomic force microscope before and after $SOCl_2$ treatment to obtain high resolution images. Absorbance and transmittance measurements were carried out using a Cary 50 UV-visible spectrophotometer under ambient condition. Scanning electron micrographs (SEM) of the graphene and G-CNT composites were obtained on a JEOL 6700 SEM. Additionally, Energy-Dispersive X-Ray spectra were obtained using an EDAX Genesis detector attached to the SEM.

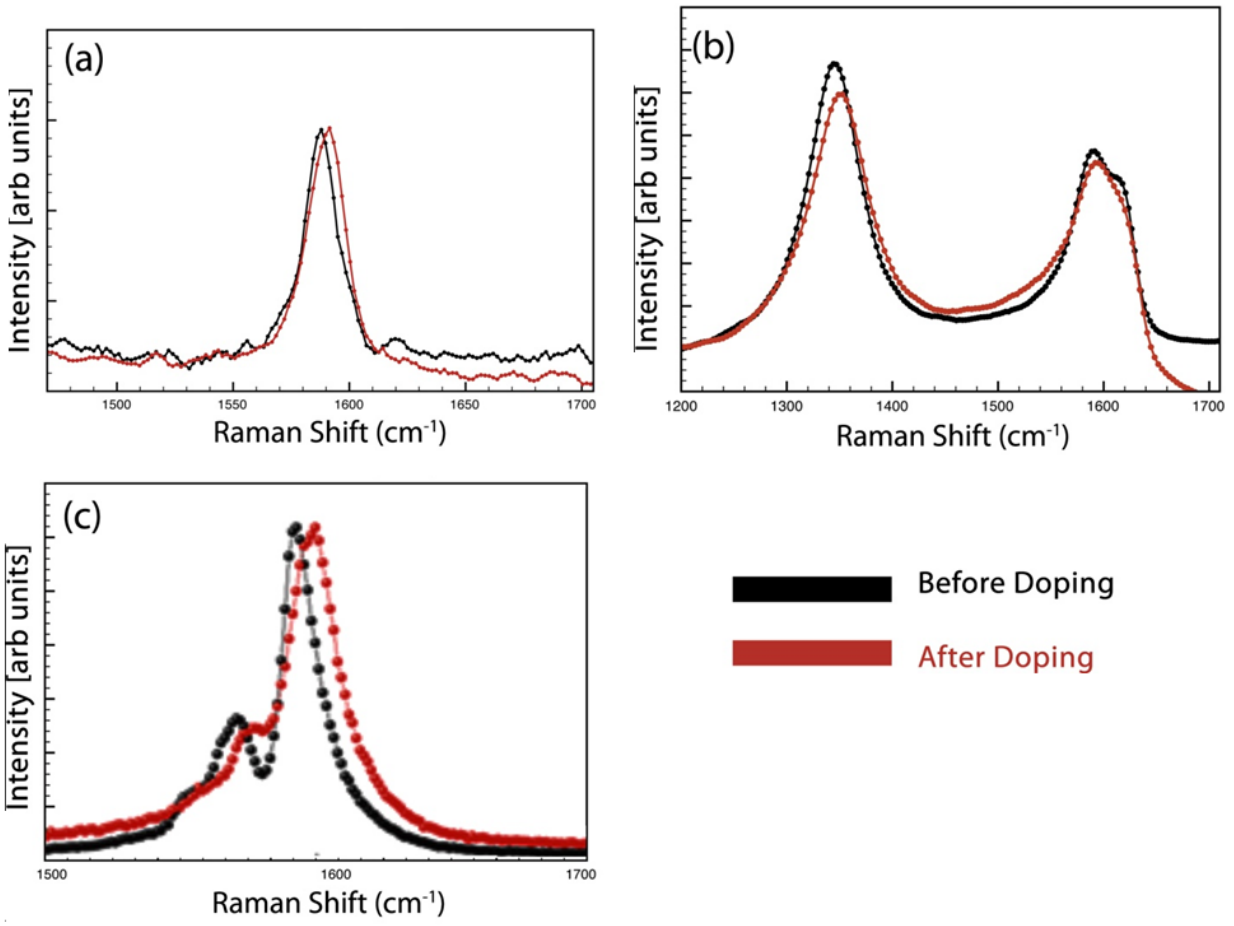

Figure 2.2 Raman spectra of the G peak in chemically converted graphene and carbon nanotubes before and after 15 minutes of thionyl chloride exposure. (a) A pristine graphene flake red shifts by 5.2 cm^{-1}; (b) a chemically converted graphene flake shifts by 4.8 cm^{-1}; and (c) a CCG-CNT hybrid film red shifts by 8.1 cm^{-1}.

Raman spectra were obtained for chemically converted graphene, mechanically exfoliated graphene (pG) and CCG-CNT composites, before and after 15 minutes of thionyl chloride exposure (Figure 2.2). The characteristic peaks exhibited in the Raman spectra before and after modification were analyzed. The G-band in graphitic materials typically exhibits a

substantial upshift for electron-acceptor dopants (e.g. bromine, iodine and nitric acid), while displaying a downshift for electron-donor (e.g. potassium) dopants.[29] Upon exposure to thionyl chloride vapor, electrons originally residing on the graphitic framework are pulled toward the more electronegative atoms, leading to charge redistribution.

The full width at half maximum for the 2D mode of the pristine graphene flake was measured to be 33 cm^{-1}, indicating a single layer was being used for this experiment. Blue-shifts in CCG (Fig. 1a) from 1595.9 to 1601.1 cm^{-1} (~5.2 cm^{-1}), pristine graphene (Figure 2.2) from 1587.7 to 1592.5 cm^{-1} (~4.8 cm^{-1}) and G-CNT (Figure 2.2) from 1592.1 to 1600.2 cm^{-1} (~8.1 cm^{-1}) are observed, which signify electron transfer from the graphitic materials to the dopant. The shape of the G band can also be used to understand the changes in the in-plane force constant and determine if a graphene flake has been intercalated.[22] As shown in Figure 2.2, no splitting of the G peak is observed, indicating that this anion interaction does not form an intercalated compound. This is important in understanding the role of the anionic dopant in the graphene system. The physical adsorption of anions is a similar effect to that of other halogen dopants such as bromine or iodine, whereas nitric acid and diazonium are believed to intercalate into the graphitic layers.[9] The shape of the G peak in the G-CNT system, as shown in Figure 2.2 (c), is an exception to the splitting since its shape is a result of combining mostly semiconducting carbon nanotubes with CCG.

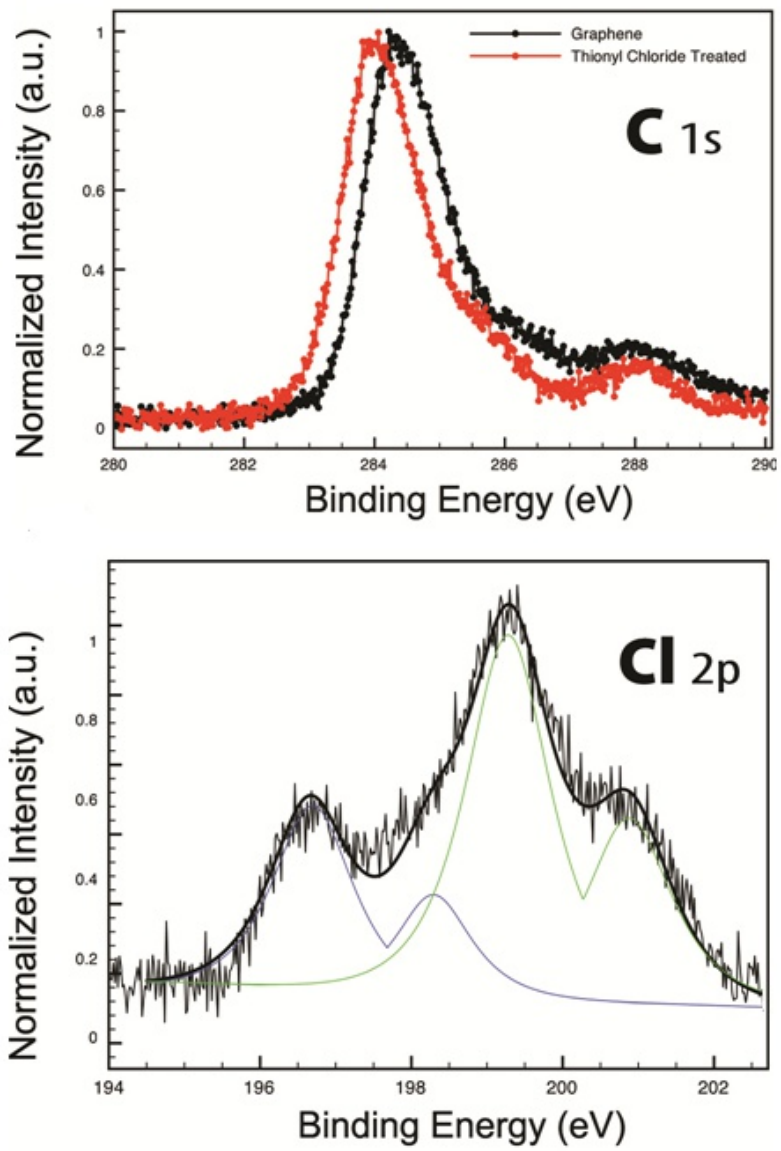

Figure 2.3 X-ray photoemission spectra of thionyl chloride treated graphene materials showing (above) the C 1s of CCG and (below) Cl 2p of mechanically exfoliated graphene.

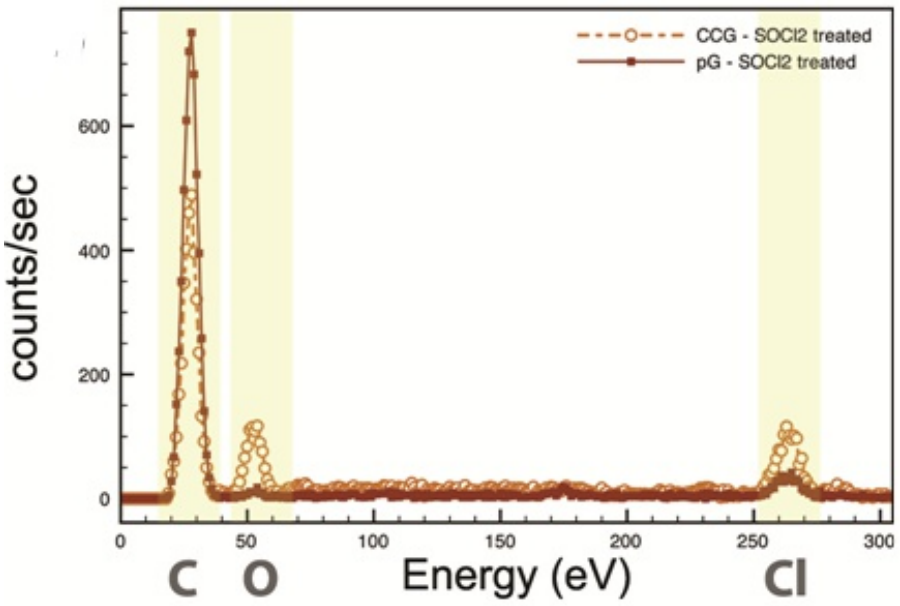

Figure 2.4 Energy dispersive X-ray (EDX) spectroscopy graph for both mechanically exfoliated pristine graphene (pG) and chemically converted graphene (CCG) to verify the presence of chlorine.

To gain insight into specific bonding effects of thionyl chloride on graphene, XPS and EDX were used on peeled graphene, CCG and G-CNT thin films. The nature of the chemical modification to the graphitic structures was determined by XPS analysis. Spectra were collected for pristine graphene, CCG and G-CNT that were deposited onto silicon substrates with a 20 nm gold layer added on top to avoid charging effects. Previous work showed that pristine SWCNT form many C-S bonds and some C-Cl bonds when exposed to liquid $SOCl_2$ at elevated temperatures,[28] so similar doping interactions with pristine graphene were expected. Full core level spectra for all three samples were collected and evidence for C 1s and Cl 2p peaks were found, but S 2p, which was observed in previous experiments with CNTs, was not found. These

results suggest that either the curvature and absence of carboxylic acid groups on the CNT allows for molecular interaction of the $SOCl_2$ with the carbon and resulting C-S bonds or the $SOCl_2$ fully decomposes in the vapor phase. In all instances the XPS show the same C 1s (for sp^2 C) and Cl 2p (C-Cl) binding energies. Figure 2.3 presents the results for CCG flakes before and after treatment. These results indicate that C-Cl interactions form from the doping process, which leads to the overall enhancement in electronic transport.

The C 1s peak at 284.4 eV for sp^2 carbon shifts by 0.5 eV to a lower binding energy (283.9 eV) after the vapor treatment, indicating that the sp^2 pi system has been affected. The Cl 2p core level spectrum shows two nonequivalent chlorine sites from the 3/2 and 1/2 levels, which are separated by 1.4 eV due to spin-orbit coupling. The more intense peak at ~200.2 eV is a result of Cl participating in C-Cl covalent bonding, while the less intense peak at ~198.8 eV is a result of Cl^- ionic bonds with the carbon on the surface. This is significant as it shows that the graphitic surfaces in the pG, CCG and G-CNT are modified by interactions with the Cl in the $SOCl_2$, instead of the S in unfunctionalized CNTs. To confirm the chemical composition of the modified graphitic species, EDX spectra were collected on both pristine and chemically converted graphene species. As shown in Figure 2.4, the spectrum verifies that only chlorine, carbon and oxygen (in the case of CCG) on the graphene and G-CNT post-$SOCl_2$ treatment are present.

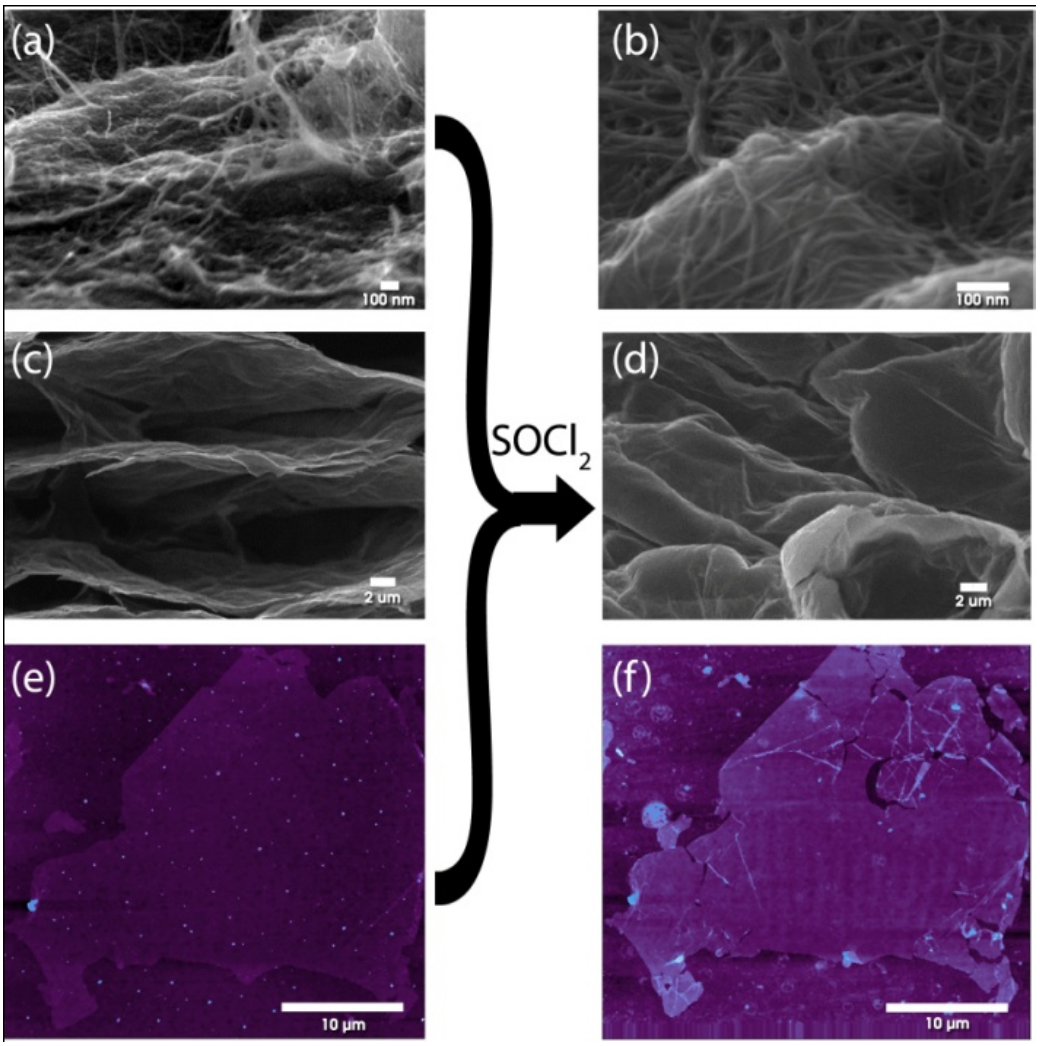

Figure 2.5 Scanning electron micrographs (SEM) of graphene-CNTs nanocomposites and CCG and an atomic force micrograph (AFM) of a single CCG sheet. The SEMs of the nanocomposite (a) before, and (b) after $SOCl_2$ treatment indicate that the CNTs bundle over the graphene layers. (c) SEMs show an increased overlap between graphene layers after (d) doping with $SOCl_2$. AFM images of CCG (e) before and (f) after treatment suggest that exposure to $SOCl_2$ can be detrimental to the fidelity of a graphene flake. This anionic dopant causes rips and wrinkles instead of intercalation and folding.

The changes in chemical structure can be correlated to the morphology of the composites using scanning electron microscopy (SEM). Thicker multilayer composites were analyzed, and the micrographs show that the treatment promotes not only aggregation and cross-linking among nanotube bundles, but also between the nanotubes and the graphene sheets. These results show that chlorine, not sulfur-bound thionyl chloride must be responsible for this morphological change. The SEM images shown in Figure 2.5 suggest that the chemical modification with $SOCl_2$ facilitates stronger interactions between the carbon nanotubes and graphene (Figure 2.5 (a) and (b)). The images of graphene layers alone (Figure 2.5 (c),(d)) show that the thionyl chloride treatment also promotes aggregation between layers and the incorporation of carbon nanotubes clearly provides an additional pathway for 3-dimensional interactions.

The bundling, coupled with the lack of G peak splitting from the Raman spectra suggests that chlorine anions, from thionyl chloride, also act as adsorbants rather than intercalants. AFM images further suggest that instead of folding along preferred crystallographic planes, the graphene flakes slightly wrinkle, and in the case of CCG, they also rip (Figure 2.5 (e) and (f)). No significant change in step height was measured on surveying the surface of the CCG with an atomic force microscope tip, implying that either these anions are not strong enough to induce folding or the concentration of the adsorbed vapor was insufficient to induce the type of folding previously seen with bisulfate anions.[30]

2.2.4 Proposed Mechanism of Chloride Anion Doping

Scheme 2.2 illustrates a proposed reaction mechanism where thionyl chloride interacts in a nucleophilic fashion with a carboxylic acid. In the presence of thionyl chloride, a carbonyl oxygen can form a chlorosulfite ester intermediate which readily reacts with nucleophiles, as it is

a good leaving group. Upon formation of the acyl chloride, the displaced chlorosulphite ion is unstable and decomposes into SO_2 and Cl^-. Analogous reactions with CCG and carbon nanotubes where the edges and basal planes are functionalized with hydroxyl and carboxylic functionalities explain how thionyl chloride modification takes place. In the case of pG, the edges are the preferred reaction sites and would likely chlorinate at terminating carbons.[14]

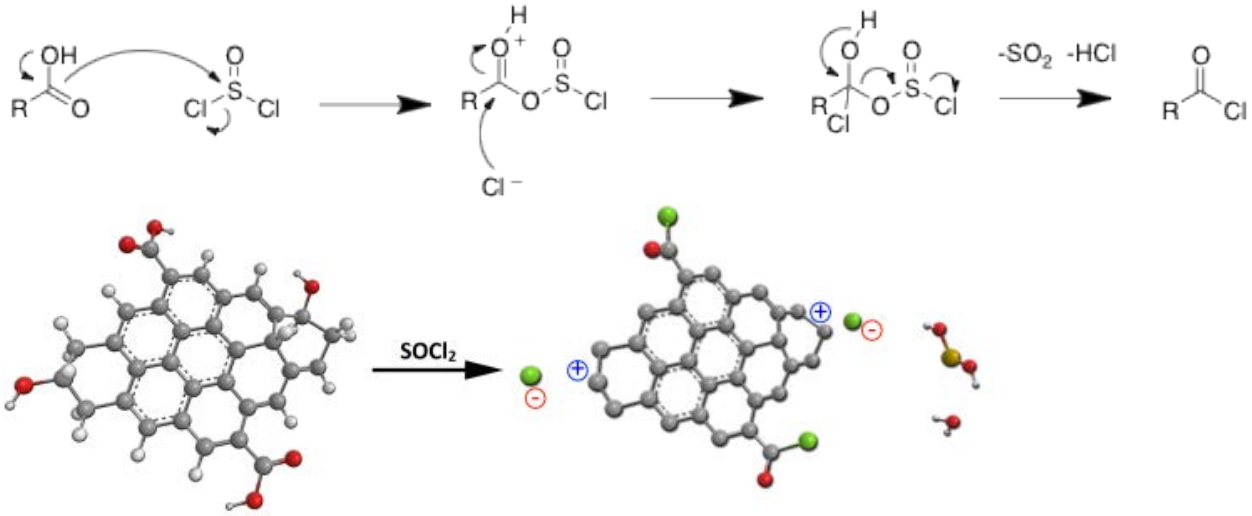

Scheme 2.2 Top: Proposed reaction mechanism in which thionyl chloride undergoes a nucleophilic interaction with a carboxylic acid releasing a chloride, which in turn can functionalize groups present on chemically converted graphenes and oxidized carbon nanotubes. R represents poly-aromatic hydrocarbon species; bottom: visualization of how chloride ions (green circles) are bonded to the carbons at the edge of a graphitic base.

Previous studies on the effects of $SOCl_2$ on CNTs found that the doping mechanism occurs predominantly via bonding of sulfur to the graphitic backbone, with very little C-Cl interactions.[11] This doping mechanism was therefore expected for pristine graphene, but that is

not the case. We find that this scheme applies to CCG and functionalized CNTs films, while for peeled graphene chlorine anions formed in the vapor phase must behave as an electrophile which adsorbs onto the surface followed by halogenation, preferably along the edges.[14]

Maintaining optical transmittance with high conductivity is vital for transparent conductor applications. Nitric acid doping of CNTs and CVD graphene show no significant drop in transmittance while reducing the resistance by about 60%.[10] However, doping with bromine and iodine imparts a significant drop in transmittance after treatment. Doping with those halogens resulted in ~20% loss in transparency with comparable reductions in resistance. As shown in Figure 2.6, optical transmittance measurements of G-CNT films across the UV-visible spectrum show that doping with $SOCl_2$ does not affect the transparency of G-CNT films, but it does enhance the electrical properties. The inset images of a G-CNT substrate before (left) and after doping (right) are shown to visually verify that essentially no change in transparency or film quality has occurred.

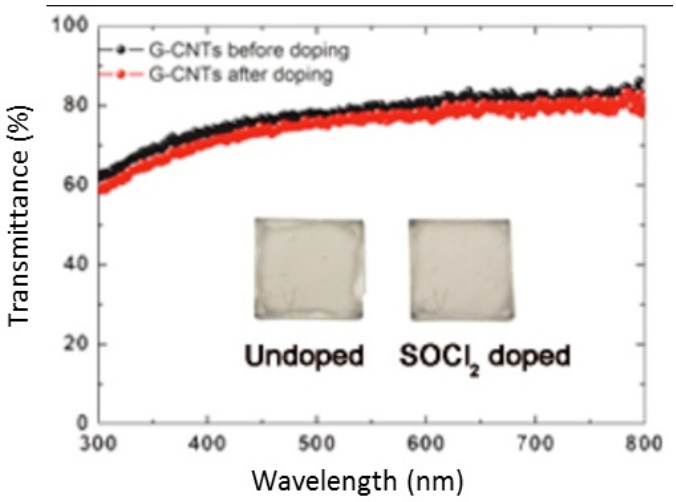

Figure 2.6 Optical transmittance of thionyl chloride treated G-CNT films. Inset: photographs of a G-CNT substrate before (left) and after doping (right) show essentially no change in transparency.

Table 2.1 Optical and electronic properties of G-CNT composite films before and after vapor-phase thionyl chloride treatment.

G-CNT Sample	Optical Transmittance (%)	Sheet Resistance (Ω/square)	Peak Raman Intensity (cm^{-1})
Untreated	82	425	1592
Doped with $SOCl_2$	82	103	1600

To further characterize the electronic properties of the different graphenes, flakes of CCG and pG were placed onto aligned substrates and gold electrodes were patterned using e-beam lithography. The resistance data were collected before and after exposure to $SOCl_2$ and plotted in Figure 2.7 (a). As metals are susceptible to corrosion when exposed directly to $SOCl_2$, *in vacuo*

gate modulation measurements were not collected to observe the shift in the Dirac point from its origin. Nevertheless, appreciable drops in the resistance were recorded, and these are attributed to the adsorbed chlorines along the basal plane of both graphenes, which contribute holes to the conjugated sp^2 network. Additionally, the enhanced properties are believed to arise from C-Cl bonds resulting from newly formed charge-transfer complexes. Figure 2.7 (c) shows a computer generated illustration of a graphene sheet being decorated with chlorine along the edges and basal plane, which increase the number of holes in the conjugated sp^2 network.

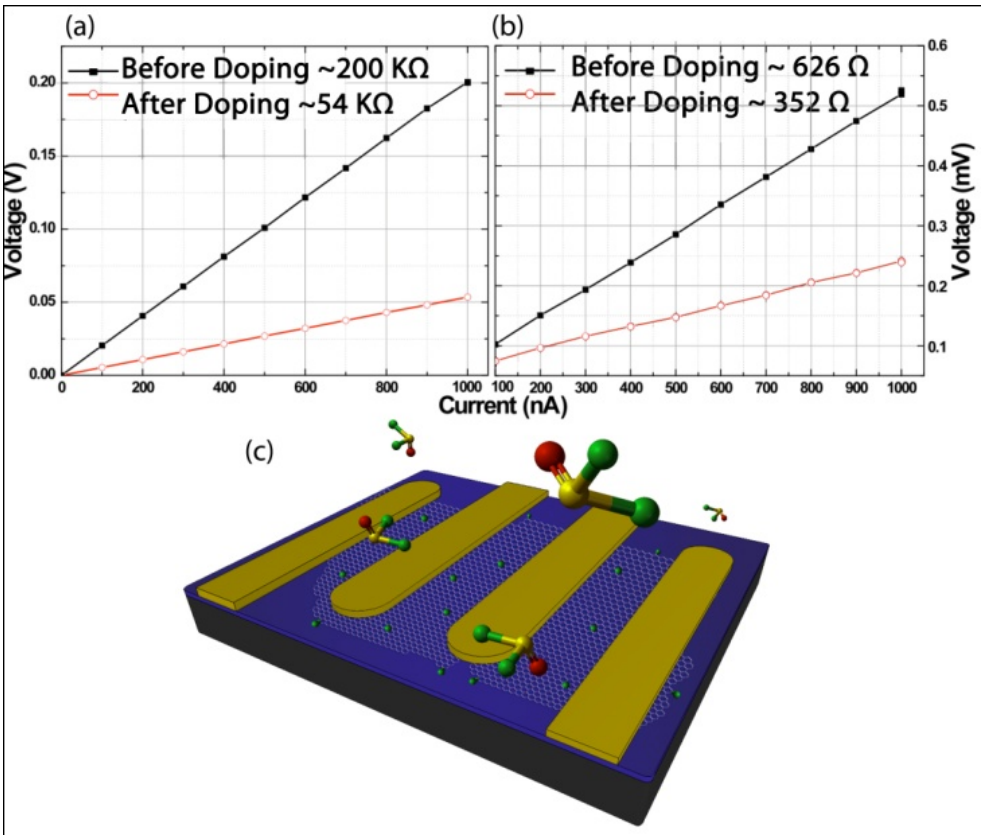

Figure 2.7 Four-point probe measurements taken across single CCG and pG flakes of similar dimensions show a significant decrease in resistance after doping. (a) A single CCG flake shows ~73% decrease in resistance while (b) mechanically exfoliated graphene shows ~44% decrease in sheet resistance. (c) An illustration of a graphene sheet being decorated with chlorine along the edges and basal plane, which increases the number of positive charge carriers in the conjugated sp^2 network.

While the bonding in pristine graphene is solely sp^2 carbon, chemically converted graphene contains sp^3 carbon and residual oxygen moieties which can be readily functionalized for other applications. It was therefore assumed that pristine graphene would be less responsive to chlorination and more susceptible to sulfonation, as seen for other graphitic systems.

However, based on the XPS, EDX and Raman spectra we conclude that vapor-phase $SOCl_2$ decomposes more readily and the resulting chlorine anions can effectively chlorinate oxygen containing graphene through a dehydration mechanism and the edges of peeled graphene through halogenation reactions. Additionally, chlorine anions adsorb onto the basal plane of graphene which also enhance the p-type behavior of the graphitic systems. Electrons residing on graphene are drawn towards the chlorine, which creates holes in the graphitic systems and leads to a substantial decrease in resistance. In addition to enhancing the electrical properties, we observe that the high optical transmittances of the G-CNT films are preserved. SEM and AFM images indicate that this vapor treatment can lead to wrinkles and induce aggregation of sheets and carbon nanotubes when they are in close proximity to each other. These results provide insights into the mechanism of functionalization of graphene and carbon nanotubes with vapor-phase ions and demonstrate a simple method to improve conductivity without sacrificing transparency of graphitic films.

2.3 Selective Registration of Graphitic Materials Using Elastomeric Stamps

2.3.1 Background and Motivation

While films of solution processible graphene can be easily cast and their conductivities modified, the practical use of chemically converted graphene also relies on its scalable deposition. Several attempts to solution process and spatially register nanoscale carbon materials have been reported; however, the dispersions typically utilized in these studies are often unstable, which ultimately adversely affects the fidelity and resolution of graphitic patterns.

In addition, devices constructed using chemically reduced graphene and carbon nanotubes are usually randomly positioned on the substrate, which could limit their scalability. Several patterning approaches to create arrays of devices are possible at the nanoscale, such as lithographic patterning (photolithography, electron beam lithography, or nanoimprint lithography). A desirable patterning method should be simple and cost effective while providing a high throughput and functional coverage over an entire wafer with minimum degradation to the active layer. Soft lithography approaches, such as microcontact printing (μCP),[31,32] fulfill these requirements and have proven useful in the registration of a variety of material and substrate combinations. Conventional μCP involves the transfer of a chemical "ink" using patterned elastomeric stamps, typically comprised of poly(dimethylsiloxane) (PDMS). PDMS stamps are well suited for these applications because they offer several advantages, including ease of fabrication and resilience to most organic solvents.

2.3.2. Procedure for Directed Deposition of Graphitic Materials from Solution

A dry μCP protocol described in the literature was adapted for this experiment.[33,34] This modified μCP technique relies on the transfer of unreacted low molecular weight oligomers from freshly prepared PDMS stamps upon conformal contact with hydrophilic substrates to produce hydrophobic patterns on hydrophilic surfaces.[35,36] A technique to transfer graphitic residues from one substrate to another using a PDMS stamp has shown the successful transfer of a large proportion of graphenes. The PDMS is able to complete the transfer because of remaining oligomers that are transferred along with the graphenes.[37] In this technique, the transfer of the graphene materials is limited to the amount of material that comes in contact with the graphitic

residues. Reversing this process, i.e. directing the location of the residues, is a more scalable method to selectively register solution-processible graphitic materials.

High resolution patterns of graphene, CNTs, or PCBM dispersed in hydrazine were achieved by first activating substrates via an oxygen plasma treatment to create a hydrophilic surface. The substrates were then immediately brought into contact with freshly prepared PDMS stamps with relief patterns molded from photolithographically prepared masters. Upon contact, low molecular weight oligomers are gradually dissociated from the stamp and released onto the silicon substrate. Scheme 2.2 provides a schematic illustration of the printing process used to register the graphitic materials via this modification to conventional μCP. Although the figures show patterns containing circular relief structures, the patterns are not limited to these shapes and it is relatively straightforward to develop more complicated patterns using PDMS stamps with different photolithographic structures.

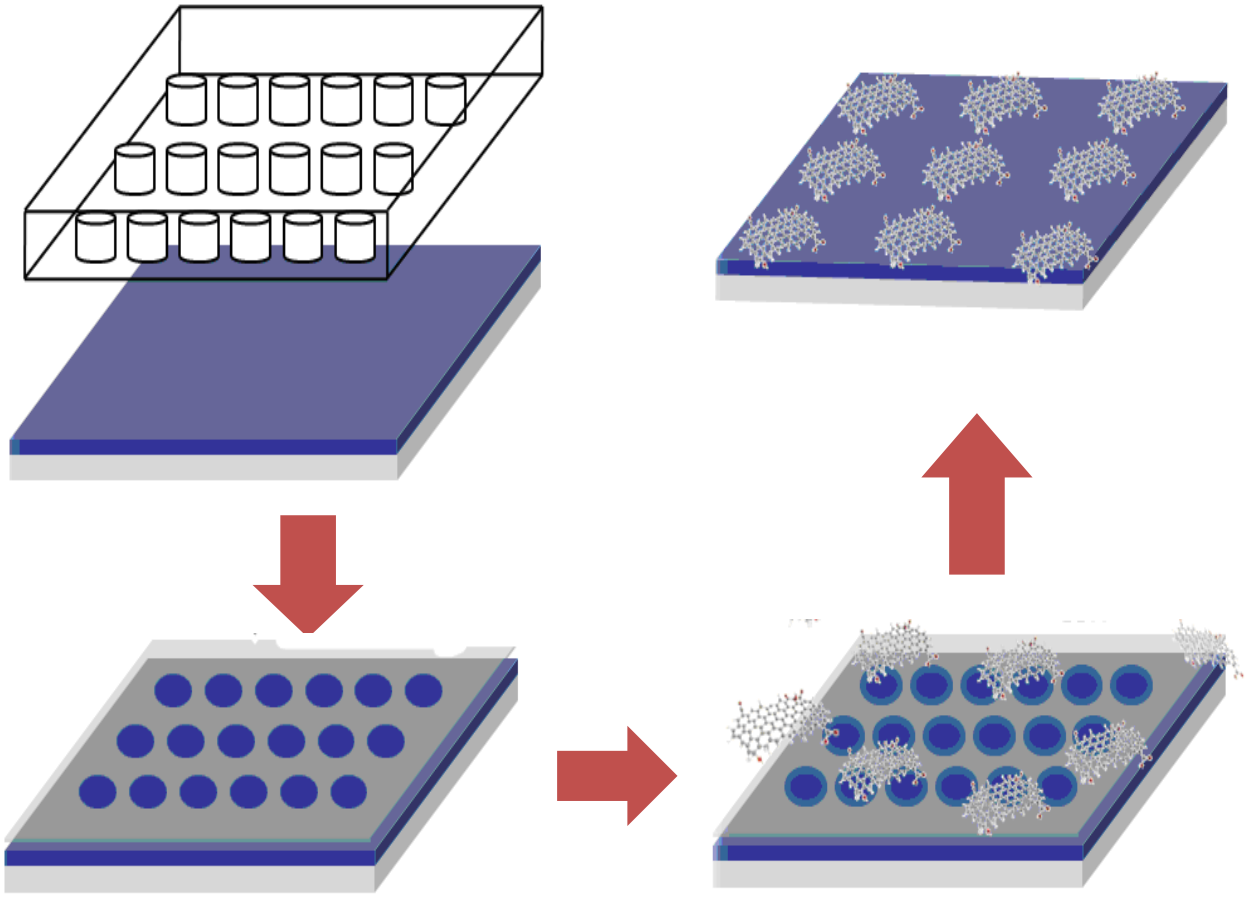

Scheme 2.2 Outline of the procedure utilized to register graphitic materials onto pre-patterned substrates by micro-contact printing. The PDMS is stamped on a clean hydrophilic surface, leaving behind oligomeric residues. The dispersion of graphene or other graphitic materials in hydrazine is deposited. After removal of the solvent and PDMS residues the materials remain in the defined pattern.

Hydrophilic surfaces are most favorable for effective deposition. For this work, silicon wafers were prepared by standard cleaning procedures, followed by oxygen plasma treatment for 3 minutes. The PDMS stamps were then pressed on the substrate with moderate pressure to

define the regions in which the materials will be located. Then, the difference in surface energies between the hydrophobic residues and the hydrophilic dispersions of graphene and CNTs in hydrazine is used to direct them into the confined areas. The graphitic materials are retained in the hydrophilic regions of the patterned substrate by selective wetting. The low molecular weight silicone oligomers transferred to the substrate have an extremely low surface energy (19.8 mJ/m^2),[38] so they can be thought of as patterned resists to the nonspecific adsorption of the graphitic materials. This method represents a simple and highly reproducible approach for patterning graphitic semiconductors from solution. For electronics applications, patterning these arrays will reduce if not eliminate parasitic current paths (crosstalk) between neighboring devices. The PDMS membranes are reusable and not limited by the shapes illustrated here.

PDMS is easy to pattern and, manipulate, and inert to many chemical and physical processes, therefore it can be employed as a mask for the deposition of graphene, carbon nanotubes and fullerenes which are dispersed in anhydrous hydrazine. As anhydrous hydrazine is a strong base that reacts violently with alkali metals, acids and other oxidants, it inhibits utilizing photoresist and metal shadow masks to pattern graphene. PDMS is a robust material that can be used for a variety of applications such microfluidics, biomedical packaging and as a method for patterning metals.[31,39]

The array patterns are fabricated through photolithographic processes and PDMS elastomeric stamps are molded to these patterns. After the membranes are prepared, a clean razor blade is used to cut out the desired features and fine tip tweezers to lift-off the membrane from the master. As the membranes are placed on to the substrate they conform to the surface and provide intimate contact for high-resolution patterning. In instances where the membrane is very

thin, isopropyl alcohol is employed to prevent the membrane from adhering to itself. The membrane-covered substrates are then briefly treated with oxygen plasma to create a hydrophilic surface before the graphitic dispersions are cast. The elastomeric membrane acts as a physical barrier while the apertures in the membrane expose bare regions of a substrate into which depositions occur. The PDMS membrane is removed to expose a defined array of patterned graphene. The coated substrates are thermally annealed to drive off residual hydrazine on the surface. The resulting arrays are identified using Raman spectroscopy to verify the presence of each material's unique spectra.

Controlled deposition and spatial registration of graphene, CNTs, and PCBM was achieved subsequent to stamping by spin coating hydrazine dispersed graphitic suspensions on to the PDMS-inked substrates followed by a low temperature annealing process to remove excess solvent. Typically, 1mg/ml of graphene, 10 mg/ml of CNTs and 17mg/ml of C_{60}-PCBM hydrazinium suspensions were used. The morphology and surface coverage within the patterned regions are essentially determined by the concentration and composition of hydrazinium solution and spin parameters. Specifically, higher concentration and lower spin speed deliver thicker patterned features comprised of multiple layers of graphene sheets or dense networks of CNTs, and vice versa.

2.3.3 Characterization of Transferred Materials

Initial characterization of the graphitic patterns was carried out using scanning electron microscopy (SEM). These images primarily provide an overview of the surface coverage relative to the spin conditions used in the patterning process. SEM images along with optical micrographs clearly indicate well defined circular regions of registered graphitic materials,

closely resembling the PDMS patterns. In most cases of graphene registration, 85% of circular patterns were filled with one to three single layer graphene sheets, but the constraint of the patterns causes multiple sheets to overlap or fold in some regions. Also, the slight agglomeration may be due to the centrifugal force of the spin-coating process. As a result, multilayer sheets possessing higher molecular mass tend to distribute away from the center of the patterned features. Arrays of CNTs were patterned in the same manner. By varying the concentration and composition, we are capable of delivering different morphologies that may be useful for a variety of sensor or nanoelectronic applications such as circuit design.

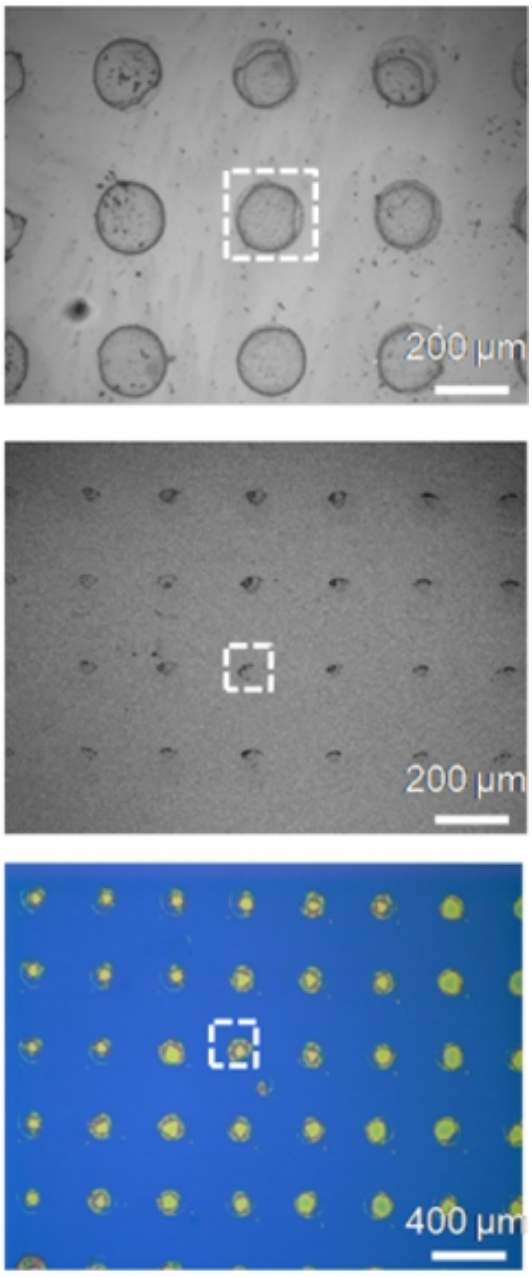

Figure 2.8 Images of deposited graphitic materials in arrays after selective registration using a poly (dimethylsiloxane) stamp: (a) a scanning electron microscope image of chemically converted graphene; (b) scanning microscope image of single-walled carbon nanotubes; (c) optical micrograph of patterned arrays of the fullerene analog PCBM.

Raman spectra of CCG showed typical D and G band ratio due to the inherent disorder from post reduction. The Raman spectra of CNTs has two peaks at the G band resulting from the semiconducting and the metallic conformations. We resolved sufficient PCBM peaks, hidden beneath the strong fluorescing band in addition to the characteristic peak at 1450 cm^{-1}.[40] Scanning electron microscope (SEM) and atomic force microscope (AFM) images of individual patterns are acquired to show nanoscale topological features.

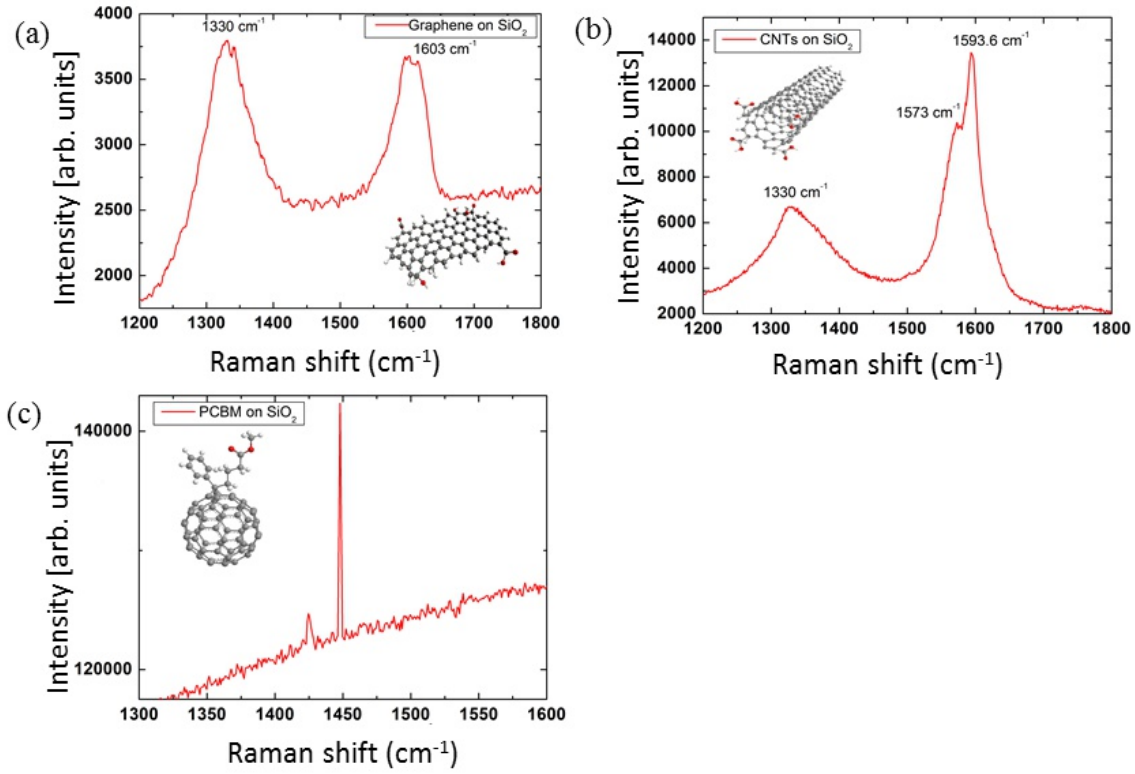

Figure 2.9 Representative Raman spectra of residues selectively transferred to a substrate: (a) chemically converted graphene; (b) carbon nanotubes; (c) PCBM. The peaks are characteristic of the materials deposited.

Infrared spectroscopy (IR) and XPS were employed to confirm the transfer of oligomeric residues to the silicon substrates during stamping as well as their stability under the hydrazine solution processing conditions. Figure 2.10 (a) shows the IR spectra of stamped silicon substrates with characteristic peaks identified as Si-O stretch (1050 cm^{-1}), CH_3 symmetric bending (1260 cm^{-1}) and C-H methyl stretching (3000 cm^{-1}). XPS performed on the oligomers transferred onto silver substrates conclusively shows that Si peak intensity and position remain the same before and after exposure to anhydrous hydrazine (Figure 2.1 (b)). These data collectively suggest that the chemical inertness of PDMS to hydrazine makes it suitable for these processing conditions. In the presence of epoxides, which are present in CCG, hydrazine forms complexes which will later form aminoaziridines that ultimately lead to the thermal elimination of diimides.[41] The backbone of PDMS, however, does not contain epoxides, and is comprised of silicone and methyl moieties which are resistant to hydrazine. The transferred PDMS layer is resistant to rinsing with common several organic solvents including chloroform, toluene, dichloromethane, isopropyl alcohol and tetrahydrofuran. It has also been shown that it is possible to remove the PDMS residue upon thermal annealing under vacuum.[37]

(a)

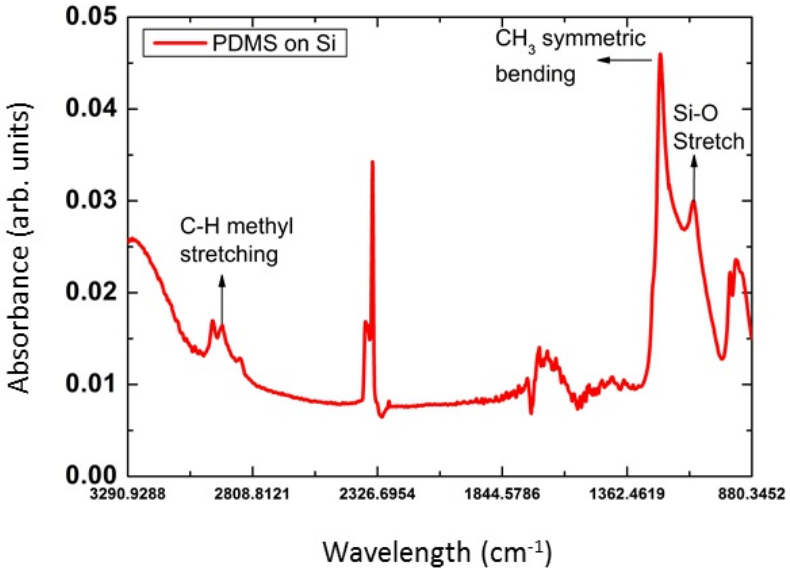

(b)

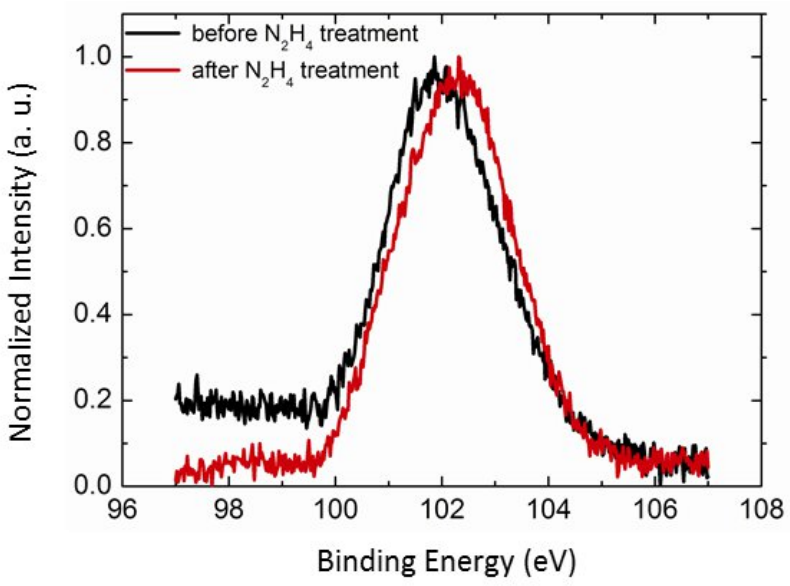

Figure 2.10 (a) Infrared spectrum of the PDMS stamp on a Si surface; (b) X-ray photoelectron spectra of PDMS residue before and after solution-casting of a graphene dispersion in hydrazine, showing the inertness of PDMS to the solvent.

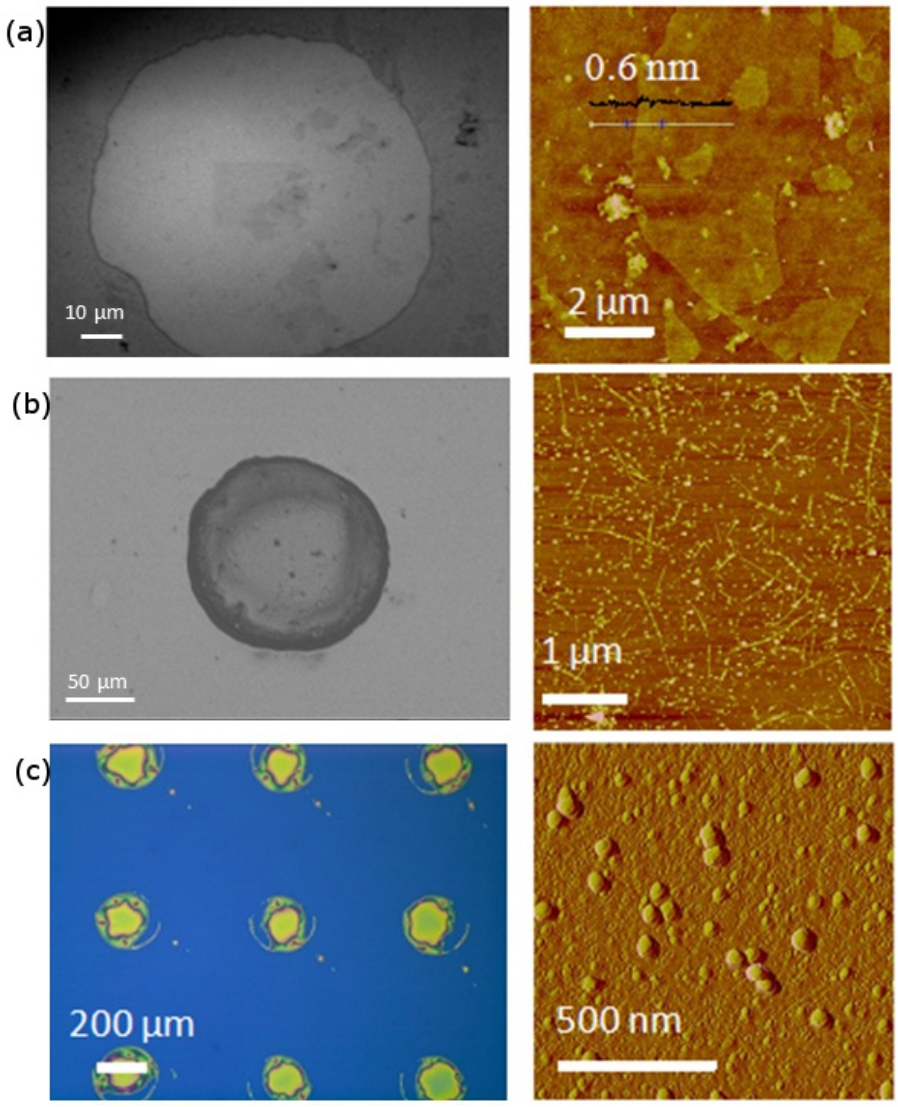

Figure 2.11 Scanning electron micrographs (SEM) of graphene deposited from solution in a defined region using the PDMS stamping method with a tapping mode atomic force microscope (AFM) image of a region showing single and few layer graphene sheets; (b) SEM of single-walled carbon nanotubes deposited from solution in a defined region using the PDMS stamping method with an AFM image of a region showing dispersion of the tubes; (c) Optical micrograph of an array of PCBM deposited from a solution in hydrazine in a defined region using the PDMS

stamping method with an AFM image of a region showing the topology and clustering of the PCBM.

The SEM technique to provide insight into surface morphology and coverage was supplemented by atomic force microscopy (AFM) to render the height profiles and domains of the graphitic materials registered to the patterned features. Figure 2.11 shows representative tapping mode AFM images of (1) single layer graphene sheets, (2) individual single carbon nanotubes along with (3) domains of C_{60}-PCBM, respectively. Step heights of 0.6 nm were obtained between the SiO2 substrate and chemically converted graphene sheets were established for a given cross-section, as shown in Figure 2.11 (a). The 3 Å discrepancy in step height compared to the theoretical value 3.4 Å for single layer carbon is attributed to the presence of physically absorbed water, oxygen molecules, or residue from oxygen functionalities under ambient conditions.[42] In addition, the AFM images provide insight into the topography of individual CNTs inside the circular patterns. Within these regions, we observe randomly distributed networks of CNTs with diameters of several nm that have percolating network structures are capable of acting as conducting channels. Unlike the surfactant-stabilized CNTs, direct assembly of individual CNTs with different density is simply achieved by a series of dilution and centrifugation. The tapping mode images of C_{60}-PCBM reveal uniform film morphology with nanometer size domains, which can be attributed to slight aggregation or molecular packing. The ability to control the shape and density of deposited graphitic materials allows us to further engineer and design integrated circuits. Most importantly, this solution based registration method provides access to desirable architectures for a variety of applications.

2.4 Conclusion and Outlook

The solution-processing of chemically converted graphene via hydrazine dispersion represents a straightforward, large scale method to deposit transparent conducting materials in large areas. The work presented in this chapter represents the versatility of this material to modification not only structurally by doping, but also in the controllable and selective deposition. Anion doping of the graphitic structure was achieved through charge transfer to the more electronegative atom, resulting in a large decrease in electrical resistance.

Solution processed graphitic materials have been registered into desired locations and patterns using a simple route based on micro-contact printing. The approach presented here is simple, high throughput, and functional over large areas. Raman, XPS, and IR spectra were used to confirm the integrity of electronic structures and assessed the surface chemistry of the patterned graphitic materials. In addition, this versatile solution based method provides a clear pathway for incorporating 0D, 1D, and 2D graphitic materials into entirely new 3D architectures that may hold great promise for future transparent electrode, hydrogen storage, and lithium battery applications. Proof-of-concept arrays of electrodes comprised of graphene and CNTs as well as nanocomposites of graphene, CNTs, and C_{60}-PCBM as absorbers in polymer solar cells are also presented. With future work, the strategies outlined here are capable of delivering entirely carbon based flexible electronic platforms that represent the building blocks for future nanoelectronic and energy storage materials.

References

(1) Hummers, W. S.; Offeman, R. E. *Journal of the American Chemical Society* **1958**, *80*, 1339.

(2) Kovtyukhova, N. I.; Ollivier, P. J.; Martin, B. R.; Mallouk, T. E.; Chizhik, S. A.; Buzaneva, E. V.; Gorchinskiy, A. D. *Chemistry of Materials* **1999**, *11*, 771.

(3) Tung, V. C.; Allen, M. J.; Yang, Y.; Kaner, R. B. *Nat Nano* **2009**, *4*, 25.

(4) Cai, D.; Song, M.; Xu, C. *Advanced Materials* **2008**, *20*, 1706.

(5) Hu, H.; Zhao, B.; Itkis, M. E.; Haddon, R. C. *The Journal of Physical Chemistry B* **2003**, *107*, 13838.

(6) Tung, V. C.; Chen, L.-M.; Allen, M. J.; Wassei, J. K.; Nelson, K.; Kaner, R. B.; Yang, Y. *Nano Letters* **2009**, *9*, 1949.

(7) Hummelen, J. C.; Knight, B. W.; LePeq, F.; Wudl, F.; Yao, J.; Wilkins, C. L. *The Journal of Organic Chemistry* **1995**, *60*, 532.

(8) Stephan, O.; Ajayan, P. M.; Colliex, C.; Redlich, P.; Lambert, J. M.; Bernier, P.; Lefin, P. *Science* **1994**, *266*, 1683.

(9) Maldonado, S.; Morin, S.; Stevenson, K. J. *Carbon* **2006**, *44*, 1429.

(10) Bae, S.; Kim, H.; Lee, Y.; Xu, X.; Park, J.-S.; Zheng, Y.; Balakrishnan, J.; Lei, T.; Ri Kim, H.; Song, Y. I.; Kim, Y.-J.; Kim, K. S.; Ozyilmaz, B.; Ahn, J.-H.; Hong, B. H.; Iijima, S. *Nat Nano* **2010**, *5*, 574.

(11) Jung, N.; Kim, N.; Jockusch, S.; Turro, N. J.; Kim, P.; Brus, L. *Nano Letters* **2009**, *9*, 4133.

(12) Ki Kang, K.; Alfonso, R.; Yumeng, S.; Hyesung, P.; Lain-Jong, L.; Young Hee, L.; Jing, K. *Nanotechnology* **2010**, *21*, 285205.

(13) Blake, P.; Brimicombe, P. D.; Nair, R. R.; Booth, T. J.; Jiang, D.; Schedin, F.; Ponomarenko, L. A.; Morozov, S. V.; Gleeson, H. F.; Hill, E. W.; Geim, A. K.; Novoselov, K. S. *Nano Letters* **2008**, *8*, 1704.

(14) Wang, X.; Li, X.; Zhang, L.; Yoon, Y.; Weber, P. K.; Wang, H.; Guo, J.; Dai, H. *Science* **2009**, *324*, 768.

(15) Crowther, A. C.; Ghassaei, A.; Jung, N.; Brus, L. E. *ACS Nano* **2012**, *6*, 1865.

(16) Schedin, F.; Geim, A. K.; Morozov, S. V.; Hill, E. W.; Blake, P.; Katsnelson, M. I.; Novoselov, K. S. *Nat Mater* **2007**, *6*, 652.

(17) Dua, V.; Surwade, S. P.; Ammu, S.; Agnihotra, S. R.; Jain, S.; Roberts, K. E.; Park, S.; Ruoff, R. S.; Manohar, S. K. *Angewandte Chemie International Edition* **2010**, *49*, 2154.

(18) do Nascimento, G. M.; Hou, T.; Kim, Y. A.; Muramatsu, H.; Hayashi, T.; Endo, M.; Akuzawa, N.; Dresselhaus, M. S. *The Journal of Physical Chemistry C* **2009**, *113*, 3934.

(19) Zhou, W.; Xie, S.; Sun, L.; Tang, D.; Li, Y.; Liu, Z.; Ci, L.; Zou, X.; Wang, G.; Tan, P.; Dong, X.; Xu, B.; Zhao, B. *Applied Physics Letters* **2002**, *80*, 2553.

(20) Cambedouzou, J.; Sauvajol, J. L.; Rahmani, A.; Flahaut, E.; Peigney, A.; Laurent, C. *Physical Review B* **2004**, *69*, 235422.

(21) Limonov, M. F.; Kitaev, Y. E.; Chugreev, A. V.; Smirnov, V. P.; Grushko, Y. S.; Kolesnik, S. G.; Kolesnik, S. N. *Physical Review B* **1998**, *57*, 7586.

(22) Brinkmann, M.; Videva, V. S.; Bieber, A.; André, J. J.; Turek, P.; Zuppiroli, L.; Bugnon, P.; Schaer, M.; Nuesch, F.; Humphry-Baker, R. *The Journal of Physical Chemistry A* **2004**, *108*, 8170.

(23) Cazayous, M.; Sacuto, A.; Horowitz, G.; Lang, P.; Zimmers, A.; Lobo, R. P. S. M. *Physical Review B* **2004**, *70*, 081309.

(24) Hall, J. W.; Arbuckle, G. A. *Macromolecules* **1996**, *29*, 546.

(25) Wang, D.; Tsukamoto, J.; Takahashi, A.; Muraki, N.; Katagiri, G. *Synthetic Metals* **1994**, *65*, 117.

(26) Geng, H.-Z.; Kim, K. K.; So, K. P.; Lee, Y. S.; Chang, Y.; Lee, Y. H. *Journal of the American Chemical Society* **2007**, *129*, 7758.

(27) Hamon, M. A.; Chen, J.; Hu, H.; Chen, Y.; Itkis, M. E.; Rao, A. M.; Eklund, P. C.; Haddon, R. C. *Advanced Materials* **1999**, *11*, 834.

(28) Dettlaff-Weglikowska, U.; Skákalová, V.; Graupner, R.; Jhang, S. H.; Kim, B. H.; Lee, H. J.; Ley, L.; Park, Y. W.; Berber, S.; Tománek, D.; Roth, S. *Journal of the American Chemical Society* **2005**, *127*, 5125.

(29) Rao, A. M.; Eklund, P. C.; Bandow, S.; Thess, A.; Smalley, R. E. *Nature* **1997**, *388*, 257.

(30) Allen, M. J.; Wang, M.; Jannuzzi, S. A. V.; Yang, Y.; Wang, K. L.; Kaner, R. B. *Chemical Communications* **2009**, 6285.

(31) Xia, Y.; Whitesides, G. M. *Annual Review of Materials Science* **1998**, *28*, 153.

(32) Gates, B. D.; Xu, Q.; Stewart, M.; Ryan, D.; Willson, C. G.; Whitesides, G. M. *Chemical Reviews* **2005**, *105*, 1171.

(33) Briseno, A. L.; Mannsfeld, S. C. B.; Ling, M. M.; Liu, S.; Tseng, R. J.; Reese, C.; Roberts, M. E.; Yang, Y.; Wudl, F.; Bao, Z. *Nature* **2006**, *444*, 913.

(34) Briseno, A. L.; Roberts, M.; Ling, M.-M.; Moon, H.; Nemanick, E. J.; Bao, Z. *Journal of the American Chemical Society* **2006**, *128*, 3880.

(35) Glasmästar, K.; Gold, J.; Andersson, A.-S.; Sutherland, D. S.; Kasemo, B. *Langmuir* **2003**, *19*, 5475.

(36) Li, X.-M.; Péter, M.; Huskens, J.; Reinhoudt, D. N. *Nano Letters* **2003**, *3*, 1449.

(37) Allen, M. J.; Tung, V. C.; Gomez, L.; Xu, Z.; Chen, L.-M.; Nelson, K. S.; Zhou, C.; Kaner, R. B.; Yang, Y. *Advanced Materials* **2009**, *21*, 2098.

(38) Krevelen, D. W. *Properties of polymers* **1990**.

(39) Herold, K. E.; Rasooly, A. *Lab on a Chip Technology: Fabrication and microfluidics*; Horizon Scientific Press, 2009; Vol. 1.

(40) Klimov, E.; Li, W.; Yang, X.; Hoffmann, G. G.; Loos, J. *Macromolecules* **2006**, *39*, 4493.

(41) Stankovich, S.; Dikin, D. A.; Piner, R. D.; Kohlhaas, K. A.; Kleinhammes, A.; Jia, Y.; Wu, Y.; Nguyen, S. T.; Ruoff, R. S. *Carbon* **2007**, *45*, 1558.

(42) Park, S.; Ruoff, R. S. *Nat Nano* **2009**, *4*, 217.

Chapter 3: Synthesis of Large Area Graphene through Low Pressure Chemical Vapor Deposition on Copper

3.1 Chemical Vapor Deposition of Graphene on Copper

The discovery of many exciting electronic properties of graphene occurred with mechanically exfoliated graphene which is of pristine quality. Therefore, interest in graphene for electronic applications has caused a demand for large quantities of the material of comparable quality to that of pristine graphene. Epitaxial growth methods on SiC have been effective but there is always interest in a lower cost process, and the electronic mobility of graphene grown from SiC is lower than that of exfoliated graphene.[1,2] Chemical methods of graphene production have so far been encouraging in producing large quantities, and have in fact opened up a new avenue of research for synthetic and physical chemists. However, for electronic applications, especially over a large area, continuity and a low structural defect concentration is of utmost importance.

It has been known for over 40 years that small amounts of graphitic materials can form upon decomposition of hydrocarbons on transition metal surfaces,[3,4] and was widely observed during heterogeneous catalysis. The interest in synthesizing large areas of graphene rekindled interest in these methods, and since then, significant effort has been undertaken to understand the nucleation, growth, and morphology of graphene on these substrates. So far, graphene growth has been reported on several transition metals including Ru,[5] Ir,[6,7] Pt, Pd,[8] Ni and Co.[9] This process occurs generally from the thermal decomposition of hydrocarbons on the metal surface, or surface segregation of carbon upon cooling from a metastable carbon-metal solid solution.[10,11] Therefore, it is dictated by the solubility limit of carbon in the metal. Work is progressing on

determining the factors influencing the growth mechanisms for the material toward being able to tailor its properties, for example crystal structure, grain size, and doping.[12-16]

An issue with graphene epitaxially grown on a metal surface turns out to be that the lattice mismatch between the metal surface and graphene typically forms a pseudomorphic interface and generally displays a moiré pattern as well as lattice strain. This can be mitigated by growth on single crystal metal substrates, although there are still misaligned domains and grain boundaries.[4,5] Using single crystal substrates under high vacuum conditions will significantly limit the use of graphene. Fortunately, polycrystalline films offer a more economical alternative that is still capable of large domains without noticeable electrical performance difference within individual domains,[17] although it was found that they could hinder its mechanical strength.[18]

Although most of the aforementioned transition metals facilitate successful growth of high quality graphene, their costs can be prohibitive, especially since these metals cannot be re-used. However, recent results of growth on relatively inexpensive polycrystalline substrates of Ni and Cu are encouraging, and therefore the growths on these metals are worth optimizing. For Ni, the process involves the dissolution of carbon atoms into the Ni at high temperature, after which they precipitate on the surface of the metal and form the graphene layers upon cooling. The thickness and crystal ordering can be controlled by the cooling rate and hydrocarbon gas concentration. A limitation to growth on Ni is that single and few layered graphene is obtained over regions of a few to tens of microns,[19] and is yet to be homogeneous over an entire substrate.[20] The number of graphene layers formed also depends highly on the carbon solubility of the substrate. Therefore, low carbon solubility in some of these metals, such as Cu and Pt, enables complete monolayer coverage.[21]

The first reports of CVD synthesis of graphene on Cu occurred in 2009,[9] and the discovery of this relatively simple method has opened a new avenue into the possibility of synthesizing large area graphene films for electronic applications. In particular, the majority of the graphene deposited on polycrystalline Cu was found to be uniformly single layered[9], of high quality, and achievable on thin copper foils which are inexpensive and readily available. In fact, copper has been shown to catalyze the growth of several other carbon allotropes such as graphite, diamond,[22,23] carbon nanotubes,[24,25] as well as graphene. The growth of graphite on copper was unintentionally achieved in 1991 in experiments designed to catalyze the growth of diamond by CVD. In these initial experiments, single and multilayered graphene were produced on (100), (110), and (111) copper surfaces via carbon implantation at elevated temperatures and subsequent out-diffusion through a carbon dissolution-precipitation mechanism.[22]

The properties of copper make it well suited as a catalyst for the formation of graphitic materials on its surface. The phase diagram shows that carbon has a very low solubility in copper, and does not form any carbide phases.[26] In addition, the stable electronic configuration of copper, $\{[Ar]3d^{10}4s^{1}\}$, contains a filled 3d electron shell,[26] and is the most stable configuration (along with the half filling $3d^{5}$) because the electron distribution is symmetrical, which minimizes reciprocal repulsions. As a result, Cu can form only soft bonds with carbon via charge transfer from the p electrons in the sp^{2} hybridized carbon to the empty 4s states of copper.[27] The controllable formation of single layers of graphene combined with its ease of deposition, low cost and relative abundance makes copper a very widely used catalyst for graphene growth, especially on a large scale.

Growth pressure is also a factor. Under atmospheric pressure (APCVD) conditions, the graphene growth is mainly limited by mass transport through the boundary layer, whereas under low pressure (LPCVD), i.e. at pressures between 0.1 to 1 torr, it was found that the surface reaction is the rate limiting step.[21] Therefore, the predominately uniform monolayer graphene grown by the LPCVD method is explained by the self-limiting nature of the growth process. However, controllable growth of multiple layers on Cu has shown to be possible through the introduction of a second growth process on an already synthesized monolayer of graphene.[28] Another method of controllably growing monolayer or multilayer graphene films is to use a Cu-Ni alloy, which can be thought of as combining the advantages of using both low and high solubility metals and enabling control of the thickness and quality of the graphene through the growth temperature and cooling rate.[29] Growth using longer chain hydrocarbon sources has also shown some bilayer characteristics.[18] Lowered growth temperatures have also been achieved with various methods. A laser-induced CVD process, which takes advantage of intense localized heating, can decompose the precursor gas at lower temperatures and also write graphene patterns directly on the surface at three times the growth rate of conventional CVD.[30] Growth has been successful at temperatures as low as 300°C using liquid precursors such as ethanol, propanol and benzene.[31,32]

A constantly improving understanding of the mechanisms of graphene growth via CVD has gone hand in hand with the development of the technique. It has been learned that growth parameters such as temperature and pressure influence the nucleation rates and growth phases. The shape of the domains formed during nucleation and growth dictates the final morphology, and varies under different conditions between flower-like structures (as shown in Figure 3.1 and

Reference 33), hexagons that have no particular epitaxy with the Cu substrate, or stochastic patchworks that join at tilt boundaries.[34]

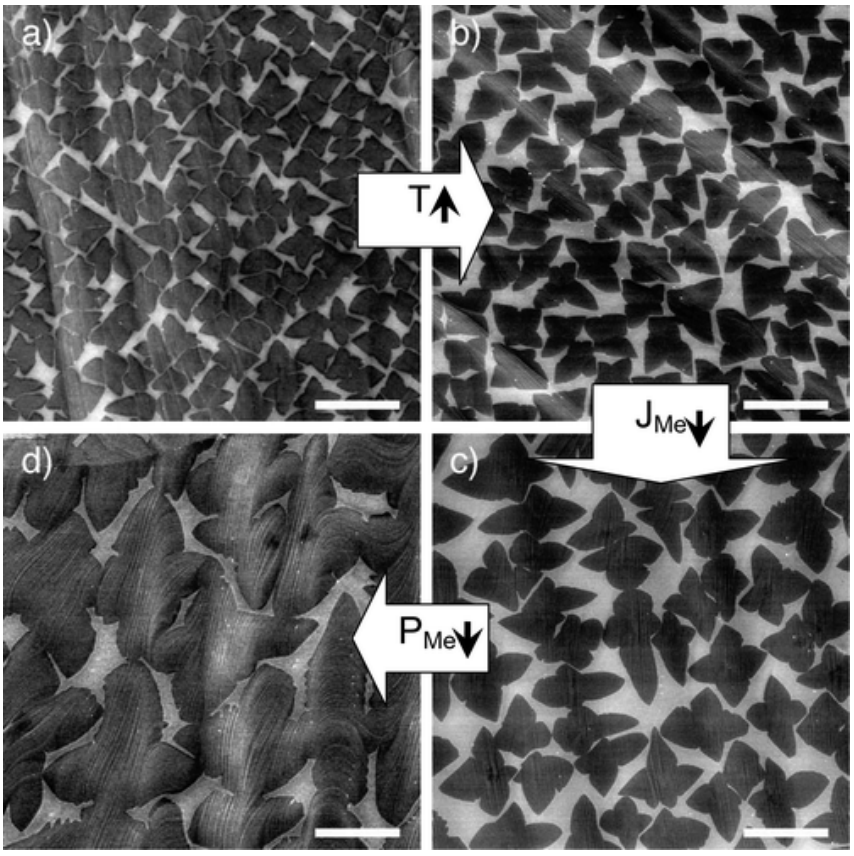

Figure 3.1 Scanning electron micrographs depicting partially grown graphene under different growth conditions: T(°C)/J_{Md}(sccm)/P_{Me}(mTorr): (a) 985/35/460, (b) 1035/35/460, (c) 1035/7/460, (d) 1035/7/160. Scale bars are 10 μm. Reprinted with permission from Reference 33. Copyright 2010 American Chemical Society.

3.2 Methods – Chemical Vapor Deposition of Graphene on Copper

Growth conditions vary among systems and are generally optimized for each CVD setup. There are three stages of the growth process on copper. Initially, the oxide on the Cu foil is

reduced by annealing in a hydrogen atmosphere, which also increases its grain size and clears surface defects. Islands of graphene nucleate according to the crystallographic orientation of the underlying Cu. These graphene domains then increase in size, and with adequate growth time, they coalesce into a continuous graphene film. Graphene growth on copper has been achieved using a variety of carbon sources, including gases, vapors and solid feedstock of varying purities.[12,35] For a methane source on a copper substrate, the graphene growth process is started after the CVD system is pumped down and heated to around 1000°C.[27]

The purchased copper foils contain dirt and oxidation residues from ambient conditions that must be eliminated to ensure a consistent and high quality grown graphene. Therefore, hydrogen gas is flowed through the tube from the start to the end of the process, which comprises of temperature ramp, growth at high temperature, and furnace cooldown. In fact, the success in graphene growth even from amorphous carbon feedstock underscores the importance of a consistent, adequate hydrogen flow in the furnace. For safety reasons, forming gas comprised of 95% Ar and 5% H_2 is used. The copper foils were loaded into a one-inch diameter quartz furnace tube. The system was pumped down to below 5.0×10^{-2} torr at room temperature before starting forming gas flow.

The furnace temperature was ramped to an intermediate temperature of 850°C at a rate of 25°C per minute. One of the important effects of annealing the copper at this temperature is the reduction of copper oxides.[36] The anneal period was varied between 20 minutes and 14 hours to determine if prolonging this step improves the quality of the graphene through an increase in the grain size of the copper foil.[9] The grain sizes appeared large when viewed with optical microscopy. After a 12 hour anneal, the average diameter of a grain was over 100 μm, as shown

in Figure 3.3. However, Raman spectra on the final transferred and cleaned graphene sheets showed no marked pattern between the anneal time and the graphene quality. After the annealing step, the furnace is ramped to the final growth temperature of 1000°C at a rate of 10°C per minute and allowed to stabilize before the methane gas flow is started.

Although the reduction of copper oxide takes place prior to growth, maintaining a high H_2 flow rate in the system during the growth process at a high flow rate improves the quality of grown graphene.[34] During the temperature ramp, the pressure of forming gas in the system was kept between 7 and 10 torr. The forming gas flow was increased to a chamber pressure of ~25 torr before methane gas flow was started. For all samples, the methane gas flow rate was kept constant between 15 and 16 scc/m during the whole growth period for a total chamber pressure of 35 to 40 torr. The growth time for this system was varied between 10 and 17 minutes to determine the minimum growth time required for a continuous layer of graphene on the copper surface. Following the growth time, the furnace was allowed to rapidly cool to room temperature. The methane gas flow was shut off around 850°C, and forming gas flow was reduced to a chamber pressure of ~8 torr and maintained during the whole cooldown step. Graphene growth is visible on the copper foil, as shown in Figure 3.2. The luster of the copper foil appears slightly blurred by the graphene.

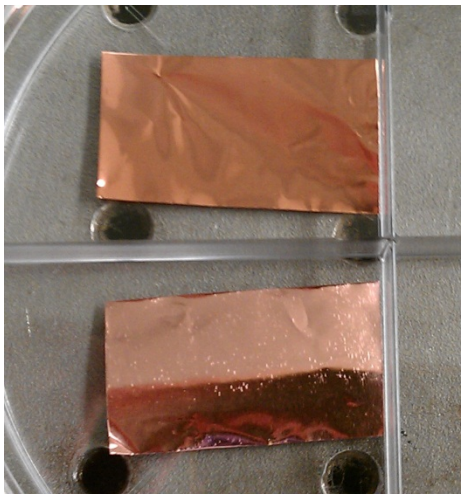

Figure 3.2 Appearance of copper foils before (above) and after (below) the graphene CVD growth process. The graphene on the surface dulls the color and luster of the copper foil.

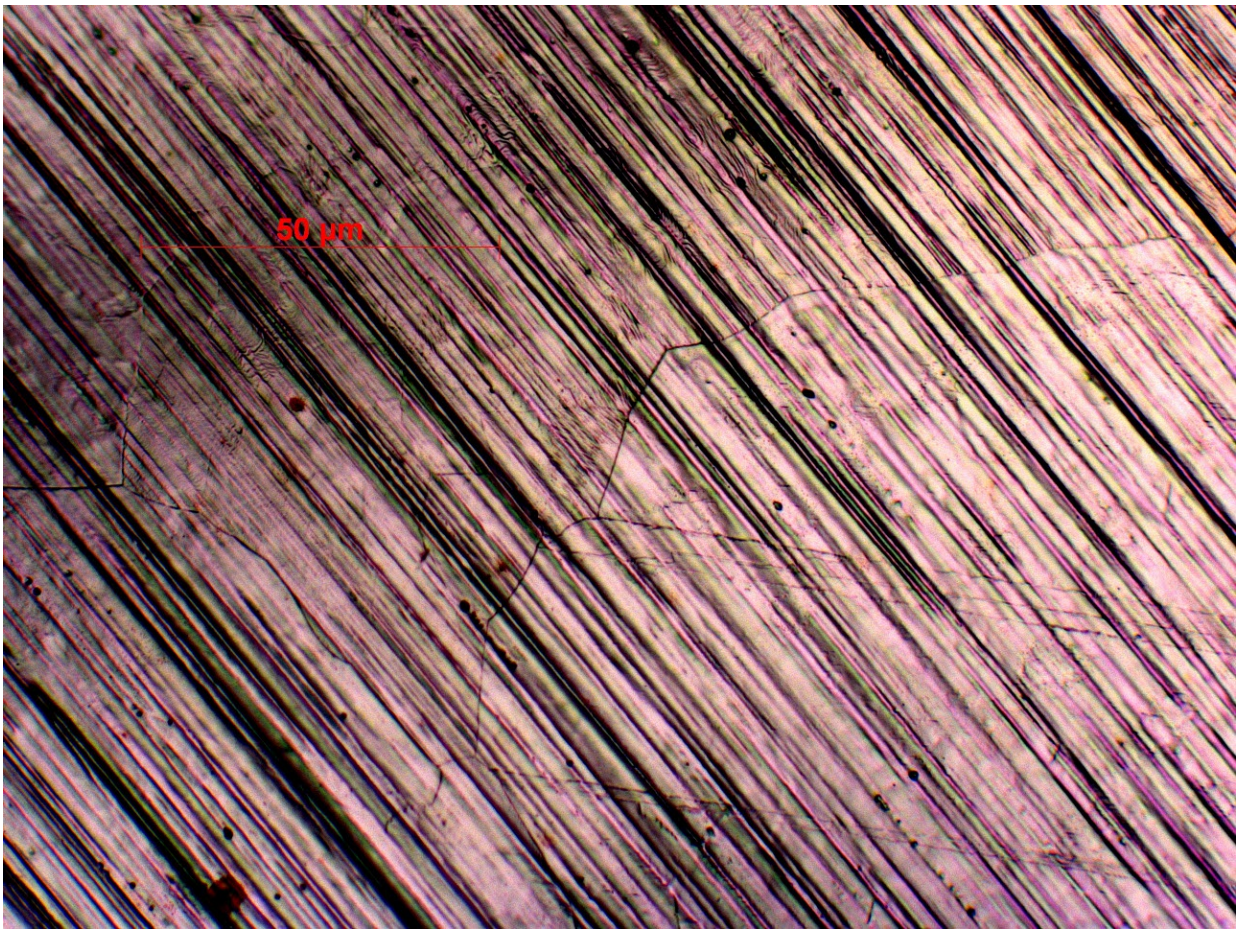

Figure 3.3 Optical micrograph of graphene grown on copper via CVD, after a 12 hour anneal at 850°C at a pressure of 8 torr, under Ar/H2 (flow rate 500 scc/m). The foil polishing lines and grain boundaries of the copper foil are clearly visible. The graphene grains terminate at these boundaries.

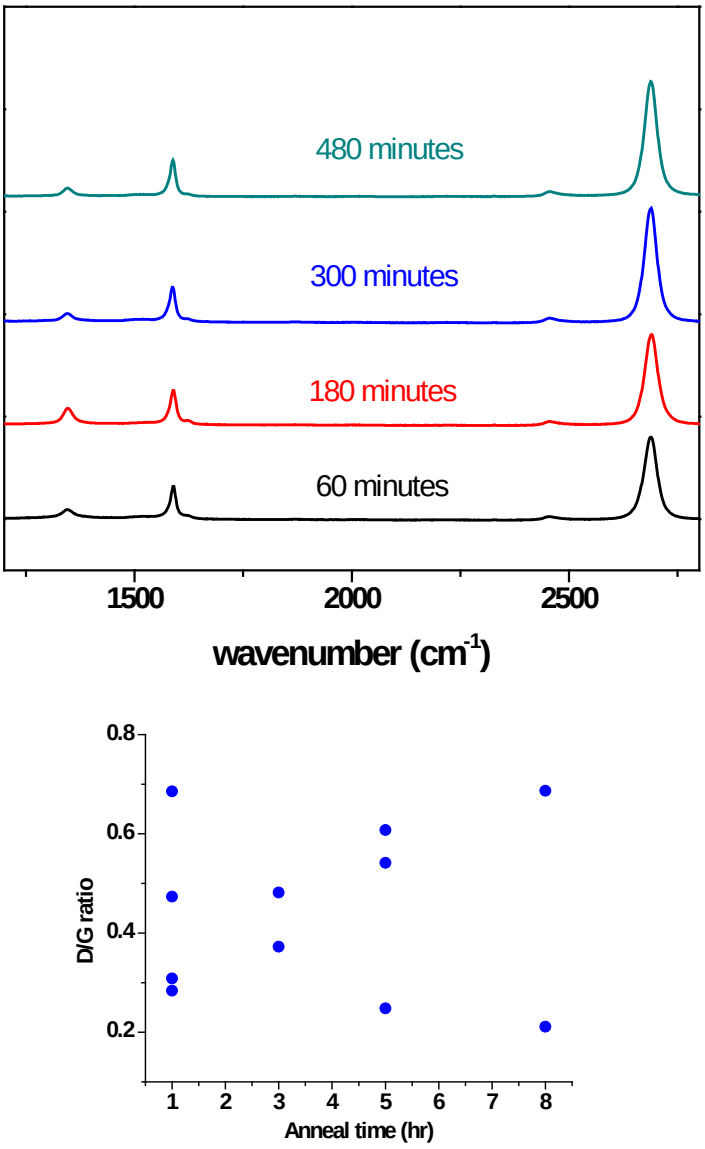

Figure 3.4 (Top) Raman spectra of graphene grown with different anneal times at 850°C for the copper foil. The ratios of the G peak (at ~1598 cm^{-1}) to the 2D peak (at ~2698 cm^{-1}) of between 2 and 3 indicate single layer graphene. (Bottom) The D peak (~1390 cm^{-1}) appeared to be the same relative to the G peak, indicating comparable level of defects and no marked improvement with a prolonged anneal step. The copper etchant used for all samples was $(NH_4)_2S_2O_8$.

3.3 Preparation of Graphene Samples on Substrates

In the majority of cases, the graphene has to be transferred from the catalyst to the substrate that is needed for further use. For many semiconductor applications, the graphene has to sit on top of an insulating substrate. Generally this is done in three steps: etching the metallic growth catalyst, transferring the graphene to the desired substrate and cleaning any organic residues. The growth, etch and transfer processes are summarized in Scheme 3.1. Each process has to be optimized in order to ensure the resulting graphene is clean with minimal defects. More recent work has shown the growth of graphene on certain insulating substrates,[37] though the commonly adopted process still involves growth on metallic surfaces. Therefore, the transfer process is still worth improving upon.

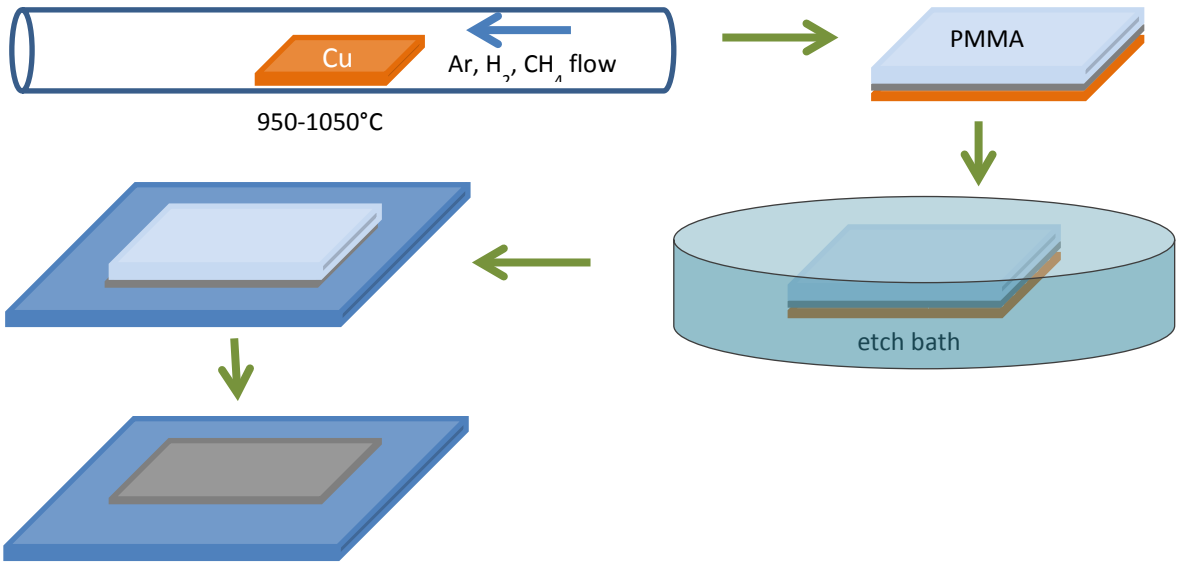

Scheme 3.1 Chemical vapor deposition growth of graphene on copper foils, followed by application of a poly(methyl methacrylate) resist layer, etching of the copper before transfer and resist removal.

3.3.1 Optimizing the Copper Etchant

The copper foils used as a catalyst during graphene growth must be etched away while minimizing damage to the graphene film. It is standard practice to coat one side of the copper foil with a protective layer that can be removed later. About 2 µm of a poly (methyl methacrylate) (PMMA) resist layer is coated on to the grown graphene and soft-baked at 180°C for 60 to 90 seconds, per manufacturer's directions. Care should be taken to not prolong the baking time, as this causes a hard cure of the PMMA which would be more difficult to dissolve and consequently damage the graphene sheet beneath the polymer.

A number of common copper etchants have been employed for CVD graphene, and they function by oxidizing copper ions. So far there have not been many detailed reports on why one etchant would be chosen over another, although the process is as simple as leaving the sample of copper foil/graphene/PMMA floating on an etchant bath until the copper is no longer visible. Although the PMMA layer is inert to these aqueous etchants, graphene is susceptible to oxidative damage. There have been some reports on new multistep etch processes that result in clean graphene with minimal defects, which can be implemented given the right conditions. These processes may be tedious at a laboratory scale. In this work, three aqueous oxidative copper etchants were examined: iron chloride hexahydrate ($FeCl_3 \cdot 6H_2O$) mixed with HCl, ammonium persulfate ($(NH_4)_2S_2O_8$) and Marble's reagent, which is comprised of a mixture of 10 g copper (II) sulfate ($CuSO_4$) and 50 mL hydrochloric acid (HCl) in 50 mL water, the goal being to select the most effective copper etchant without compromising the quality of graphene. Each etch method has been reported in the literature without much detail about any defects incurred on the

graphene during the process. The etch rate and time should be controlled to ensure that no copper remains but there is minimal exposure of graphene to the oxidizing agent.

Control of the rate of the etchant was attempted for the etchant materials by varying the concentrations of the etchants in water. Concentrations of $FeCl_3$ and $(NH_4)_2S_2O_8$ in water were varied between 0.05 M and 0.2 M, while Marble's reagent was made in the commonly prescribed proportions as mentioned above. It was observed that at 0.1M $FeCl_3$ solution in water etched about 95% of the copper foils within minutes but took a much longer time to oxidize the final traces of the metal. At a concentration of 0.1M, the $(NH_4)_2S_2O_8$ etchant appeared to have a more controlled copper etch rate, removing a 1 cm x 1.5 cm area of metal in about two hours. Nevertheless, Raman spectra for both etch conditions showed presence of the D peaks. In contrast, spectra for a sample etched with Marble's reagent showed a much diminished D peak (Figure 3.5). The etch time for a 1 cm x 1.5 cm sample was about an hour. X-ray photoelectron spectra (XPS) of graphene samples transferred after etching with $FeCl_3 \cdot 6H_2O$ and $(NH_4)_2S_2O_8$ were obtained and are shown in Figure 3.6. The C1s binding energies were 285.41 eV for $FeCl_3$ and 285.23 eV for $(NH_4)_2S_2O_8$, which is higher than the binding energy for C1s in the sp^2 configuration of 284.8 eV (Figure 3.6). These shifts, coupled with the shoulders on the peaks, are indicative of oxidative defects.[38,39]

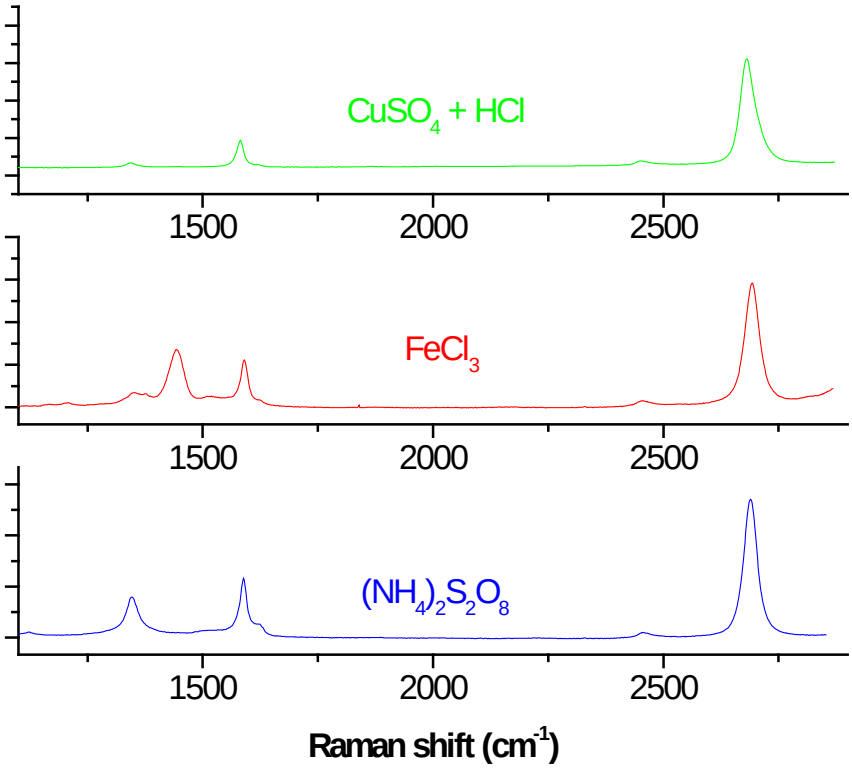

Figure 3.5 Raman spectra for graphene grown via chemical vapor deposition of methane on copper foils, with various copper etchants: (top) Marble's reagent; (middle) 10 mg/mL $FeCl_3$; (bottom) 0.1M $(NH_4)_2S_2O_8$. The degree of defects, as shown by the appearance and intensity of the D peak at around 1340 cm^{-1}, appears to be the lowest with Marble's reagent, and highest with the $FeCl_3$. All samples were transferred to SiO_2 substrates after etching and the PMMA resist dissolved in acetone.

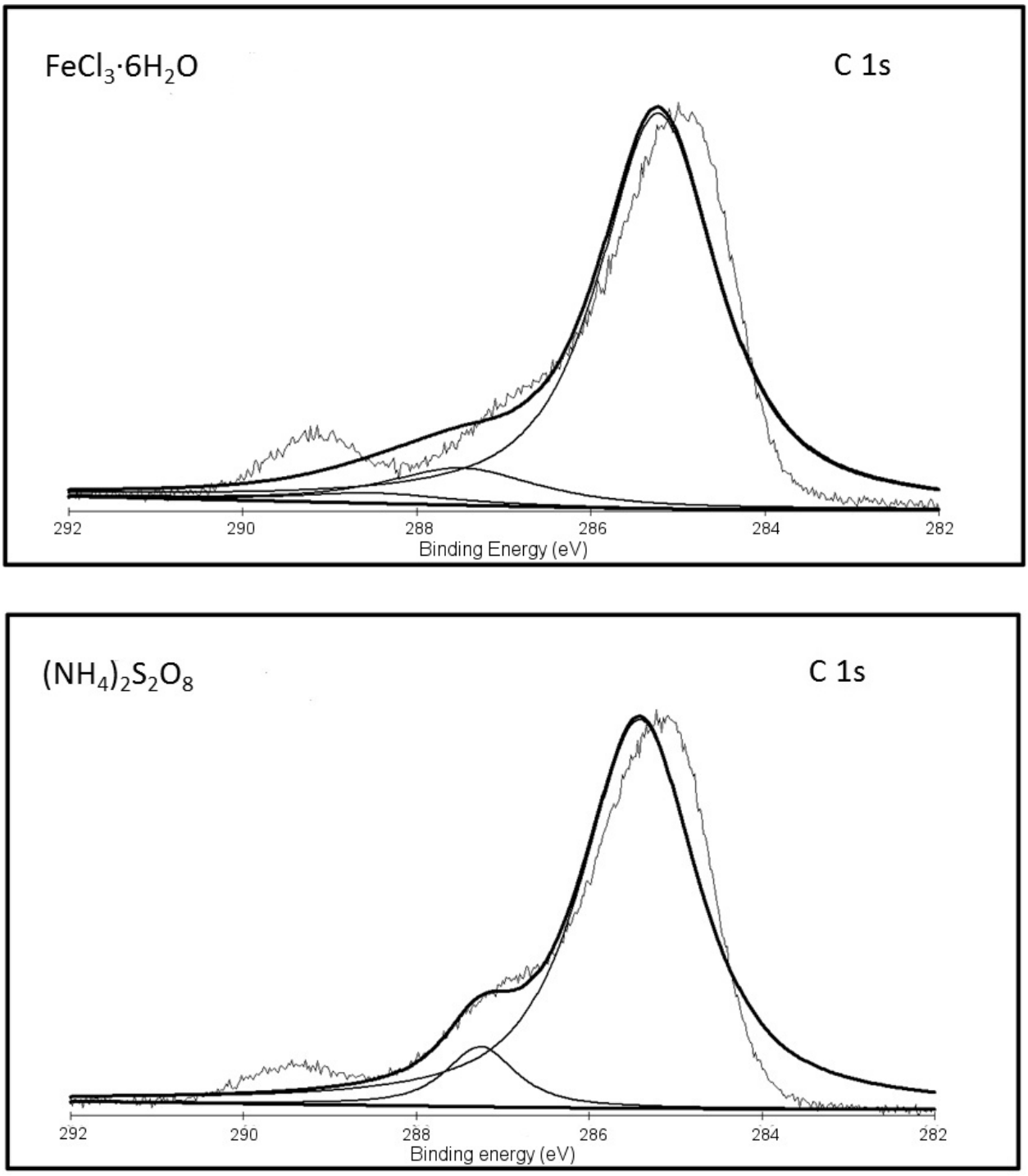

Figure 3.6 Deconvoluted X-ray photoelectron spectra of graphene etched from copper foils using (top) $FeCl_3 \cdot 6H_2O$ and (bottom) $(NH_4)_2S_2O_8$. The shoulders on the C1s peaks are indicative of oxidation of the C-C bonds.

3.3.2 Removal of Organic Residue and Final Etch Process

Complete transfer of the graphene sheet to a substrate is very much dependent on the adhesion between the graphene and the substrate. Incomplete adhesion, inadvertently caused by air bubbles or wrinkles, can result in delamination during the final stages of the transfer process. Samples were drawn vertically out of the bath to minimize water between the substrate and the graphene/PMMA film. The sample was then air-dried briefly and baked on a hotplate at 150°C to remove remaining traces of water. The final step in the etch/transfer process is to remove the protective PMMA layer. This layer should be completely removed to leave a clean graphene sample, but in some instances the elimination of all organic residues was incomplete, predominantly from the PMMA support. A number of techniques have been used to determine the most effective and complete removal: for example, solvent baths and reduction in hydrogen at high temperatures.[19] In this work, the samples were immersed in an acetone bath for at least 8 hours to dissolve the PMMA layer. The samples were then rinsed well with additional acetone and alcohol and dried. Reduction in a 95% Ar-5% H_2 gas mixture at 300°C was attempted, but did not appear to further remove any further traces of PMMA.

3.4 Conclusion and Outlook

Chemical vapor deposition of graphene on metal catalysts is an effective method of synthesizing high purity graphene, and reports in the literature suggest that the thickness and purity of the graphene can be controlled. Copper is one of the most attractive catalyst materials because of its low cost without sacrifices in quality and the predominantly single layer character of the synthesized graphene. In this work, chemical vapor deposition was used to grow single layers of graphene on polycrystalline foils of copper using a two-step heating process from a

methane precursor and transferred to substrates. The growth and transfer parameters such as the growth time, hydrogen gas flow and copper etchant were optimized. As the applicability of CVD graphene expands beyond large area single layer sheets into patterned arrays and sheets of varying dimensions with tunable band gaps, the controllability of the growth and transfer processes will continuously improve.

References

(1) Berger, C.; Song, Z.; Li, X.; Wu, X.; Brown, N.; Naud, C.; Mayou, D.; Li, T.; Hass, J.; Marchenkov, A. N.; Conrad, E. H.; First, P. N.; de Heer, W. A. *Science* **2006**, *312*, 1191.

(2) Emtsev, K. V.; Bostwick, A.; Horn, K.; Jobst, J.; Kellogg, G. L.; Ley, L.; McChesney, J. L.; Ohta, T.; Reshanov, S. A.; Rohrl, J.; Rotenberg, E.; Schmid, A. K.; Waldmann, D.; Weber, H. B.; Seyller, T. *Nat Mater* **2009**, *8*, 203.

(3) Banerjee, B. C.; Hirt, T. J.; Walker, P. L. *Nature* **1961**, *192*, 450.

(4) Wintterlin, J.; Bocquet, M. L. *Surface Science* **2009**, *603*, 1841.

(5) Sutter, P. W.; Flege, J.-I.; Sutter, E. A. *Nat Mater* **2008**, *7*, 406.

(6) Coraux, J.; N`Diaye, A. T.; Busse, C.; Michely, T. *Nano Letters* **2008**, *8*, 565.

(7) Vo-Van, C.; Kimouche, A.; Reserbat-Plantey, A.; Fruchart, O.; Bayle-Guillemaud, P.; Bendiab, N.; Coraux, J. *Applied Physics Letters* **2011**, *98*, 181903.

(8) An, X.; Liu, F.; Jung, Y. J.; Kar, S. *The Journal of Physical Chemistry C* **2012**, *116*, 16412.

(9) Li, X.; Cai, W.; An, J.; Kim, S.; Nah, J.; Yang, D.; Piner, R.; Velamakanni, A.; Jung, I.; Tutuc, E.; Banerjee, S. K.; Colombo, L.; Ruoff, R. S. *Science* **2009**, *324*, 1312.

(10) Arnoult, W. J.; McLellan, R. B. *Scripta Metallurgica* **1972**, *6*, 1013.

(11) Siller, R. H.; Oates, W. A.; McLellan, R. B. *Journal of the Less Common Metals* **1968**, *16*, 71.

(12) Sun, Z.; Yan, Z.; Yao, J.; Beitler, E.; Zhu, Y.; Tour, J. M. *Nature* **2010**, *468*, 549.

(13) Wei, D.; Liu, Y.; Wang, Y.; Zhang, H.; Huang, L.; Yu, G. *Nano Letters* **2009**, *9*, 1752.

(14) Yu, Q.; Jauregui, L. A.; Wu, W.; Colby, R.; Tian, J.; Su, Z.; Cao, H.; Liu, Z.; Pandey, D.; Wei, D.; Chung, T. F.; Peng, P.; Guisinger, N. P.; Stach, E. A.; Bao, J.; Pei, S.-S.; Chen, Y. P. *Nature Materials* **2011**, *10*, 443.

(15) Li, X.; Cai, W.; Colombo, L.; Ruoff, R. S. *Nano Letters* **2009**, *9*, 4268.

(16) Sutter, P.; Sadowski, J. T.; Sutter, E. *Physical Review B* **2009**, *80*, 245411.

(17) Rasool, H. I.; Song, E. B.; Allen, M. J.; Wassei, J. K.; Kaner, R. B.; Wang, K. L.; Weiller, B. H.; Gimzewski, J. K. *Nano Letters* **2010**, *11*, 251.

(18) Wassei, J. K.; Mecklenburg, M.; Torres, J. A.; Fowler, J. D.; Regan, B. C.; Kaner, R. B.; Weiller, B. H. *Small* **2012**, *8*, 1415.

(19) Reina, A.; Jia, X.; Ho, J.; Nezich, D.; Son, H.; Bulovic, V.; Dresselhaus, M. S.; Kong, J. *Nano Letters* **2008**, *9*, 30.

(20) Obraztsov, A. N.; Obraztsova, E. A.; Tyurnina, A. V.; Zolotukhin, A. A. *Carbon* **2007**, *45*, 2017.

(21) Bhaviripudi, S.; Jia, X.; Dresselhaus, M. S.; Kong, J. *Nano Letters* **2010**, *10*, 4128.

(22) Ong, T. P.; Xiong, F.; Chang, R. P. H.; White, C. W. *J. Mater. Res* **1992**, *7*, 2429.

(23) Hartsell, M.; Plano, L. *J. Mater. Res*, *9*, 921.

(24) Zhou, W.; Han, Z.; Wang, J.; Zhang, Y.; Jin, Z.; Sun, X.; Zhang, Y.; Yan, C.; Li, Y. *Nano Letters* **2006**, *6*, 2987.

(25) Yuan, D.; Ding, L.; Chu, H.; Feng, Y.; McNicholas, T. P.; Liu, J. *Nano Letters* **2008**, *8*, 2576.

(26) López, G. A.; Mittemeijer, E. J. *Scripta Materialia* **2004**, *51*, 1.

(27) Mattevi, C.; Kim, H.; Chhowalla, M. *Journal of Materials Chemistry* **2011**, *21*, 3324.

(28) Yan, K.; Peng, H.; Zhou, Y.; Li, H.; Liu, Z. *Nano Letters* **2011**, *11*, 1106.

(29) Wu, Y.; Chou, H.; Ji, H.; Wu, Q.; Chen, S.; Jiang, W.; Hao, Y.; Kang, J.; Ren, Y.; Piner, R. D.; Ruoff, R. S. *ACS Nano* **2012**, *6*, 7731.

(30) Park, J.; Xiong, W.; Gao, Y.; Qian, M.; Xie, Z.; Mitchell, M.; Zhou, Y.; Han, G.; Jiang, L.; Lu, Y. *Applied Physics Letters* **2011**, *98*, 123109.

(31) Zhang, B.; Lee, W. H.; Piner, R.; Kholmanov, I.; Wu, Y.; Li, H.; Ji, H.; Ruoff, R. S. *ACS Nano* **2012**, *6*, 2471.

(32) Li, Z.; Wu, P.; Wang, C.; Fan, X.; Zhang, W.; Zhai, X.; Zeng, C.; Li, Z.; Yang, J.; Hou, J. *ACS Nano* **2011**, *5*, 3385.

(33) Li, X.; Magnuson, C. W.; Venugopal, A.; An, J.; Suk, J. W.; Han, B.; Borysiak, M.; Cai, W.; Velamakanni, A.; Zhu, Y.; Fu, L.; Vogel, E. M.; Voelkl, E.; Colombo, L.; Ruoff, R. S. *Nano Letters* **2010**, *10*, 4328.

(34) Huang, P. Y.; Ruiz-Vargas, C. S.; van der Zande, A. M.; Whitney, W. S.; Levendorf, M. P.; Kevek, J. W.; Garg, S.; Alden, J. S.; Hustedt, C. J.; Zhu, Y.; Park, J.; McEuen, P. L.; Muller, D. A. *Nature* **2011**, *469*, 389.

(35) Ruan, G.; Sun, Z.; Peng, Z.; Tour, J. M. *ACS Nano* **2011**, *5*, 7601.

(36) Vlassiouk, I.; Regmi, M.; Fulvio, P.; Dai, S.; Datskos, P.; Eres, G.; Smirnov, S. *ACS Nano* **2011**, *5*, 6069.

(37) Yan, Z.; Peng, Z.; Sun, Z.; Yao, J.; Zhu, Y.; Liu, Z.; Ajayan, P. M.; Tour, J. M. *ACS Nano* **2011**, *5*, 8187.

(38) Moulder, J. F.; Chastain, J.; King, R. C. *Handbook of X-ray photoelectron spectroscopy: a reference book of standard spectra for identification and interpretation of XPS data*; Physical Electronics Eden Prairie, MN, 1995.

(39) Hawaldar, R.; Merino, P.; Correia, M. R.; Bdikin, I.; Grácio, J.; Méndez, J.; Martín-Gago, J. A.; Singh, M. K. *Sci. Rep.* **2012**, *2*.

Chapter 4: Incorporation of Graphene into Organic Electronic Devices

4.1 Graphene as a Transparent Electrode

As has been described in Chapter 1, graphene has many unique electrical properties that position it to be a very promising transparent conductor material. One of the major applications of transparent electrodes is in optoelectronic devices such as light emitting diodes (LEDs) and photovoltaics. Its high electrical conductivity and optical transmittance is encouraging for a field that aims to find alternatives to indium tin oxide, particularly in energy harvesting. The earth abundance of carbon, coupled with rapidly evolving techniques for generating graphene from bulk carbon sources, further add to its advantages. In organic electronics, graphite oxide derivatives have also been used as light emitting or absorbing materials,[1-3] indicating its potential to be a versatile material in electronic devices. In recent years, numerous reports have been published on graphene as a transparent anode in organic devices, particularly in photovoltaics.

The basic structure of an organic photovoltaic device and its corresponding energy level alignment diagram is shown in Figure 4.1. It is comprised of an active layer sandwiched between a cathode and an anode. Light enters the cell from the anode in a regular structure device. The role of the anode and cathode is to collect separated holes and electrons, respectively. To further extract these charge carriers, layers may be added between the active layer and electrodes. The active layer is comprised of an electron donor and electron acceptor. In a bilayer device, these two layers are separated. In a bulk heterojunction device, the interpenetrating donor-acceptor layer greatly increases the number of interfaces present for charge separation, leading to higher extraction of charges. Current research focuses on extracting the maximum number of charge

carriers from either electrode through multiple steps including extracting more electron-hole pairs, improving charge carrier mobility, and minimizing recombination at interfaces.[4]

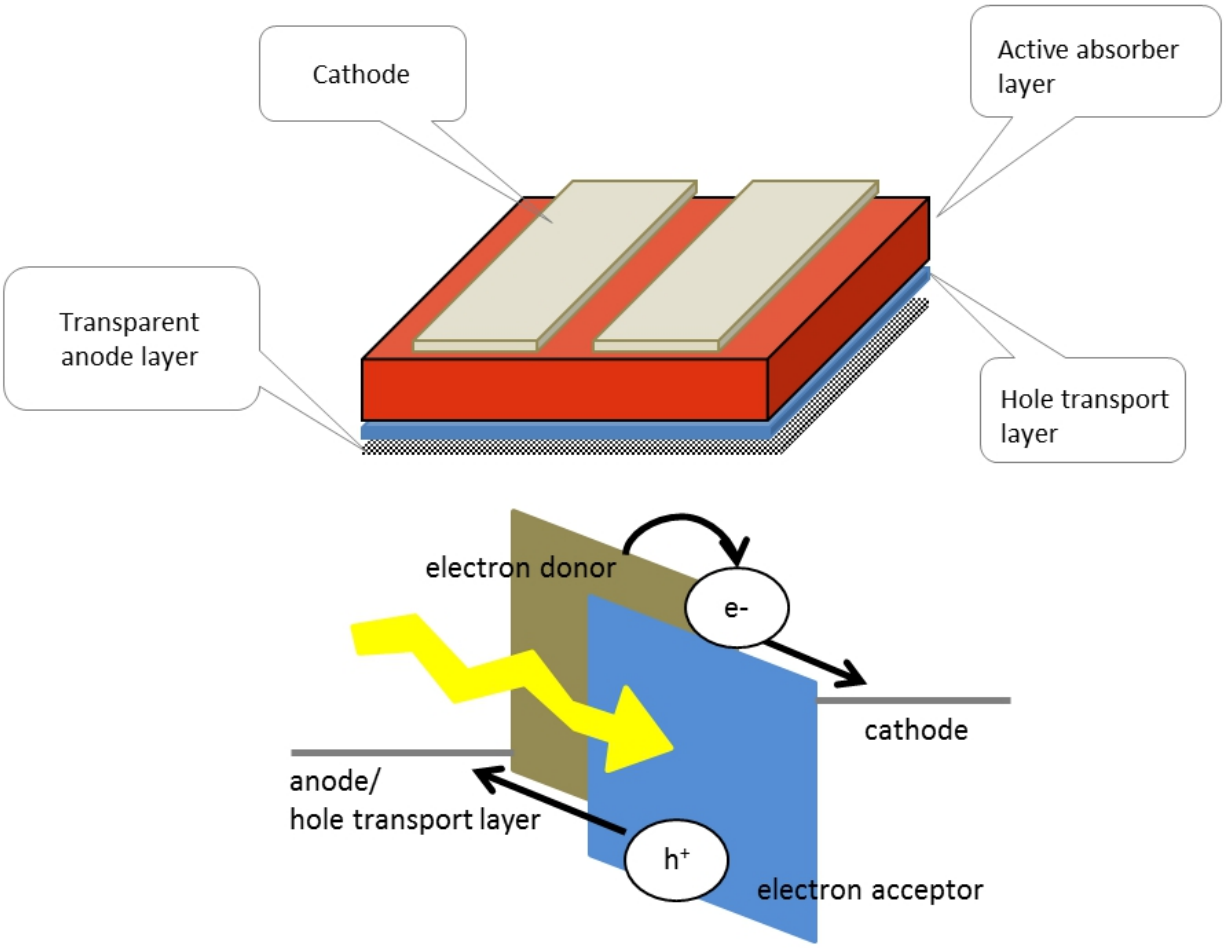

Figure 4.1 Schematic diagram of a regular bulk heterojunction organic photovoltaic device structure, from bottom to top: the transparent anode; hole transport or buffer layer; absorber layer with the electron donor and acceptor; cathode.

4.2 Organic Photovoltaic Devices with Graphene as the Transparent Anode

In organic donor-acceptor systems, the effectiveness of charge collection depends in part on the energy band alignments on the materials. Before graphene was produced on a large scale, reports were published on carbon nanotube films as the anode in organic devices.[5,6] These electrodes were found to be reasonably compatible with the PEDOT:PSS and organic layers from an energy level standpoint. The measured work function of graphene and carbon nanotubes is 4.2 eV, which is close to the value measured for graphite, and within the range needed for hole collection from many organic donor materials. Therefore, in theory, graphene satisfies the general requirements for a transparent anode, with the added advantage of a higher optical transmittance than CNTs.[7]

The advancements in obtaining high conductivities in solution processed reduced graphene oxide mean they could, in principle, be used in single or few layers as a transparent anode, but is a challenge for large area devices. As a consequence of the graphite oxidation process which can tear apart sheets with a large starting lateral area, a single CCG sheet would measure, on average, tens of microns. It is difficult to ensure a continuous conducting pathway on the area (~0.1 cm^2 or larger) necessary. Therefore, the hybrid graphene-CNT film, highlighted in Chapter 2, was used as the transparent anode layer to minimize the number of coatings necessary for a conductive layer. This layer was cast on to a glass substrate in the desired area after half of it was masked using elastomeric stamping. The graphene-CNT layer was spin-coated from a hybrid solution and baked at 150°C to remove traces of the solvent.

Graphene deposited via CVD was also used in a device as the transparent anode. The desired dimension of graphene was cut from the copper foil before the etch step. After the copper

etch, the graphene was transferred to a glass substrate before PMMA removal and rinsing. For higher conductivity, this step is repeated on the same substrate to produce multiple layers of graphene. The OPV device processing step was also carried out in the same manner as a standard device: a poly(3,4-ethylenedioxythiophene) poly(styrenesulfonate) (PEDOT:PSS) hole transport coating, active layer deposition and cathode deposition.

A few proof-of-concept devices have been constructed with the bulk heterojunction OPV with a graphene-based transparent electrode. The devices were constructed using the standard bulk heterojunction system with P3HT as the donor and PCBM as the acceptor. A ca. 10 nm layer of PEDOT:PSS was coated on to the surface of the graphene layer after ozone treatment for 10 minutes. Prolonged ozone treatment oxidizes the graphene and degrades its electrical conductivity. The P3HT:PCBM blend was deposited from a 20 mg/mL solution in dichlorobenzene to yield a ca. 200 to 300 nm thick film. The films were then solvent annealed and then baked at 110°C for ten minutes, according to established methods in the field for this donor-acceptor system.[8] The Ca and Al cathode layers were then deposited via thermal evaporation at 10^{-6} torr pressure.

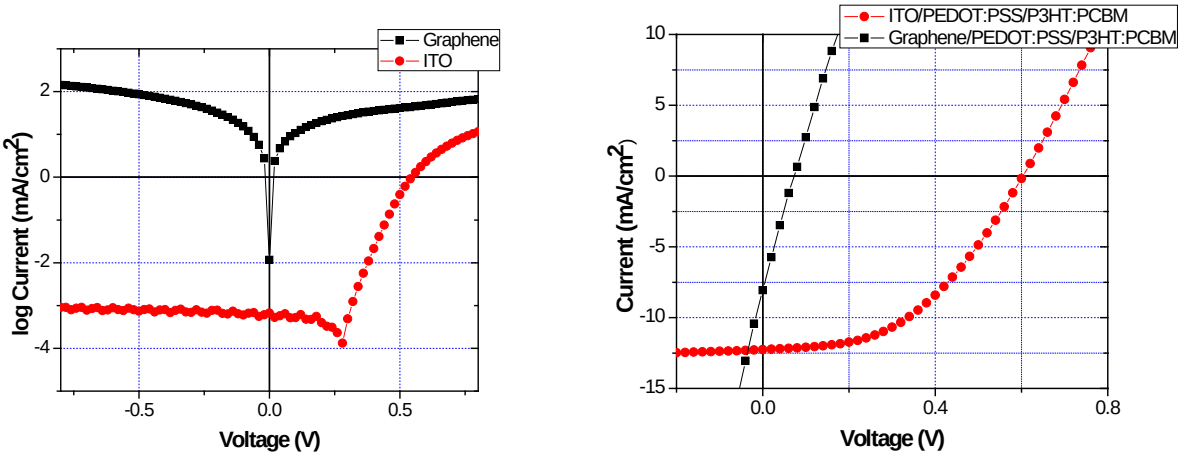

Figure 4.2 Current-voltage characteristics under (left) dark and (right) AM 1.5 light conditions for an organic bulk heterojunction photovoltaic device with poly(3-hexylthiophene) and C_{60}-PCBM. The device constructed on ITO had an efficiency of ~3.5%, while the device with a graphene anode had 0% and clearly does not exhibit diode characteristics due to shorting.

The measured current-voltage characteristics (Figure 4.2) indicated that the devices with graphene as a transparent electrode for the most part do not have diode characteristics, destroying the device performance. A number of explanations for this are the high resistance of the anode, film nonuniformity and the lack of surface compatibility between the graphene-CNT layer and the polymer layers. This is because in using hydrazine to cast the reduced graphene layer and subsequent removal of the solvent, the recovered graphene-CNT film with a majority of its oxygen functionalities removed is hydrophobic. Indeed, the organic devices fabricated by evaporation have seen greater success with a graphene anode than a solution-processed layer because of the hydrophobic nature of the deposited materials and the conformity of the materials to the surface of the graphene. With regards to surface uniformity, the decreased surface energy

of the graphene-CNT material compared with an ITO layer is detrimental for compatibility with a solution process. Static water contact angle measurements on films of graphene-CNT and PEDOT:PSS are 61° and 12°, respectively, showing a large difference in the surface energy.

In fact, surface modification has been employed in organic electronic devices, predominantly in transistors and memory devices. These efforts have led to higher mobility and lowered barriers for charge transport.[4] This has been extended to organic photovoltaics by a number of methods, such as addition of a charge transport layer, modification of the graphene layer, or a planarization layer between graphene and the organic material.[9] A study showed that oxygen plasma treatment possibly increases the bonding strength even though the dangling bond generated by plasma treatment could degrade mobility. It is consistent with the results of the present study and can be explained to be a result of the improved adhesion due to the presence of the hydroxyl group, which increases the polarity of the surface.

Thus, mitigating the problems of adhesion of graphene to the organic layer whilst maintaining its structural integrity and electronic conductivity using relatively simple processing conditions are dramatic step towards creating graphene-based organic devices. A method of polymerization directly on a graphene surface would create good adhesion, and possibly surface modification due to chemical bonding to the graphene.

4.3 Electropolymerization of Conducting Polymers on Graphene

4.3.1 Motivation

Because graphene also combines high optical transmittance with high electrical conductivity, it has been heavily researched as a transparent electrode in place of ITO. This has

been largely successful in devices constructed via physical deposition methods, some showing performance comparable to or better than established transparent electrode material.[10] At the same time, the synthetic methods of conducting polymers have been heavily researched and have led to some very high quality materials with unique properties that can be used in energy generation and storage applications. Poly(3,4-ethylene dioxythiophene), commonly known as PEDOT, is a well-known conducting polymer that has electrochromic properties and serves as a hole transport layer in organic optoelectronic devices. While PEDOT itself is insoluble, its insolubility is circumvented by the use additives such as poly(styrene sulfonate) (PSS). This soluble form is then compatible with solution-processed methods and thus widely used in constructing organic and hybrid optoelectronic devices.[11] This solution is very hydrophilic and is compatible with the standard indium tin oxide that is used for these applications. So far, the surface incompatibilities of graphene with PEDOT:PSS has hindered its widespread application as a transparent electrode in solution-processed devices. In the best cases, PEDOT is substituted, or surface modification of the graphene film through the use of an interfacial layer is performed,[12,13] which, cumulatively, is time consuming in the device preparation process.

Electropolymerization is a well-studied technique for growing conducting polymers on conductive substrates such as Au and Pt, and on carbon-based materials, particularly on glassy carbon. *In situ* polymerization of conducting polymers has been applied to carbon surfaces and the results have generally shown increases in electrochemical capacitance.[14] Various methods of combining PEDOT with graphene, predominantly in the form of reduced graphite oxide, have also shown enhanced capacitive behavior, mechanical strength, or conductivity.[15-17] In fact, recent research shows that graphene, synthesized via a variety of methods, can facilitate

polymerization of conducting polymers, including PEDOT. Successful electropolymerization can occur in the presence of carbon materials, and a few solution-based and vapor-phase approaches to building the polymer on graphene have been published. The high capacitive performance of hybrid materials comprising conducting polymers and reduced graphene oxide and carbon nanotubes are generally possible because of their large surface areas and mixture of sp^2 and sp^3 bonds. Graphene synthesized by chemical vapor deposition (CVD) has a lower instance of sp^3 bonding but can be highly conductive, so it is expected that it would have potential as an electrochemical electrode. Stacked hybrids of graphene-conducting polymers would offer the advantage of decreased surface resistance, especially for charge transport functions.

A direct electropolymerization of the conducting polymer PEDOT on single layer graphene produced by CVD has been achieved. The polymer was characterized by Raman spectroscopy and the evolution of the film properties was tracked by microscopic methods. The variation of polymer growth as a function of the graphene surface and other factors was also characterized.

4.3.2 Electropolymerization Process of Poly(3,4-ethylenedioxythiophene) on Graphene

Graphene was grown via chemical vapor deposition from methane precursors on copper foil as described in Chapter 3. Transfer of the graphene to substrates was also performed using the aforementioned methods. A thin layer (~3 um) of poly (methyl methacrylate) (PMMA) was spin-coated on the graphene/copper foils. The copper foils were etched using Marble's reagent, and then rinsed well with deionized water. This transfer process was repeated to create multilayer graphene films. Chemical activation of some of the graphene surfaces was done by immersion in concentrated HNO_3 for approximately 30 seconds.

Electrochemical polymerization was performed in a standard three-electrode, single compartment, electrochemical cell that contained a solution of the monomer 3,4-ethylenedioxythiophene (EDOT), and the electrolyte, 0.1M lithium perchlorate in acetonitrile. The concentrations of EDOT used were 0.1M, 0.05M and 0.025M. Platinum wire and $Ag/AgNO_3$ were used as the counter and reference electrodes, respectively. The polymerization was carried out at a constant potential of 1.2V. This potential was used after a preliminary deposition using cyclic voltammetry to determine the onset potential of oxidation of the polymer, which was about 1.1V. The cell was deaerated with nitrogen for about ten minutes before applying potential. After the electropolymerization cycle, the film was briefly washed with monomer-free electrolyte, rinsed with ethanol and dried.

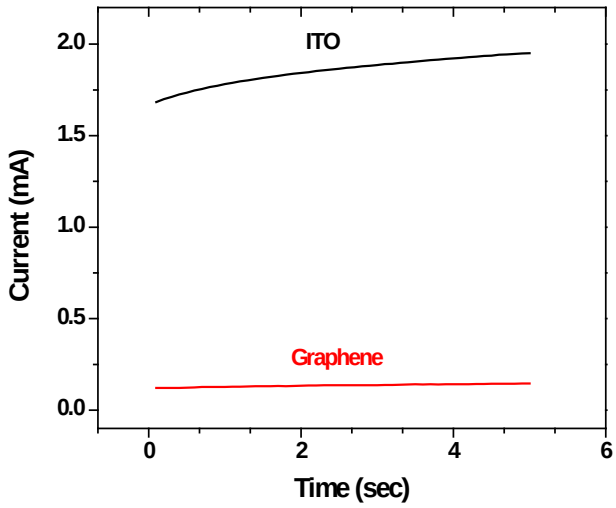

Figure 4.3 A sample current-time plot of the electropolymerization of 3,4-ethylene dioxythiophene (EDOT) on graphene and on ITO from a 0.0025M solution of the monomer in acetonitrile. The polymerization on ITO proceeds at a higher current because of its much higher electrical conductivity.

4.3.3 Properties of the Electropolymerized Film

Potentiostatic growth in the doped state (i.e. a positive potential) was performed, and the visible characteristic blue shade for thicker films show that the growth was successful on single layer and multilayer graphene samples. The thickness of the film was correlated to the charge during film growth. Although great effort was made to ensure the consistency of the graphene quality and experimental conditions, it was found that the thickness and smoothness of the films heavily depended upon the contact between the potentiostat and the film. Another factor contributing to the large deviation of film thickness is the variation of electrical conductivity at different points on the graphene sample. As a consequence, the current and film thickness did not increase linearly with the growth time as expected. Varying the concentration of the monomer did provide some control over the film thickness, as the lowering in growth rates led to films with less spikes.

Table 4.1 Values of the charge per area and overall film thickness as a function of PEDOT growth time.

Growth time (sec)	0.0025M Charge per area (C/cm^2)	0.0025M Average measured thickness (nm)	0.005M Charge per area (C/cm^2)	0.005M Average measured thickness (nm)
5	0.00138	250	0.00455	533
10	0.00847	966	0.00748	1186
30	0.0116	1609	0.01799	2024
60	0.0259	4125	0.03475	949*

* The films at this condition consisted of multiple large spikes which indicate a very high film roughness and a high standard deviation for the film thickness.

Raman spectroscopy was used to confirm and track the growth of the polymer on the graphene film, transferred to a SiO_2 or glass substrate. As shown in Figure 4.4, the Raman peak intensities match very well with known characteristics of PEDOT, the most dominant being the peaks at 1568 and 1508 cm^{-1}, which are attributed to the asymmetrical stretching of $C_\alpha = C_\beta$.[18] The most intense peak at 1434 cm^{-1} arises from the symmetrical stretching of $C_\alpha = C_\beta$. In the EDOT monomer, the C_α is the carbon atom connected to the sulfur atom, while C_β is the atom connected to the C_α (Figure 4.4, inset).[19] Other characteristic peaks are symmetric C-C stretching at 1367 cm^{-1}, antisymmetric stretching of C-C at 994 cm^{-1}, C-S-C bending at 700 cm^{-1}, inter-ring C-C stretching at 1257 cm^{-1}, and the =C-O vibration at 1110 cm^{-1}. It is apparent that the peak at 1434 cm^{-1} increases in intensity along with the growth time/thickness of the PEDOT. On samples with a low thickness of PEDOT on the graphene, the characteristic G and 2D peaks of the graphene are still visible. On thicker samples, the graphene peaks are eclipsed by the PEDOT peaks. The graphene as an electrode does not affect the structure of the polymer. The G and 2D peaks of graphene (at 1590 and 2690 cm^{-1} respectively) are visible at low thicknesses of PEDOT, but with increasing thickness, the PEDOT peaks eclipse the graphene peaks.

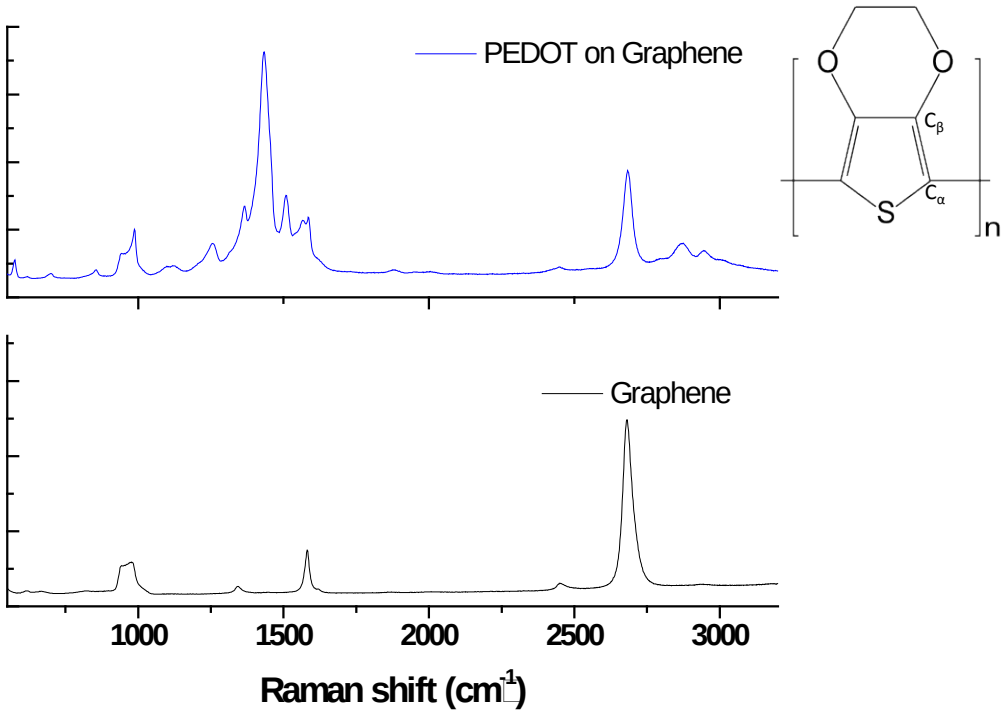

Figure 4.4 Raman spectra of single layer graphene before and after polymerization of EDOT. The most intense peak at 1434 cm^{-1} arises from the symmetrical stretching of C_α=C_β. In the EDOT monomer, the C_α is the carbon atom connected to the sulfur atom, while C_β is the atom connected to the C_α (inset). The peaks at 1568 and 1508 cm^{-1} are attributed to the asymmetrical stretching of C_α=C_β. Other peaks are symmetric C-C stretching at 1367 cm^{-1}, antisymmetric stretching of C-C at 994 cm^{-1}, C-S-C bending at 700 cm^{-1}, inter-ring C-C stretching at 1257 cm^{-1}, and the =C-O vibration at 1110 cm^{-1}.

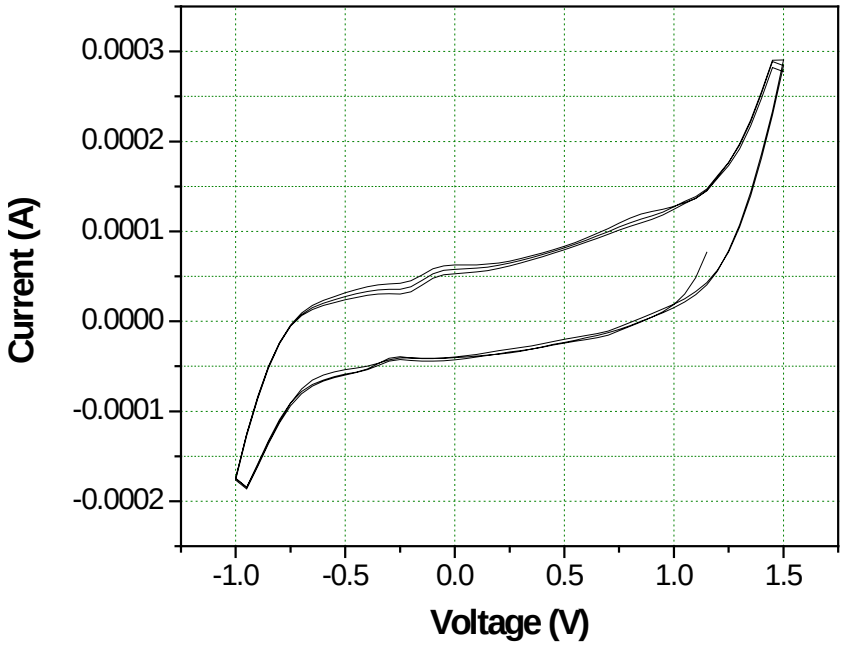

o

Figure 4.5 A sample cyclic voltammogram of a PEDOT film electropolymerized n graphene. The consistent presence of the peaks between 0 and -0.5V indicate a reversible redox process. The CV was recorded 0.1M $LiClO_4$ in acetonitrile vs. $Ag/AgNO_3$ for the voltage range indicated in the figure, at a sweep rate of 50 mV/s.

In the doped state, the as-grown films appeared mostly clear with a slight tinge of blue for the shorter growth times, and pale blue for the longer growth times. During cyclic voltammetry, the films switched to dark blue. Reversible redox behavior was exhibited, which enables us to derive the reduction and oxidation potentials for the film. The electrochemical HOMO level, after subtracting from a ferrocene couple, was -6.0 eV, which is deeper than the Fermi level of -5.2 eV often cited for PEDOT:PSS. The graphene/PEDOT stack is robust and does not dissolve after repeated rinsing with acetone and alcohols. The measured sheet

resistances of the stack are lower than the graphene alone, depending on the thickness of the film. Generally, the resistance is decreased further with a thicker PEDOT layer (Table 4.2). The absorbance spectrum of the films grown showed a broad peak stretching into the n-IR, which is characteristic of the doped state of PEDOT. Nonetheless, the optical transmittances of the films of a thickness over 100nm (10 second growth in Figure 4.6) is still over 85% in the visible region) which would be advantageous for devices requiring transparency in this area.

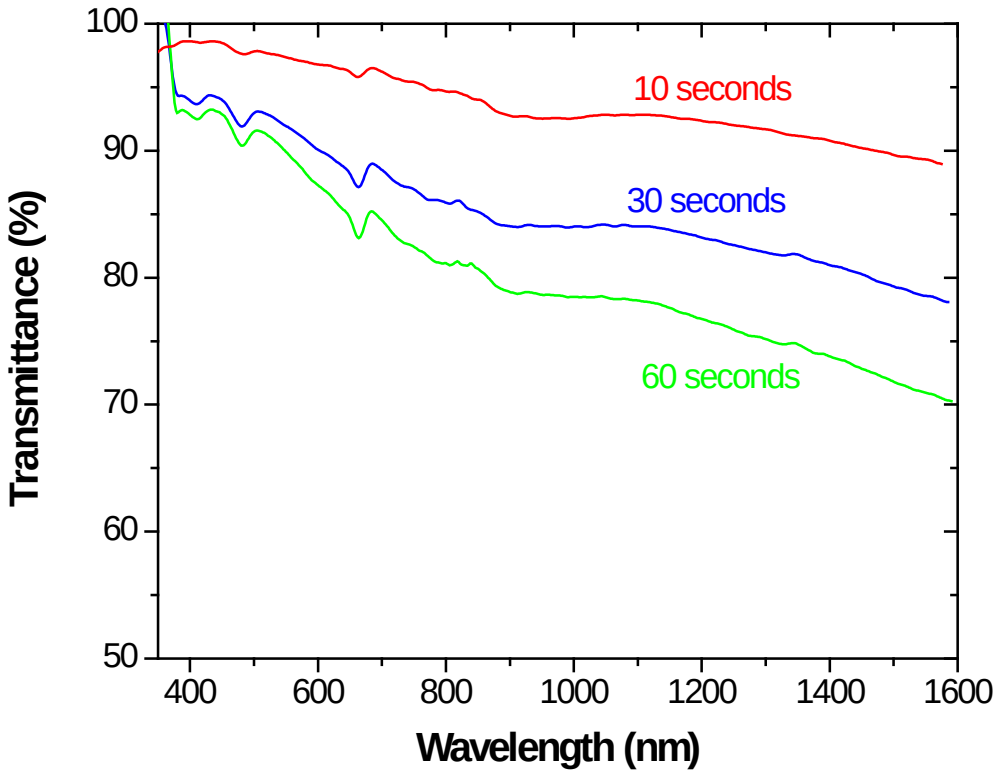

Figure 4.6 UV-visible-nIR transmittance data for samples of PEDOT grown on graphene on glass at different growth times. The dips at ~500 nm and ~650 nm are caused by the changes in the detectors in the instrument.

Table 4.2 The influence of PEDOT growth on the electrical conductivity of the graphene, as shown by the decrease in sheet resistance. The average resistance of the graphene was taken from measurements on all the samples prior to polymerization.

Growth time (seconds)	Average R_s of Graphene (Ω)	Average R_s of Graphene-PEDOT stack (Ω)
10	665	584
30	665	339
60	665	117

As shown in Figure 4.7, the resulting morphology of the polymer differs from the flower-likes structure grown on ITO in the same anion/electrolyte system. It is also evident that the polymer grows conformal to the graphene surface, as the tears in the graphene sheet are also devoid of any polymer growth. Figure 4.8 shows the topology of the films with increasing growth time or thickness. Films grown with the same lithium perchlorate electrolyte in two different solvents, namely propylene carbonate and acetonitrile, did not show significantly different surface morphologies after 10 minutes of growth. It appears that the PEDOT growth begins as islands before merging to form networks.

Electropolymerized films lack the smoothness or planarization capability of polymers synthesized in the solution phase and cast on to a surface. Therefore, control of the growth of the polymer is essential for attaining uniform films, especially when used in a stacked configuration such as organic LEDs or solar cells. It was found that the shortest growth times yielded the thinnest but roughest films. For instance, films produced after a 5 second growth time in a 0.0025M monomer solution showed an overall measured step height of 200 to 300Å but

contained several spikes measuring up to 2000Å. The longer growth times yielded thicker films with spikes of smaller deviation. A possible solution for controlling the polymer growth would be to examine the growth at an applied under potential of oxidation.

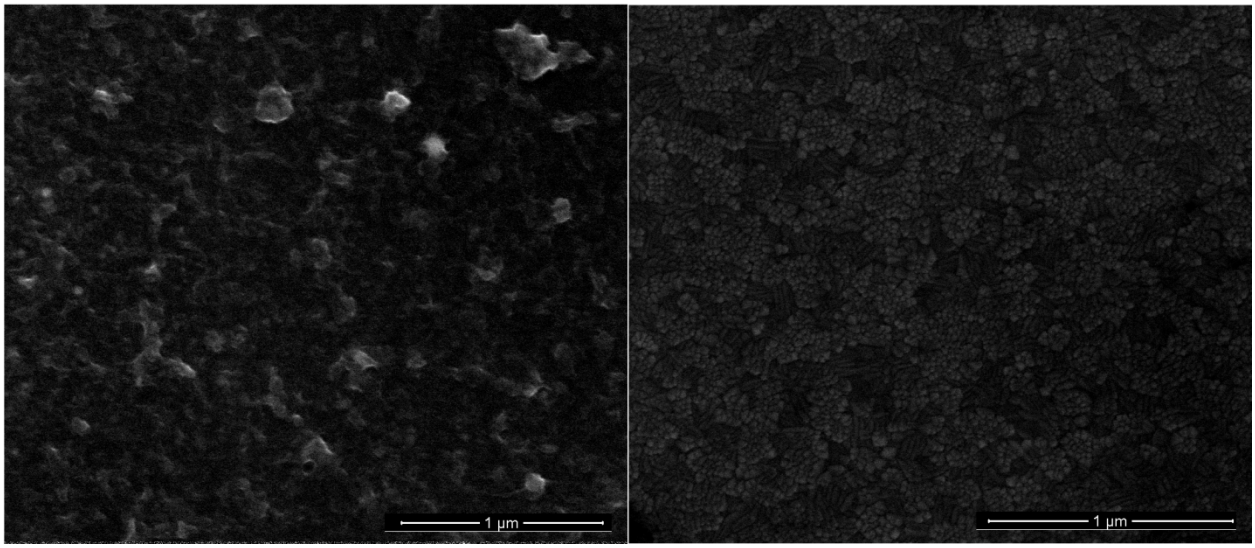

Figure 4.7 Comparison of morphology of PEDOT grown on (left) single layer graphene and (right) indium tin oxide, with the same monomer concentration of 0.05M and growth time of 10 seconds. On graphene, the polymer chains form clusters, while on ITO, they simultaneously form small lamellar bunches.

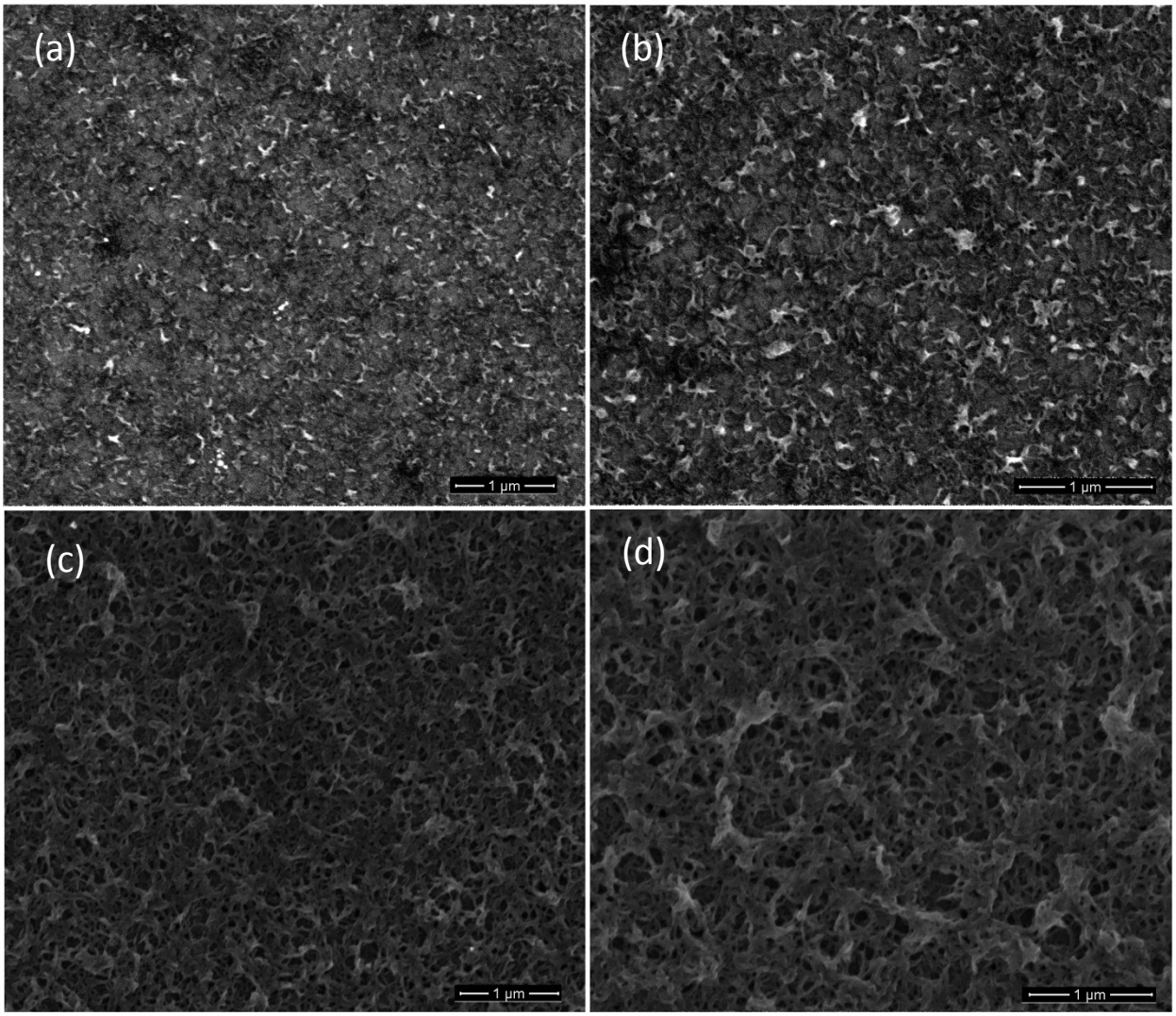

Figure 4.8 Morphological evolution of PEDOT growth from a 0.0025M EDOT solution in acetonitrile through scanning electron micrographs: (a) 5 seconds; (b) 10 seconds; (c) 30 seconds; (d) 60 seconds.

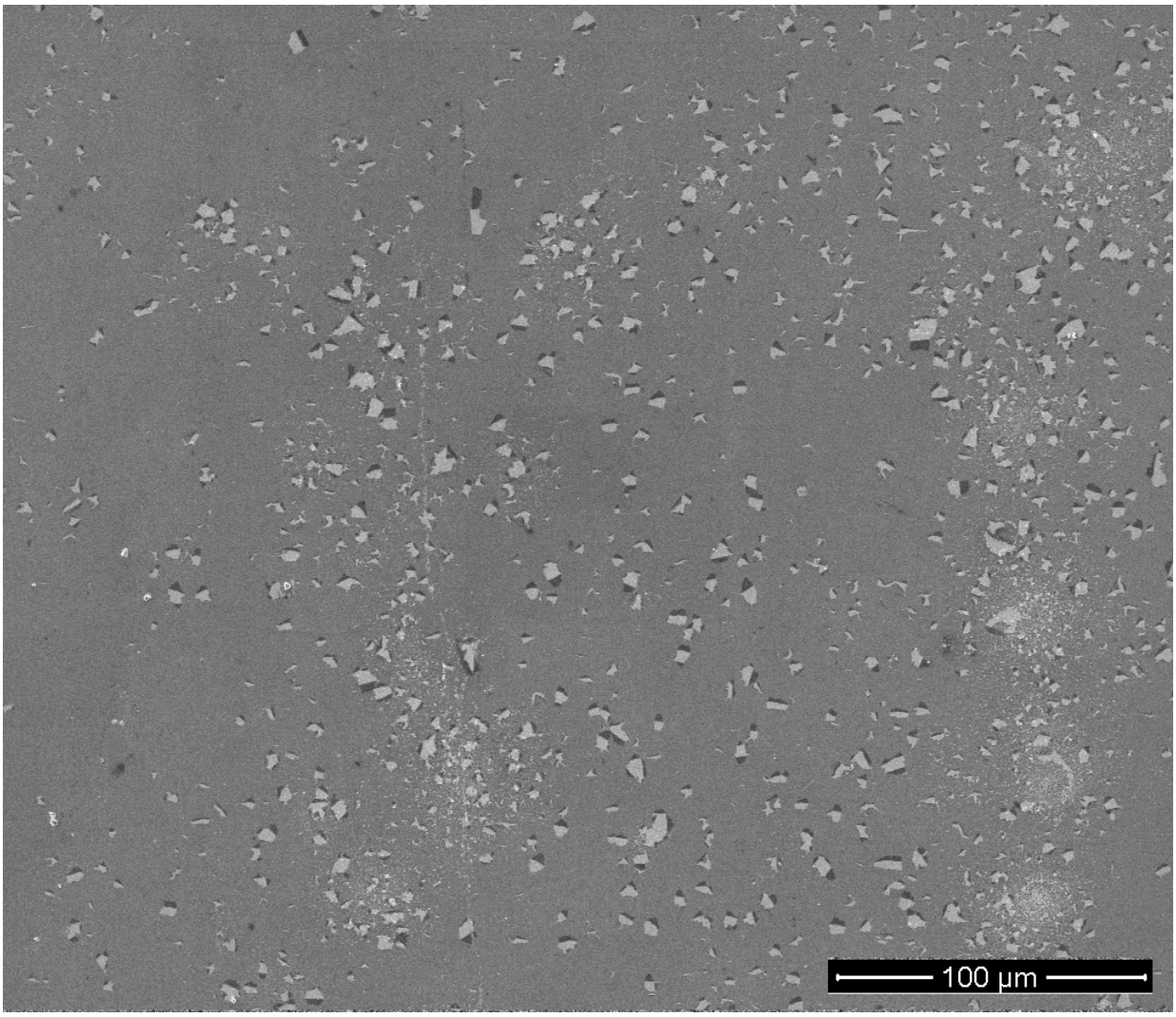

Figure 4.9 A scanning electron micrograph of a large area of the electropolymerized PEDOT on graphene. This section of the graphene film has several rips and gaps which are also devoid of polymer growth, showing that the growth is conformal to the graphene.

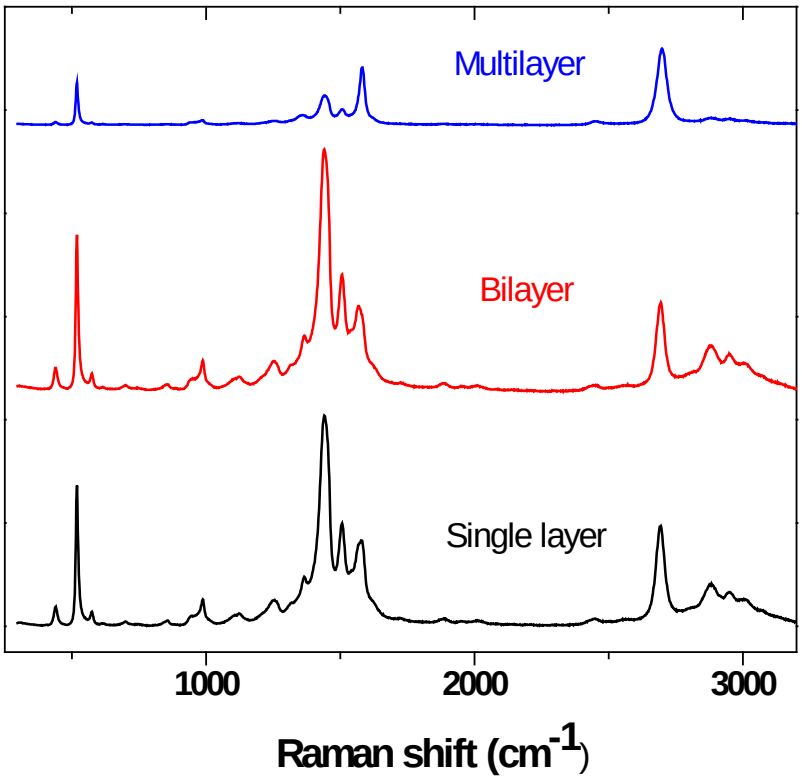

Figure 4.10 Raman spectra of PEDOT grown on single layer, bilayer and multilayer regions of a graphene sheet. After 5 seconds, notable growth on the multilayer region does not appear to have occurred, as the graphitic peaks are still dominant. However, as shown in Figure 4.11, the growth advances rapidly after an initial barrier.

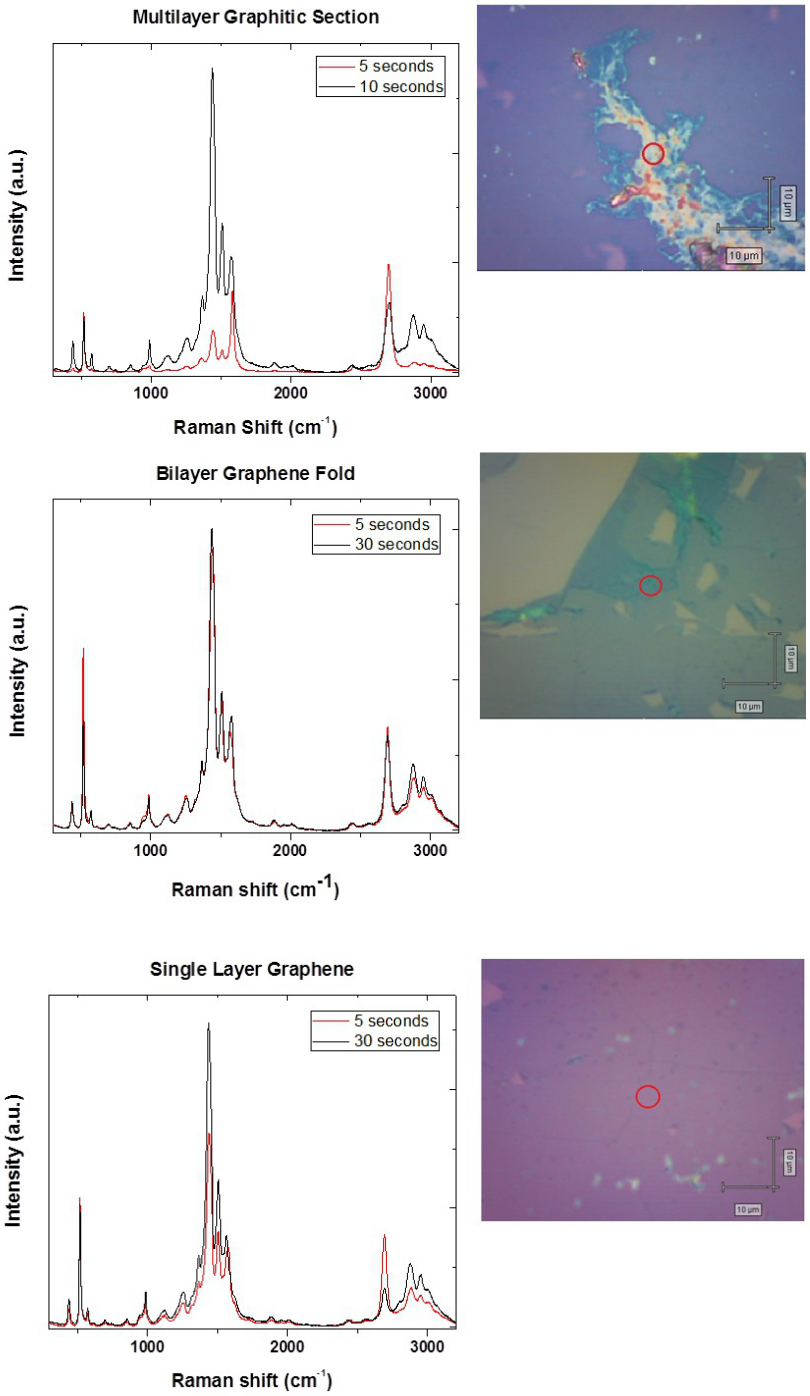

Figure 4.11 Raman spectra showing the difference in peaks in PEDOT grown on multilayer, bilayer folds and single layer graphene after the indicated growth times. The imaged areas on the 5 second sample are circled in red on the corresponding optical micrographs.

The static water contact angle measurements were taken on surfaces of PEDOT:PSS and the graphene/PEDOT stack. The average contact angles were 12° and 49°, respectively, showing that the PEDOT modifies the surface of graphene, reducing its hydrophobicity. As such, the challenge of adhesion of PEDOT to the graphene surface is addressed by this direct electropolymerization method. A detailed study should be done to investigate the influence of the growth and film parameters on the surface characteristics.

4.4 Conclusion and Outlook

The application of graphene as transparent conductors in organic devices required circumventing the challenge of surface compatibility as it greatly affects the ability to transport and/or extract charges from the active materials. To do so, a method has been developed to grow films of the conducting polymer PEDOT directly and conformally on single layer CVD graphene via a simple electrochemical method without the use of any catalysts. This technique, which has historically most commonly been employed on metals and ITO, is surprisingly suitable for single layer graphene grown by CVD, even with the predominantly sp^2 character of the bonding. The film properties of the electropolymerized PEDOT on graphene were studied and found to differ from PEDOT grown on ITO and via other conventional synthesis methods. This PEDOT also enhances the conductivity of graphene, which shows promise for high conductivity and transmittance applications. A few challenges, such as controlling the roughness of the films and establishing a good contact between the potentiostat and the graphene working electrode, have to be overcome in order for incorporation into devices. Nevertheless, this growth process creates a new bilayer composite material with potential for further optimization.

References

(1) Liu, Z.; Liu, Q.; Huang, Y.; Ma, Y.; Yin, S.; Zhang, X.; Sun, W.; Chen, Y. *Advanced Materials* **2008**, *20*, 3924.

(2) Liu, Z.; Liu, L.; Li, H.; Dong, Q.; Yao, S.; Kidd Iv, A. B.; Zhang, X.; Li, J.; Tian, W. *Solar Energy Materials and Solar Cells* **2012**, *97*, 28.

(3) Subrahmanyam, K. S.; Kumar, P.; Nag, A.; Rao, C. N. R. *Solid State Communications* **2010**, *150*, 1774.

(4) Park, H.; Brown, P. R.; Bulović, V.; Kong, J. *Nano Letters* **2011**, *12*, 133.

(5) van de Lagemaat, J.; Barnes, T. M.; Rumbles, G.; Shaheen, S. E.; Coutts, T. J.; Weeks, C.; Levitsky, I.; Peltola, J.; Glatkowski, P. *Applied Physics Letters* **2006**, *88*, 233503.

(6) Rowell, M. W.; Topinka, M. A.; McGehee, M. D.; Prall, H.-J.; Dennler, G.; Sariciftci, N. S.; Hu, L.; Gruner, G. *Applied Physics Letters* **2006**, *88*, 233506.

(7) Tung, V. C.; Chen, L.-M.; Allen, M. J.; Wassei, J. K.; Nelson, K.; Kaner, R. B.; Yang, Y. *Nano Letters* **2009**, *9*, 1949.

(8) Li, G.; Shrotriya, V.; Huang, J.; Yao, Y.; Moriarty, T.; Emery, K.; Yang, Y. *Nature materials* **2005**, *4*, 864.

(9) Wang, Y.; Tong, S. W.; Xu, X. F.; Özyilmaz, B.; Loh, K. P. *Advanced Materials* **2011**, *23*, 1514.

(10) Gomez De Arco, L.; Zhang, Y.; Schlenker, C. W.; Ryu, K.; Thompson, M. E.; Zhou, C. *ACS Nano* **2010**, *4*, 2865.

(11) Ouyang, J.; Chu, C. W.; Chen, F. C.; Xu, Q.; Yang, Y. *Advanced Functional Materials* **2005**, *15*, 203.

(12) Wang, Y.; Tong, S. W.; Xu, X. F.; Özyilmaz, B.; Loh, K. P. *Advanced Materials* **2011**, *23*, 1514.

(13) Hsu, C.-L.; Lin, C.-T.; Huang, J.-H.; Chu, C.-W.; Wei, K.-H.; Li, L.-J. *ACS Nano* **2012**, *6*, 5031.

(14) Wang, D.-W.; Li, F.; Zhao, J.; Ren, W.; Chen, Z.-G.; Tan, J.; Wu, Z.-S.; Gentle, I.; Lu, G. Q.; Cheng, H.-M. *ACS Nano* **2009**, *3*, 1745.

(15) Saxena, A. P.; Deepa, M.; Joshi, A. G.; Bhandari, S.; Srivastava, A. K. *ACS Applied Materials & Interfaces* **2011**, *3*, 1115.

(16) Choi, K. S.; Liu, F.; Choi, J. S.; Seo, T. S. *Langmuir* **2010**, *26*, 12902.

(17) Zhang, J.; Zhao, X. S. *The Journal of Physical Chemistry C* **2012**, *116*, 5420.

(18) Wang, X. J.; Wong, K. Y. *Thin Solid Films* **2006**, *515*, 1573.

(19) Sakmeche, N.; Aaron, J. J.; Fall, M.; Aeiyach, S.; Jouini, M.; Lacroix, J. C.; Lacaze, P. C. *Chemical Communications* **1996**, 2723.